M.Sc. thesis in chemistry

Determination of partitioning coefficients and protein binding using high performance liquid chromatography: Towards *in vitro* pharmacology in radiotracer development

Mona Milde Spilhaug

Department of Chemistry, University of Oslo, Norway

May 2017

Address correspondence to: Mona Milde Spilhaug,
University of Oslo, Department of Chemistry,
Boks 1072 Blindern
0316 OSLO
E-mail: m.m.spilhaug@kjemi.uio.no

2017

Determination of partitioning coefficients and protein binding using high performance liquid chromatography: Towards *in vitro* pharmacology in radiotracer development

http://www.duo.uio.no/

Print: Repro central, University of Oslo

Table of Contents

Acknowledgements

I wish to thank my supervisor in this project, Prof. Patrick Riss, for project planning, funding and administration, and the co-supervisor Prof. Bent Schoultz for supervision and technical assistance. I am thankful for their facilitation of the process of completing this thesis work despite the obligations arising from work and motherhood. A big thankyou also goes to my many colleagues for assistance and training with the equipment used and feedback during the experimental and writing phases. Thank you to Fatland Oslo AS, who provided several deliveries of pig blood, and thanks also to Tine Olsen Linderud (Fürst Medicinal Laboratory) for lending equipment and assistance with withdrawal of human blood. I acknowledge proof reading of this thesis by Prof. Paul Cumming, and my great appreciation to everyone who helped me with all my questions and problems. Finally, my biggest thanks to my family and friends, who helped with babysitting, housekeeping, and even walked my dog, for having supported me in all my decisions, re-decisions, frustrations over problems, and who shared my happiness when things went well. None mentioned, none forgotten.

1. Summary

We present RP-HPLC methods for the determination of the distribution coefficient at pH 7.4, as log D, and plasma protein binding. Although there are several methods available to determine distribution coefficient (log D) and protein binding, none of them involves a general and user-friendly approach that gives the opportunity to screen large libraries of compounds for both log D and plasma protein binding, with low cost and less time-consuming assays. The log D methods are amenable to rapid determinations and offer an excellent reproducibility. Standard deviation from literature was only 0.1 as an average for method A and 0.2 in method B, though method B eluted compounds earlier and worked for a broader range of complex compounds. The plasma protein binding determination made use of Microcon centrifugal filters whereas incubated test compound in porcine plasma where ultrafiltrated and the supernatant were measured by RP-HPLC. The high-throughput protocols described herein, for determination of log D and plasma protein binding, are straightforward to set up and require very small quantities of sample (< 1 mg for both lipophilicity and protein binding). In addition to the optimized methods, trends between chemical properties and lipophilicity/plasma protein binding were investigated, with no clear correlation useful for screening purposes.

2. Aim

The aim of this project was to develop, calibrate and test new methods for ascertaining the physicochemical molecular properties of small molecule radiotracers for positron emission tomography (PET) imaging. In the past decade, HPLC methods for lipophilicity and protein binding measurements have become more and more popular in preliminary characterization of radiopharmaceuticals designed to have affinity for specific receptors or other molecular targets. There are also literature reports on using HPLC for to measure binding of radiopharmaceuticals to porcine plasma protein, although with rather narrow aims in relation to specific proteins and peptides. There has not hitherto emerged any general screening method for using HPLC to measure plasma protein binding, although this physicochemical property can be decisive in the success of a new PET tracer. We therefore wanted to develop practical methods for characterizing tracers over a wide range of lipophilicity, and to then to establish a correlation between lipophilicity and plasma protein binding with tissue uptake and distribution. We foresee that such a method would facilitate screening of new tracer compounds, and, therefore save research time and resources.

3. Introduction

3.1. Imaging and PET

PET is a powerful and minimally invasive molecular imaging technique based on the tracer principle, as developed by Georges de Hevesy (Nobel Prize in Chemistry, 1943), and now finding a wide range of clinical and research applications. The PET technique relies on the detection of ionizing radiation emitted by a molecular probe as it makes its way through the organism. Specific small molecular weight probes (radiotracers) are used in clinical care to detect cancer and measure cellular metabolism, and in basic brain research. PET methods enable the study of biological function on the molecular level in both healthy and diseased tissues. Thereby, PET enables molecular imaging in contrast to nuclear magnetic resonance imaging (MRI) and computed tomography (CT) modalities, which primarily image tissue morphology and density. PET more closely resembles single-photon emission computed tomography (SPECT), but generally provides higher sensitivity, spatial and temporal resolution and diagnostic accuracy. Tomographic imaging (from the Greek: tomos = section and graphikos = written, displayed) allows for three-dimensional visualization of organs and tissues of the body. PET is used to map the distribution of a molecule in the living organism by mapping the emanations from a short-lived positron-emitting radionuclide which as ^{11}C ($t_{1/2}$ = 20 min) or ^{18}F ($t_{1/2}$ = 110 min), which must be prepared in a cyclotron and rapidly reacted with a precursor. The classic example of a PET tracer is 2–[^{18}F]fluoro-2-deoxyglucose (FDG), which behaves much as natural glucose in certain physiological processes [2]. Today, PET imaging with FDG is the standard of care in clinical oncology and nuclear medicine [1, 3-5].

PET recordings with FDG follow the pathway for glucose, as visualized by fluorine-18, which decays by release of a positron or *anti*-electron. In the medium of the brain, the positron soon encounters an electron, and their mutual annihilation results in releasing a pair of photons in diametrically opposite directions, in accordance with conservation of momentum. The released gamma photons (512 keV) contain the entire rest mass energy of the electron-positron pair ($E=mc^2$). A radial detector array counts both photons using a coincidence circuit (Figure 1), and the accumulation of many such decay events is reconstructed into a source map.

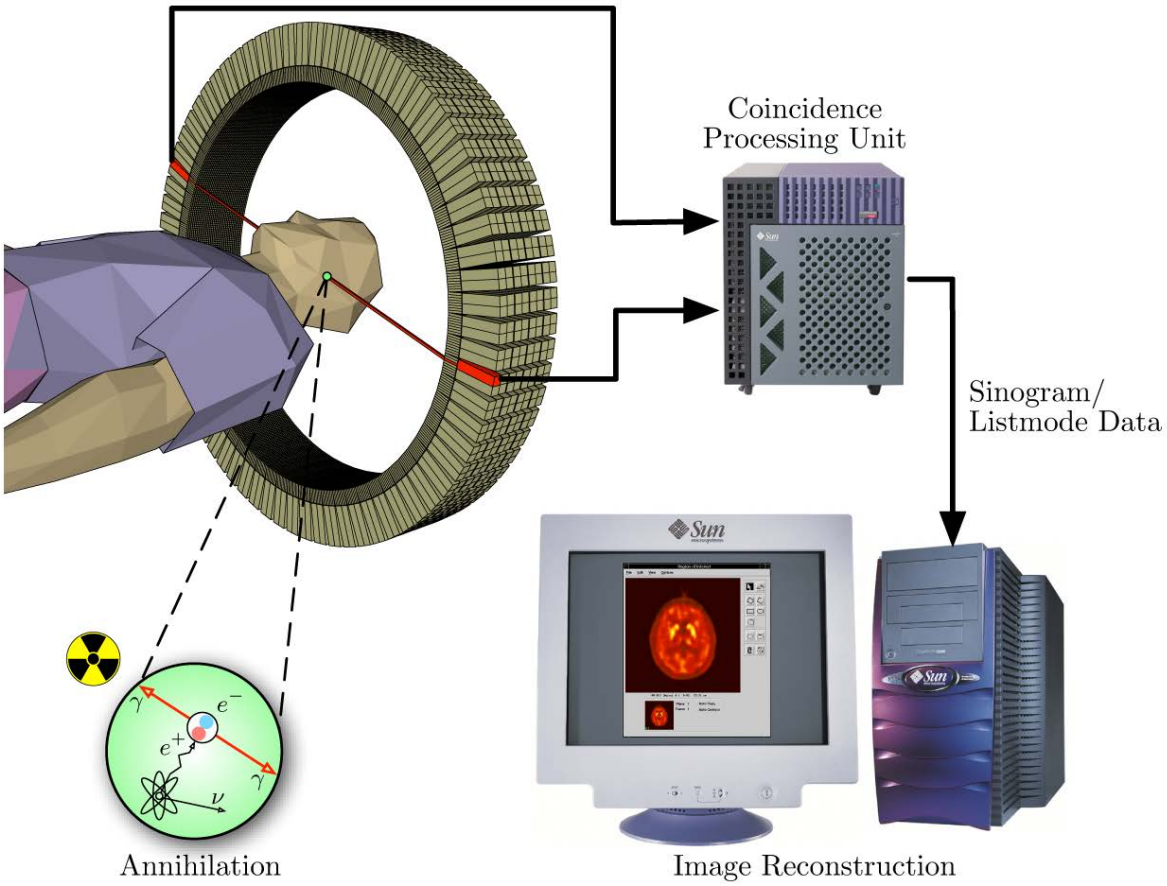

Figure 1: Schema of a PET acquisition process

After an intravenous injection of FDG to patient there are millions of decays per second, so the final images are reconstructed from a vast number of single decays. In some quantitative studies, the dynamics of FDG uptake in three dimensions is followed with the additional dimension of time, where source maps are generated in a series of time windows known as frames. Since the radioactivity A of FDG or any radioactive tracer is strictly proportional to the mass of substance and its physical decay constant ($A = N \times \lambda$), and the temporal distribution of the radiotracer is governed by its biomolecular properties, PET provides quantitative information about physiological parameters, such as the rate of influx or transport from blood into tissue and the rate of trapping in the tissue. In the special case of FDG, the trapping indicates the enzymatic activity in living tissue of glucose hexokinase, which catalyses the first step in the glycolytic pathway. For many other tracers, the trapping in tissue is mediated by binding to a neurotransmitter receptor or transporter.

The development of new pharmacologically specific PET probes is difficult because it is not possible to predict the performance of new radioactive molecules in the living organism. Following intravenous injection, the tracer is carried in the blood target sites, but several parameters affect its access to the intended tissue or destination. These parameters include binding to plasma proteins, metabolism in liver, and permeability to the blood-brain barrier.

To test these parameters *in vivo* is expensive and time consuming in humans and results are in experimental animals do not always generalize to humans. As an alternative to studies in vivo, simple models can be used to simulate specific aspects of a tracer's behavior in the living system. Tissues composed of individual cells, which are small compartments of cytoplasm contained by the lipid bilayer of the cell membrane; entry of a small molecule into a living cell entails transit across the membrane. The preference of a molecule for the lipid environment is known as lipophilicity, which is commonly expressed as Log D, that is to say the logarithm of the distribution coefficient between an aqueous and a lipophilic phase, usually water versus octanol (This measurement method will be presented in detail in chapter 3.3. "Lipophilicity"). Molecular within a certain range of lipophilicity diffuse across cell membranes with ease.

Simulation model studies such as the octanol/water partition measurement are useful for initial screening of candidate tracer molecules. However, the value of such models for predicting the success of intravenously injected radiotracers is rather limited, due to an abundance of factors. Therefore, there is a need for translating straightforward methods for quantification of molecular lipophilicity into their *in vivo* correlate.

3.2. Reversibly binding radiotracers

Following injection into the blood stream, small lipophilic molecules may bind to blood cells and plasma proteins or remain unbound in the plasma. Plasma protein binding is a key factor limiting bioavailability, since the partitioning of a tracer or radiopharmaceutical molecule between the aqueous phase and a plasma protein bound state (known as the free fraction in plasma) determines its availability for diffusion into tissues, which is in turn defined by the molecular weight and lipophilicity of the compound. Only after reaching the target tissue the binding affinity of the radiotracer for its molecular target comes to play a role. These considerations highlight the importance of the molecular physicochemical properties, as discussed above.

PET imaging of proteinaceous targets in the human brain has revolutionized understanding of brain function and behaviour. Quantitative analysis and interpretation of PET imaging data has undergone significant advances in recent years [6]. Researchers in the pharmaceutical industry and academic medicine now use PET biomarkers to report on drug-target engagement and measurements of drug efficacy and/or toxicity. Clinical diagnosis and staging of brain diseases such as dementias and other neurodegenerative diseases is another area where PET imaging methods have been transformative. FDG-PET studies of brain energy metabolism as well as PET studies with tracers for β-amyloid are being used to provide endpoints in large scale prospective studies of Alzheimer`s disease, and for the differential diagnosis of Alzheimer`s disease from other dementias.

Radiopharmaceuticals used in brain PET can have different principles governing their passage across the blood-brain barrier (BBB). The class example of FDG, like natural glucose, enters the brain by process of facilitated diffusion mediated by a specific transporter embedded in the BBB. The majority of radiopharmaceuticals enter the brain by passive diffusion, and then undergo binding to a protein target, such as in the case of [^{18}F]altanserin for PET studies of serotonin 5HT2 receptors in brain. Members of this class of targets is often referred to as saturable systems; the small number (~10^2) of available radiotracers targeting saturable systems stands in stark contrast with the tremendous number of functional protein receptors in the mammalian proteome (10^5-10^6). There is clearly enormous scope for expanding the range of PET targets [1, 2].

Candidate radiotracers must have an appropriate affinity (K_D) relative to the number of binding sites per volume of target (B_{max}), where K_D and B_{max} are the saturation binding parameters; this ratio is frequently presented as the binding potential (BP), B_{max}/K_D. In a case where the target abundance is 100 nM and the radiotracer affinity is 10 nM, BP is predicted to have a value of 10. Selectivity of binding for the target protein *in vivo* is of the utmost importance; ideally the radiotracer only binds to a single molecular species tissue volume of interest.

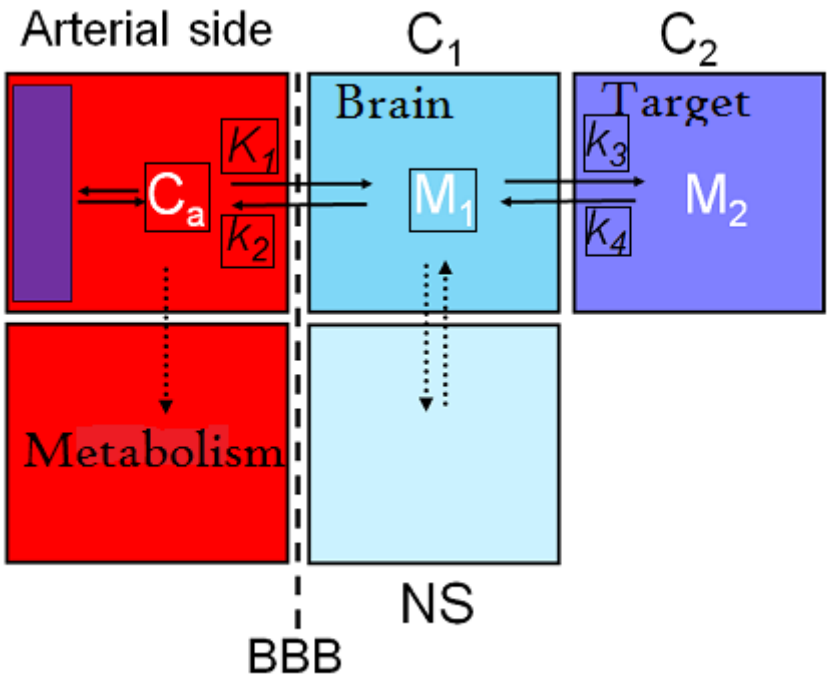

Figure 2: A general compartmental model for a radiotracer

In Figure 2 the tracer has concentration C_a in arterial blood, and reversibly (K_1, k_2) crosses the blood brain barrier (BBB) The free tracer concentration in brain M1 occupies the first tissue compartment (C_1), and is available for reversible binding (k_3, k_4) to the target, where M_2 is the bound mass in the second tissue compartment (C_2), or can enter a non-specific binding compartment (NS). Tracer in blood can be metabolized, but plasma metabolites generally do not cross the BBB. Unmetabolized tracer on the arterial side that is bound to

plasma proteins (depicted as the purple sub-compartment) is not available for transfer across the BBB.

As depicted in Figure 3, the radiotracer concentration in tissue is made up of at least three components, unbound radiotracer in tissue (M_1), radioactivity specifically bound to the target (M_2) and tracer bound non-specifically to the tissue; it is M2 that imparts the specific signal of interest in the PET study. The tracer in blood enters the brain by exchange across the capillary endothelium of the BBB. In cases where radiometabolites do enter the brain, the specific binding component of the PET signal (M_2) can be difficult to separate from the additional background radioactivity in brain. In summary, an ideal PET tracer should not be entirely bound to plasma proteins, should have good permeability to the BBB, and should not yield brain-penetrating metabolites [1]. For quantitative analysis of the PET data, a fast pharmacokinetic profile is also highly desirable. In general, the tracer must reach a transient equilibrium of binding within less than 5 half-lives of the radionuclide (i.e. 100 min for carbon-11) to sustain adequate image quality for quantitation. To develop radiotracers that comply with these criteria is challenging, because few experimental techniques are available to predict uptake and equilibration of a candidate radiotracer in vivo.

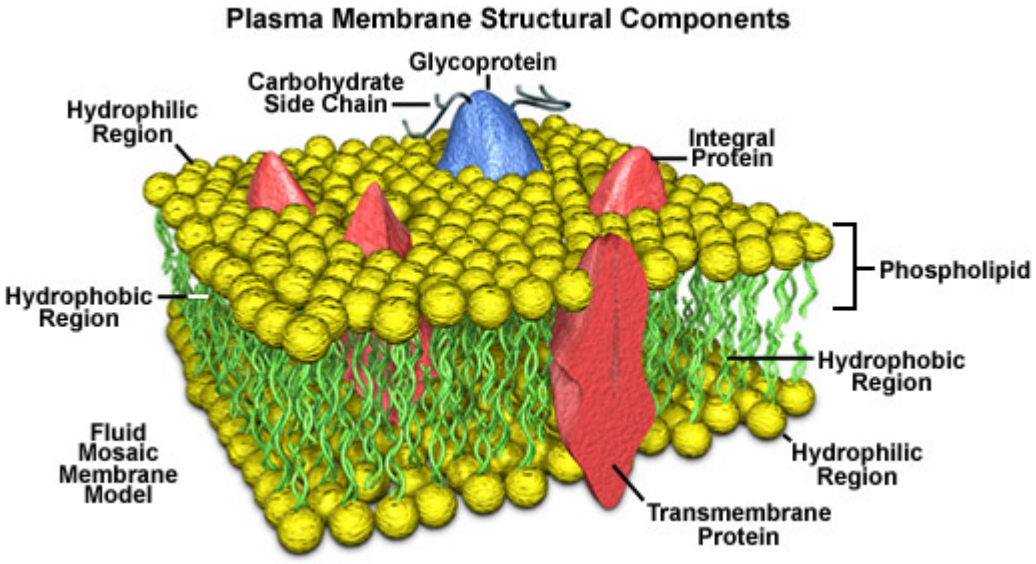

Figure 3: The layers of a cell membrane

Transit of a small molecule across the BBB or any cell membrane is a complex process. As suggested by Figure 2, passage across a lipid bilayer is opposed by the inner and outer hydrophilic (from Greek hydro = water; philic = dear, friendly) domains, and the intramembrane lipophilic (from Greek lipo = fat, oil; philic = dear, friendly) or hydrophobic (from Greek hydro = water; phobic = fear). A given small molecule in brain or blood first encounters the hydrophilic surface of the membrane, and must then pass across the hydrophobic/lipophilic inner part of the membrane. In a manner of speaking, permeability

across the cell membrane is a tradeoff between hydrophobic and hydrophilic properties. Hydrophilic and highly charged compounds often require specific transport mechanisms to be taken up into cells and tissues [1]. Nutrients such as sugars, essential ions or amino acids are also hydrophilic, and specific molecular mechanisms exist to facilitate their trafficking from the blood to tissues, and across cell membranes. As such, individual cells are protected from uncontrolled trafficking of ions and certain molecules. On the other hand, small lipophilic compounds may diffuse very quickly across cell membranes, and thus reach equilibrium distribution within minutes after i.v. administration. This property favors reaching the target compartment without the need for specialized transport systems, which often limit permeability. Since uncontrolled diffusion of bioactive lipophilic compounds, many of which are toxic, may have a negative effect on cells and tissues, efflux pumps such as the ABC proteins are embedded in the cellular membrane. In addition, oxidoreductase enzymes metabolize lipophilic molecules absorbed via food, drink, breathing or skin contact by converting them into more hydrophilic metabolites, which are then eliminated by the kidneys. While an essential adaptation, these mechanisms also affect the handling of radiopharmaceuticals. For example, lipophilic tracers can be rapidly metabolized in the liver [7], thus creating a need for designing candidate molecules with an optimal balance of properties. Overall, the lipophilicity of a radiopharmaceutical plays a major role in determining whether its reaches its target tissue and binding site.

3.2.1. PET groups aim for radiotracers

The PET group at the University of Oslo works on developing radiotracers for applications within PET imaging in various fields. The main groups of compounds that were investigated during this project are showed in Table 81 in Appendix C “General data concerning both lipophilicity and protein binding”. Opioid receptors are a class of inhibitory G protein-coupled receptors, within a large family of receptors that detect signaling molecules outside the cell and then activate internal signal transduction pathways and, ultimately, cellular responses. The natural ligands are the opioid peptides, whereas opiates are natural products or synthetic molecules that mimic the response to the endogenous peptides [8, 9]. Opioid receptors fall into three pharmacologically distinct categories, which are designated μ, κ or δ receptors. The aim for the compounds designated W-group was to obtain a tracer with high affinity (low K_D) specifically for μ receptors, and low affinity for κ or δ receptors, which is a necessary property for a μ-specific PET ligand. The compounds designated L-group were aimed for Alzheimer´s disease detection, based on high affinity for the pathological τ protein aggregates in brain. Many tracers have been promoted as τ-imaging agents, but none are yet sufficiently selective for the intended target. While some of the commercial compounds show good selectivity in vitro, they have failed to reveal specific signal in PET studies, which justifies our search for agents with improved properties.

3.3. Lipophilicity

3.3.1. Blood Brain Barrier

The Blood Brain Barrier (BBB) is an arbitrary concept, a tool where brain tracers are used due to the cleanliness compared to peripheral ones. The BBB only simplifies the model for the brain tracer development though, it either goes through or it doesn't, so the experimental part is to see how fast and how clean the novel radiotracer enters the brain. Using this model is recognized and useful in many aspects, but uptake in the brain cannot solely be interpreted from this model. The theory has still been central in the development and understanding of uptake in the brain and helps characterizing comprehensive mechanisms and will be explained in this chapter. As noted above, the BBB is a hindrance to the free diffusion of pharmaceuticals and PET tracers into the central nervous system (CNS). As such, the BBB is a major consideration in medicinal chemistry. The brain, like all living tissues rely upon blood perfusion for the supply of oxygen and nutrients. Since the brain is a complicated organ containing hundreds of types of specialized cells that communicate by chemical messenger (neurotransmitter) molecules, brain tissue is very sensitive to exogenous toxins arriving in the blood. Furthermore, there is very little neurogenesis in human brain after the first postnatal years, which means that the population of neurons at birth must be protected from environmental stressors throughout life to maintain healthy functioning. Neurons are polarized by the action of the Na^+/K^+-ATPase and neuronal homeostasis requires tight control of ion concentrations, which is maintained by a constant expenditure of ATP produced by glycolysis and aerobic respiration. The energy demand of brain tissue is thus very high, which requires an uninterrupted supply of oxygen, glucose and nutrients, without any compromise of protection against entry of potentially disruptive or toxic chemicals. Hence, the brain vasculature is characterized by a very fine, structure that is an obstacle to diffusion by molecules of mud weight (MW) greater than 500. The composition of the BBB and factors that influences the permeability of molecules has been reviewed in several articles [10-12]. Figure 4 shows a schematic representation of the BBB. The brain microvasculature is composed of capillary endothelial cells (BCECs) with so-called "tight junctions", structurally unlike the junctions in most other capillary beds. Since certain nutrients and messengers would otherwise be excluded from entry to the brain, the BECSs also express several specific transporters, such as the glucose and amino acid transporters [2]. The BBB is not permeable for large molecules like proteins, and only two percent of small molecules administered to man are detected in brain in a significant concentration. The key function of the BBB is best illustrated by the significant effort expended in developing model systems to facilitate CNS drug development. A team from Pfizer Inc. developed the rule of five (sometimes referred to as Lipinski's rule) in 1997 to formalize the factors determining BBB permeability. This model only addresses parameters relevant for passive diffusion, solubility and binding. Given that most pharmaceuticals are administered orally, the Pfizer model also considers the effects of a molecule´s charge in relation to absorption via the digestive tract, a consideration that is less important for BBB permeability.

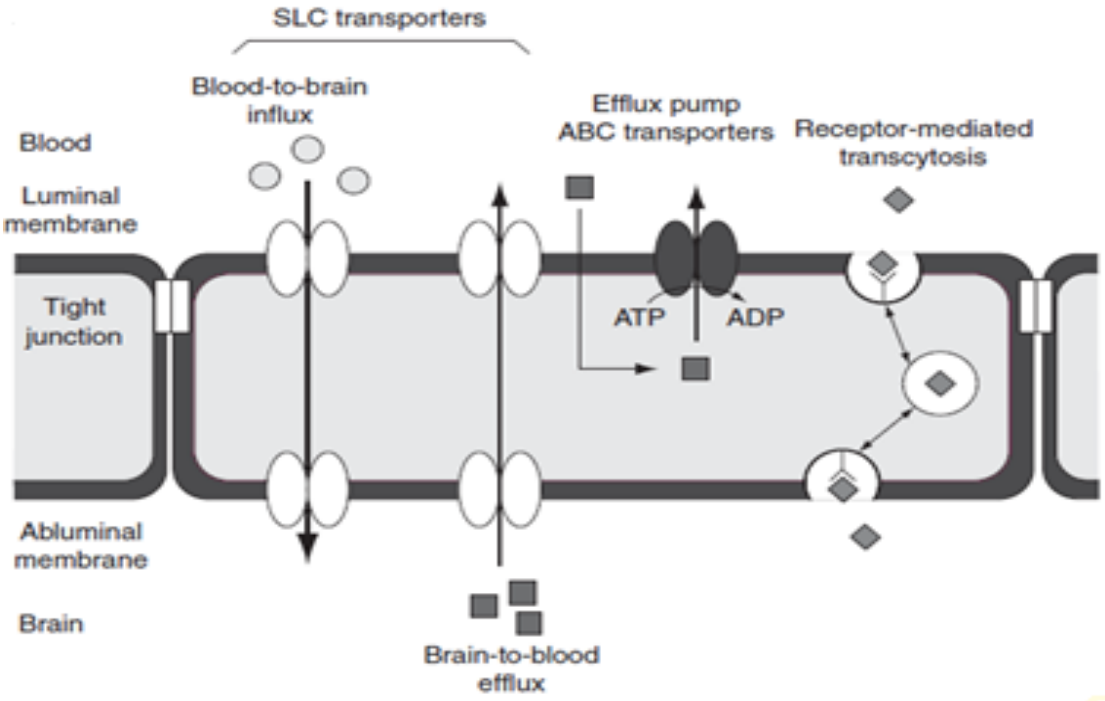

Figure 4: A schematic view of transportation through the BBB

For PET imaging, the rule of five is not sufficient. This is partially due to the nearly exclusive use of intravenous administration, and partially to the tracer principle itself. A major distinguishing factor relates to the orthogonal pharmacokinetic requirements of PET imaging and pharmacotherapy; quantitative PET imaging is favored by fast kinetics, but pharmaceuticals require steady-state for prolonged action in brain. In either circumstance, the concentration of the drug in the brain is directly related to BBB permeability, and generally correlates with the area under the plasma drug concentration- time curve (AUC) [13, 14]. Therefore, new pharmacokinetic models are required to adequately describe the requirements for successful PET radiotracers.

The figure above illustrates three modes of solute transporter at the BBB. The first is blood-to-brain passive influx (K_1), which favors the entry of many lipid-soluble molecules into the brain [15]. The tracer influx can be reduced or completely blocked by extrusion back into circulation even before the tracer enters the brain; this extrusion is mediated by efflux transporters of the ATP-binding cassette (ABC) family, which includes the P-glycoprotein (ABCB1, P-gp or MDR1), breast cancer resistance protein (ABCG2 or BCRP) and multidrug resistance-associated protein (ABCC1 or MRP1), which are not just a hindrance for PET tracers, but can hamper pharmacotherapy using chemotherapeutic drugs. As the third mechanism, the radiotracer in blood is vulnerable to metabolism; since the primary route of administration is intravenous injection, radiotracers are immediately exposed to an array of metabolizing enzymes in the blood, liver and other tissues. This process reduces the

availability of tracer for crossing the BBB, but fortunately the radiometabolites are usually less lipophilic than its parent radiotracer, and hence do not enter the brain as easily [1, 16]. Understanding the various modes of transport and diffusion across the BBB in vivo is the key to understanding BBB permeability and drug distribution in the brain.

Liver also contains a similar system of enzymes and ATP-binding cassette (ABC) transporters which regulate the access of blood-born molecules to hepatocytes. ABC efflux transporters can have a big effect on drug bioavailability. Drugs that are not absorbed or extracted by the liver will be excreted in the bile or bypassed to the kidneys and eliminated in the urine. In tissues, such as the liver and small intestine, Pgp-mediated excretion occurs conjointly with metabolism by the cytochrome p450 (CYP) family of enzymes and by glutathione-S-transferases. Certain drugs that are good substrates of the CYP are reported to have less than 50% oral bioavailability, which limits their effectiveness by oral administration, especially when compounded by Pgp-mediated extrusion. 60% of drug molecules and 75% of PET tracers are metabolically altered via hepatic CYP, mainly in the liver and kidneys. The formation of the radioactive metabolites can be problematic for PET imaging, especially in cases where metabolites remain in circulation during the scan. Many CYP metabolites are more hydrophilic than the parent compounds (which facilitate their renal elimination) and some plasma metabolites can enter the target tissue. In PET studies, the resulting radioactivity distribution will increase the non-specific binding signal, and in some cases, the radiometabolites can have undesirable specific binding components. As such, CYP metabolism can interfere in the utility of candidate PET tracers [1].

Solubility in plasma membranes of the BBB and interactions with certain transporters is strongly influenced by lipophilicity, i.e. hydrophobic interactions. Indeed, drug receptor interactions are governed by very much the same intermolecular forces as partitioning of solutes between water and organic biphasic mixtures. Before a drug or radiotracer ever reaches its pharmacological target, a given compound´s lipophilicity determines its solubility, reactivity and degradation, as well as the manner of formulation [2]. Log D is the logarithm of the distribution-coefficient (*D*), which is the measured ratio of equilibrium concentrations of a compound in a mixture of two immiscible phases such as octanol/water. Log P is similarly defined, but applies for non-ionized solutes. While both measures are used early in the drug discovery process, log D at pH 7.4 (log D (7.4)) is much to be preferred over Log P, as it applies to the physiological condition. Indeed, Log P has a poor correlation with physiological data for BBB permeability [17].

3.3.2. Lipophilicity influences in biological systems

In formal and quantitative terms, permeability to the BBB can be defined as the extraction fraction, which is the percentage of tracer entering brain as the blood passes through the capillary bed. Since extraction fraction is relative to the cerebral perfusion rate, permeability is more conveniently expressed as the brain concentration at some early time after tracer

injection, in standard uptake units (% injected dose per gram of tissue). Using this metric, a parabolic relationship between measured lipophilicity and *in vivo* brain penetration of pharmaceuticals can be seen. Hydrophilic compounds have low permeability because ionizable functional groups having a charge disfavors transit across cell membranes. Compounds of moderate or intermediate lipophilicity often have highest uptake; whereas very higher lipophilicity have reduced permeability due to their greater binding to plasma proteins [18]. The above considerations relate to an inherent property of a molecule governing its partitioning between the blood and brain compartments. However, it has been shown that high drug lipophilicity also correlates with high affinity and binding to certain enzymes and efflux pumps [18]. This is mainly due to the hydrophobic interactions that drive drug binding to the active center of the relevant enzyme. This kind of interaction is a topic to be examined in this thesis. Many radiolabeled drugs with known behavioral or therapeutic effects in the CNS do not appear to enter the brain when administered at low mass dose, as is typical in PET tracer studies. In such cases, lipophilicity might not predict brain uptake due to mass effects, but if binding to efflux pumps or other biological barriers can be neglected from consideration, lipophilicity should correlate with brain uptake in the ascending limb on the parabolic relationship, until lipophilicity exceeds some value at which binding to plasma proteins or binding in lung or hepatic tissue become dominant factors, thus disfavoring brain uptake. The trade-off between these factors determines the parabolic relationship between drug lipophilicity and both brain uptake and behavioral effects of drugs as discussed above [19].

Figure 5 indicates that the brain uptake of low molecular weight radiotracers has a parabolic relationship with lipophilicity [20]. The Log P range here corroborates general findings that brain penetration is favored when Log P < 4. (From *Waterhouse*, 2003)

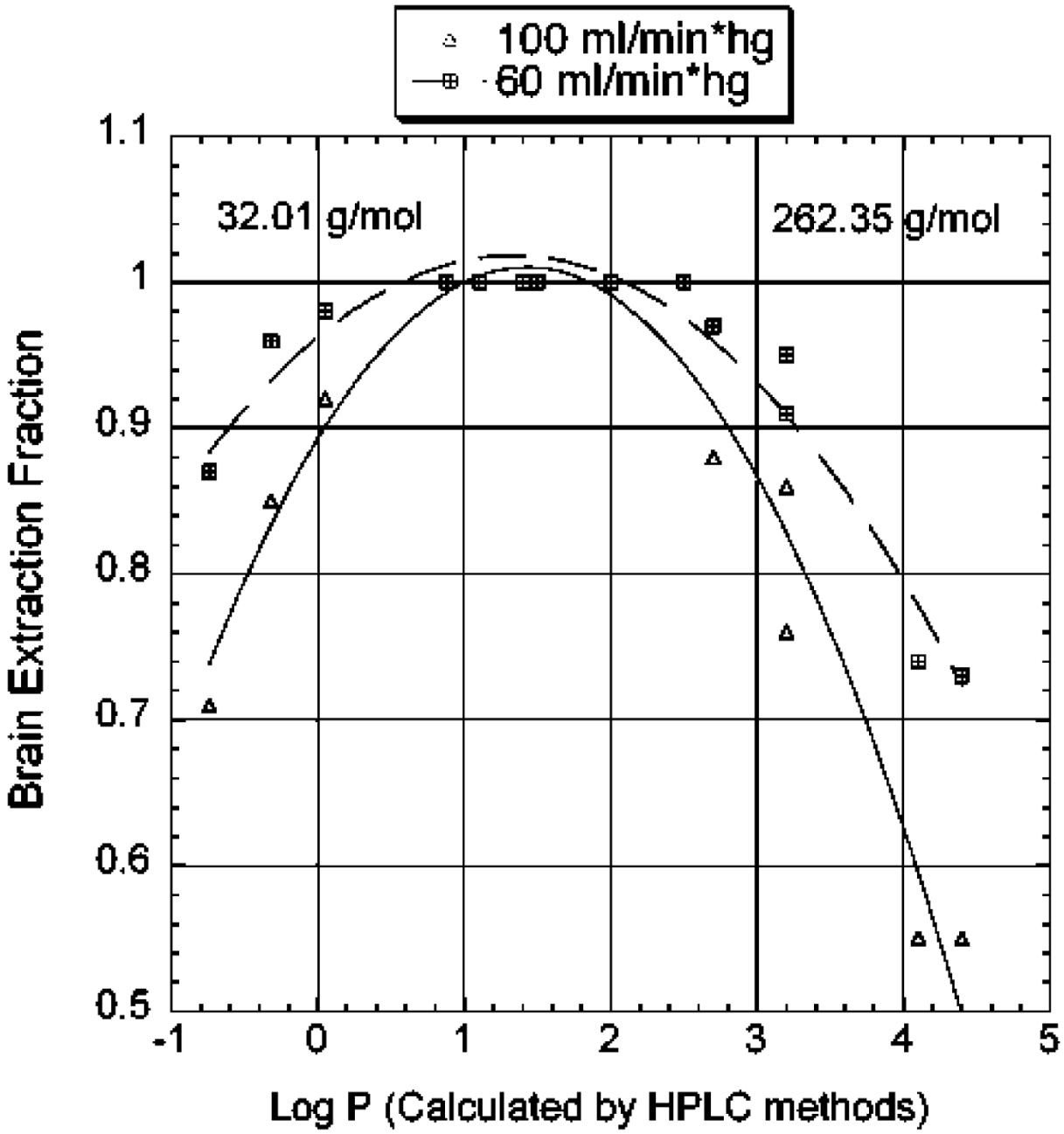

Figure 5: Early studies in tracer development [24]. Lipophilicity versus brain uptake for simple radiolabeled compounds

Lipophilicity of drug candidates also seems to have a major impact on absorption, distribution, metabolism, excretion and toxicity properties. The partition coefficient between the aqueous phase in blood and tissues determines its exposure to hepatic metabolism, which influences its elimination rate. Toxicity is often the reason for withdrawal of a drug candidate, and this should ideally be estimated at the earliest possible stage of drug development, preferably even before synthesis [21, 22]. Even though PET tracers are usually administered at very low mass doses, toxicity can be an issue, as in the case of very potent opioid agonists, which are pharmacologically active at microgram doses.

3.3.3. Lipophilicity determination

Solvent Extraction

Several experimental protocols for lipophilicity determination can be found in the literature, but most often lipophilicity is measured through its partitioning between an aqueous and a hydrophobic phase. The classical method for partition coefficient measurement is called shake-flask procedure, which is a simple extraction in *n*-octanol and water (Figure 6). Octanol is often used because its lipophilicity and polarity is comparable to the lipid bilayer in cell membranes. However, methods using hexane, decane and branched chain alcohols have been used [4].

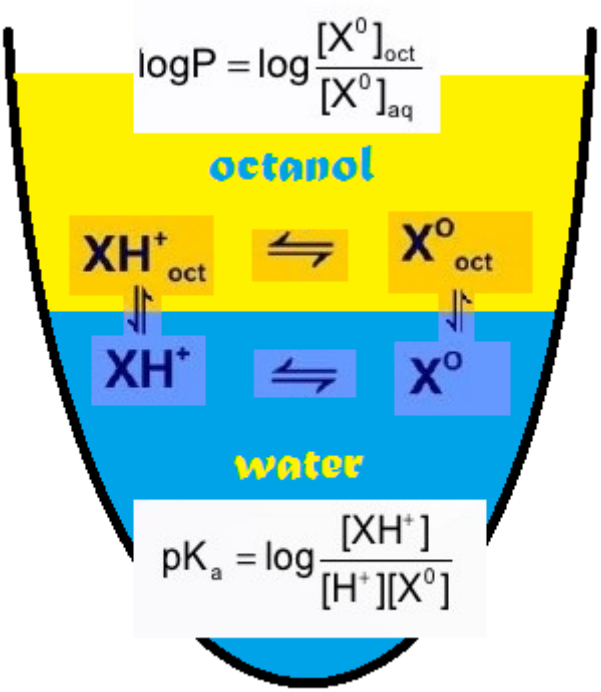

Figure 6: A solution of the sample is titrated in a two-phase system (water and octanol). The sample can ionize in water (pK_a), or it can partition into octanol (log P).

The quantitative description of lipophilicity, i.e. the partition coefficient P, is defined as the ratio between the concentrations of a neutral compound in organic (c_{org}) and aqueous (c_{aq}) phases under equilibrium, $P = c_{org}/c_{aq}$. After equilibrium between all interacting components is attained, an appropriate analytical method (for example UV/VIS spectroscopy or radiometric methods) is used to determine concentrations of the substances dissolved in both phases, and calculated as a ratio. The partition coefficient is normally expressed in a logarithmic scale, and applies for non-ionized species. A logarithmic scale is a nonlinear scale used when there is a broad range of quantities, here extending over many orders of

magnitude. This Log P +1 indicates a ten-fold concentration difference between the two phases and log P +4 a ten-thousand-fold concentration gradient favoring the organic phase.

In measuring Log P, the pH of the aqueous phase is adjusted so that the predominant form of the compound is non-ionized. For ionizable species, the partitioning is represented as the distribution coefficient Log D, which measures the contributions of all natural and ionized species at a specific pH. Of particular interest for some biological systems is the Log D at pH = 7.4, as this is the physiological pH of blood serum and thus reflects the practical chemical environment of drugs partitioning between blood and brain.

In the standard shake-flask measurement, the compound is partitioned between equal volume of aqueous and organic phases by agitation, followed by separation and measurement of the analyte concentrations in the two phases. This method is time-consuming, requires a lot of validation and calibration for each individual sample, and allows Log P determination in only the narrow range of -3 to 3. Log P has to be corrected for ionization, and furthermore relatively large amounts (10 mg) of high purity samples are necessary, which complicates assaying of compound libraries. In recent years, the method has been optimized significantly, resulting in a substantial shortening of the time required for each experiment, and a reduction in fluid volumes from above 100 ml per phase to less than 1 ml. A parallel shake-flask procedure employing 96-well plates has been proposed, which makes the method less time consuming but requires a high degree of automation and special instrumentation in combination with elaborate validation of the results. Several variations of the shake-flask method and other direct methods have been described in the literature [2]. As alternatives to the classic shake-flask procedure, methods such as reversed phase HPLC (RP-HPLC) and reversed phase thin layer chromatography (RP-TLC) have much to commend them in terms of simplicity and reproducibility [23]. Indeed, chromatography is a cost-effective method to quantify molecular lipophilicity being straight forward and offering an adequate throughput compared to other methods [18, 24, 25]. The chromatographic analysis is often done by measuring the concentration of a compound in a biphasic system (water/organic phase), and the results may be expressed as permeability coefficient P_e, partition coefficient log P, or distribution coefficient log D. [18, 24, 25].

High Performance Liquid Chromatography

In reversed phase chromatography, the solute migrates in a mobile phase, and is presented with a charged silica phase immobilized in the analytical column or TLC plate (Figure 7). As such, chromatographic retention time in reversed phase format is comparable to *n*-octanol / water partitioning. The retention time of a compound in reversed phase liquid chromatography (RP-LC) is strongly affected by the lipophilicity of the sample, since it is a function of the partition of the solute between the lipophilic stationary phase and the aqueous mobile phase. Hence, a well-designed HPLC method can give relevant information about compound properties with respect to lipophilicity [23]. Chromatographic methods are

often faster than the shake-flask method. The HPLC apparatus is accessible in many laboratories, the method is precise, and retention data is reproducible under controlled conditions. Furthermore, HPLC can be automated and has consequently become a standard procedure for lipophilicity measurements. Compared to direct shake-flask methods, impurities do not affect the measurements, as chromatographic separation is inherently part of the process. It is consequently possible to measure a broader range of chemicals, with smaller quantities of the samples [23].

The Organization for Economic Cooperation and Development (OECD) has published guidelines for testing of chemicals; OECD test # 117 "Partition Coefficient (n-octanol/water), High Performance Liquid Chromatography (HPLC) Method" and this was the starting point for the lipophilicity methods described in this thesis.

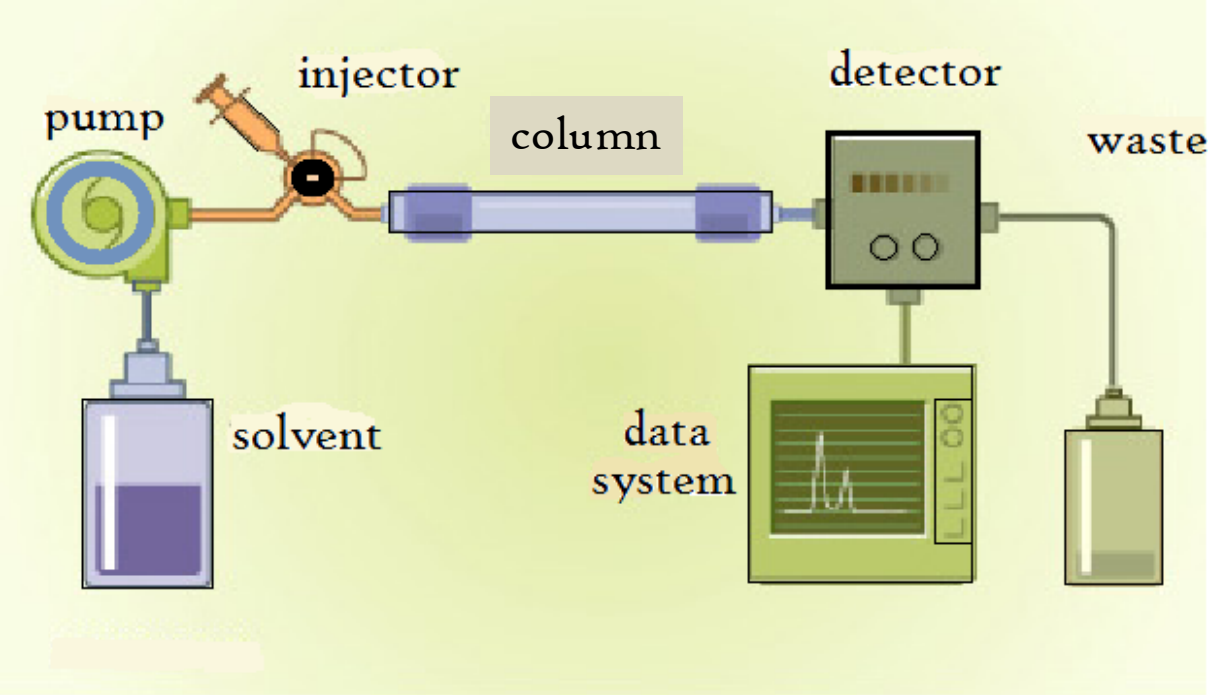

Figure 7: Schematic view over an HPLC system where the mobile phase is being pumped through the system, which carries the sample from the injection valve through the analytical column. A UV/Vis detector sends the data to viewable software according to the retention time of the compound.

Calibration curves with compounds of known Log P /Log D values are made, and test samples can be analyzed. The retention volume relative to the void volume of the analytical system is used to calculate the capacity factor and the Log P /Log D is calculated relative to the calibration curve. At best, the calibration curve is generated using homologues of the test compound, so that the calibration curve will emulate the test compound's behavior in the analytical system. Compounds with different functional groups have different retention mechanisms, and can sometimes thus be difficult to compare. When measuring several different compounds, a broader approach is still necessary to minimize the workload. Using a set of compounds spanning the range of lipophilicity to be measured will yield a more

general calibration curve for a group of structurally diverse molecules. The more reference compounds are added, the more robust the calibration curve will be.

The capacity factor k is a measure of a retention peak that is independent of column geometry or mobile phase flow rate. It is given by the expression:

Equation 1

$$k = (t_R - t_0)/t_0$$

where t_R and t_0 are the retention time of the test compound and of an unretained compound (dead volume), respectively.

Due to ease of operation and calibration combined with straightforward means for validation, HPLC provides a robust method with moderate throughput for assessing lipophilicity of structurally diverse compound libraries. Once established, UV/Vis reversed phase HPLC serves as a routine method to determine chemical purity of compounds and Log P/Log D of test compounds.

3.4. Protein binding

Albumin and other plasma proteins present binding sites with moderate affinity and high capacity for certain ligands and radiotracers. As with saturable sites encountered at the BBB, plasma protein binding, by removing tracer from the diffusible compartment, can inhibit entry into the brain during transit across the capillary bed [21]. However, non-specifically bound drugs can still enter the brain by free diffusion, which could explain why some radiotracers with over 90% plasma protein binding under equilibrium conditions, may still enter the brain relatively unhindered [10]. An issue is the association/dissociation kinetics of ligand binding to plasma protein relative to the brief transit time across the capillary bed. In some measure, the binding of ligands to plasma proteins is likely driven by hydrophobic interactions. If this hypothesis holds true, there are real implications of lipophilicity for brain uptake; the analysis of brain neuroreceptor imaging data can be critically dependent of the free fraction of the PET tracer in plasma. Brain uptake data is often quantified relative to the tracer concentration in blood (or plasma). Reversible binding of the radiotracers to plasma protein would result in continuous equilibration of the bound and free fraction of the drug, whereas irreversible binding removes some fraction of the tracer from the exchangeable blood pool. In either case, the total radioactivity concentration in whole blood or plasma remains the same.

The question if non-specific binding of a PET tracer to plasma proteins always reduces BBB penetration is a matter of debate. A common argument is that irreversible binding certainly makes the tracer unavailable for diffusion, since only the free fraction in plasma can enter the brain. But the notion that reversible binding occurs with equilibration of plasma free and

plasma protein bound fraction is also supported [19, 26, 27]. In conventional PET radiotracer experiments, the plasma concentration is normally within the picomolar to nanomolar range. It is therefore necessary to establish if the biological effects of saturable sites might substantially alter the free plasma concentration, and at what point mass effects emerge. The serum albumin concentration is normally 35-50 g/L (MW 67 kDa), corresponding to approximately 500 µM. Given one binding site per albumin molecule, it follows that the capacity for drug binding is very high. However, the mass of a given drug bound at equilibrium will depend critically on its affinity, and the extent of competition from all other blood constituents.

Given these consideration, the role and impact of plasma protein binding on the effective concentration of a drug or tracer available for diffusion into tissues is a matter of discussion. [28]. Figure 8 shows a schematic depiction of free fraction of a compound diffusing into tissue. This only depicts the protein binding at a hypothetical condition of complete equilibrium. In practice, the rate of diffusion of a tracer across the BBB is also influenced by factors noted above, i.e. the molecular weight of the compound, its charge, permeability and other parameters. In pharmacokinetics and receptor-ligand kinetics the binding potential is the ratio of the density of "available" neuroreceptors (B_{max}) to the affinity of the tracer for that target (K_D) under the conditions prevailing in the living organism.

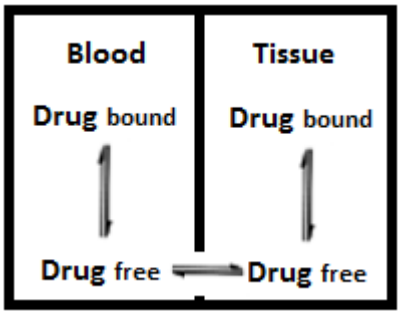

Figure 8: Free drug distribution at equilibrium [28]

The effects of plasma protein binding on drug or tracer availability can vary between species. Eldredge et.al. did a species comparison of plasma protein binding for a reversible binding compound; pig plasma proteins bound on average 8.6% less drug than did human plasma proteins. Samples of plasma from different human individuals showed binding for the same drug that differed by 13.1% [29]. While, mean human serum binding is higher than for pigs, this species difference may be overwhelmed or obscured by batch differences in human plasma samples. For example, the canonical range of human albumin concentration is 35-50 g/L, but lower values may occur, for example, in individuals with impaired liver function. Over, the binding capacity of human plasma resembles that of the pig more than a number of other common laboratory animals, i.e., dog, rabbit, rat and mouse [29]. Using porcine plasma, a method was developed for fast screening of protein binding ranking within a group

of compounds. After incubation in plasma, the samples were centrifuged through filter membranes, and the free fraction of the test compounds measured with HPLC with UV detection. The objective was to develop a high throughput and cost-effective assay of plasma protein binding suited for the existing laboratory environment and instrumentation.

3.5. Correlation between lipophilicity, protein binding and tissue distribution

Screening of new PET tracers would be facilitated if physicochemical properties could be shown to correlate with plasma protein binding and/or lipophilicity results. Relevant physicochemical properties would include polar surface area, molecular weight and molecular volume.

3.6. Statistics

Statistics is the science of collecting, analyzing and making inferences from data. Statistics is a particularly useful branch of mathematics that is not only a topic for advanced research, but is used in routine manner by researchers in many fields to organize, analyze, and summarize data. In statistics, standard deviation (SD) is a quantity expressing by how much the members of a group differ from the mean value for the group. For the slope and the intercept in a curve, the standard deviation can show the uncertainty of the numbers. The term F refers to the Fisher F- statistics, which is the ratio of the variance in the data explained by the linear model divided by the variance unexplained by the model. The F-statistic is calculated from the regression sum of squares and the residual sum of squares. The residual sum of squares is the sum of the squared residuals, or squared deviations from the line. The regression number R^2 is a statistical measure of how close the data points are to the fitted regression line. It is also known as the coefficient of determination, or the coefficient of multiple determinations for multiple regressions. The R^2 value is used for evaluating the models, but it is only a rough indicator of the goodness of fit. It is calculated from the total sum of squares, which is the sum of the squared deviations of the original data from the mean.

In the present context, the OECD repeatability recommendations is that the value of log D derived from repeated measurements made under identical conditions and using the same set of reference substances should fall within a range of ± 0.1 log units. The reproducibility should be ± 0.5 log units: If the measurements are repeated with a different set of reference compounds, results may differ. Typically, R^2 for the relationship between log k and log D for a set of test substances is around 0.9, corresponding to an octanol/water partition coefficient of log Pow ± 0.5 log units. Per OECD standards, inter-laboratory comparison tests have shown that log D values obtained with the HPLC method should agree to within ± 0.5 units of the shake-flask values. [30]

4. Experimental

For all measurements performed on the HPLC, blanks were measured between each sample. If there were any UV readings of the blanks (mobile phase, PBS, DMSO or pig plasma), this would be subtracted from the sample readings in each case. All samples were measured with wave length range of 190 to 300 nm, but 254 nm was used as a general parameter.

4.1. Lipophilicity

Procedures for making buffers

1 liter 50 mM 3-morpholinopropane-1-sulfonic acid (MOPS) buffer

50 ml stock solution of MOPS (1 M from Sigma Aldrich) was added to 950 ml ddH_2O and the solution was stirred for 3-5 minutes. The pH was adjusted to 7.4 by pipetting drops of 1 M NaOH and measuring with a pH-meter. The buffer was filtered through a 0.45 µm membrane filter using a filter unit and a vacuum pump before the ready-to-use buffer were stored in glass bottles at 4 °C.

1 liter 1 M phosphate buffer

- 106.47 g (1.33 mol) sodium phosphate dibasic was weighed up and dissolved in 745 ml ddH_2O.
- 29.99 g (4.00 mol) sodium phosphate monobasic was dissolved in 245 ml ddH_2O.
- These two salt solutions were mixed together in a measuring cylinder and the final volume was adjusted to 1 liter.
- Before use, the buffer was diluted to 50 mM by adding 50 ml 1 M stock solution to 950 ml ddH_2O, with stirring for 5 minutes.
- The pH was adjusted to 7.4 with phosphoric acid (85%) and measured with a pH-meter.
- The buffer was filtered through a 0.45 µm membrane filter using a filter unit attached to a vacuum pump before the ready-to-use buffer were stored in glass bottles at 4 °C for no longer than 2 weeks.

Equipment

Chromolith High Resolution RP-18 end capped 100-4.6 mm HPLC column
Shimadzu Prominence-i LC-2030C HPLC
VWR vacuum gas pump
Thermo Scientific Orion Star A211 pH-meter
Eppendorf Safe-Lock microtubes
Screw vial for chromatography from Technolab as
Eppendorf Research Plus pipettes, 0-10 µl, 10-100 µl, 100-1000 µl and 0.5-5 ml
Origin 2015 graphing and Analysis Program

Chemicals

Acetaminophen from Sigma Aldrich, ≥ 99.0%
Acetophenone from Fluka, ≥ 99.0%
AH-7921 from Acorn Pharma, 99%
Anisaldehyde from Fluka, ≥ 98%
Astemizole from Sigma Aldrich, ≥ 98%
Benzaldehyde from Sigma Aldrich, ≥ 99%
Benzene from Prolabo, ≥ 99.8%
Benzophenone from Sigma Aldrich, 99%
Bifonazole from Sigma, ≥ 98.0%
Br-benzene from Fluka, ≥ 99.5%
2-butanone from Fluka, ≥ 99%
4-chlorobenzaldehyde from Sigma Aldrich, 97%
Chlorthalidone from Sigma Aldrich, ≥ 98%
Clonidine from Sigma Aldrich
Dexamethasone from Sigma Aldrich, ≥ 98%
DMSO from Sigma Aldrich, ≥ 99.5%
Estradiol from Sigma
4-ethyltoluene from Sigma Aldrich, 90%
Flumazenil from Biotech > 99%
Flutamide from Sigma Aldrich
4-fluorobenzaldehyde from Sigma Aldrich, 98%
2-hydroxybenzaldehyde phenylhydrazone from Sigma Aldrich, 97%
Iodobenzene from Fluka
2-I-ethylbenzene from Sigma Aldrich, 97%
Lansoprazole from Sigma Aldrich, ≥ 99.0%
Loperamide HCL from Sigma Aldrich, ≥ 98%
Loratadin from Fluka
Methanol HPLC grade (99.8%)
MOPS solution from Sigma Aldrich, 1M

Naphtalene from Fluka, ≥ 99%
Omeprazole from Fluka, analytical reference material
PBS pH 7.4 (10X) from Gibco
Phosphoric acid from Fluka, > 97.5%
Promethazine from Sigma Aldrich, European Pharmacopoeia reference standard
Protriptyline HCl from Sigma Aldrich, ≥ 99%
Sodium hydroxide from VWR chemicals, 99.3%
Sodium phosphate dibasic from Sigma Aldrich, ≥ 99.0%
Sodium phosphate monobasic from Sigma Aldrich, ≥ 99.0%
4-tert-butylbenzaldehyde from Sigma Aldrich, 97%
Testosterone from Sigma, ≥ 99.0%
Tolnaftate from Sigma
Tolnaftate from Sigma Aldrich, European Pharmacopoeia reference standard
Toluene from Sigma Aldrich, ≥ 99.7%
Trans-Cinnamaldehyde from Alfa Aesar, 98+%
Trazodone from Sigma Aldrich, ≥ 99%
Trichlormethiazide from Sigma Aldrich, ≥ 98%
Triflupromazine hydrochloride from Fluka, ≥ 99.9%
Trimipramine from Sigma Aldrich, ≥ 98%
Tryptophan from Sigma Aldrich, pharmaceutical secondary standard
Uracil from Sigma, ≥ 99.0%
Warfarin from Fluka, analytical standard

4.1.1. Methods

The calibration curves were made according to OECD guidelines 117 [30]. Reverse phase HPLC was performed on a high performance 100 x 4.6 mm Chromolith analytical column.

Sample preparations

Approximately 1 mg samples of each compound were weighed into an HPLC glass vial of 1.5 ml and PBS or DMSO was added in sufficient volume to make stock solutions of 1 mg/ml. All stock samples were prepared in glass vials and thoroughly mixed on a vortex mixer. The stock solutions were stored at -80 °C and allowed to defrost to room temperature before use.

To make 10 µg/ml test samples, 10 µl from the stock solutions was added to 990 µl solvent, preferably PBS for those compounds with sufficient aqueous solubility, or otherwise in DMSO. Test samples were prepared directly into HPLC vials, vortexed for about ten seconds and placed into HPLC injector trays for analysis.

Choice of method

The choice between two methods depended on the approximate lipophilicity of the analyte (estimation was done with ChemDraw 15.1). For compounds with Log D in the range 0.5 to 3.5 method A was used. For compounds with Log D in the range 2.5 to 4.8 method B was used. Table 1 shows the two methods for measuring different ranges of lipophilicity.

Table 1: Two methods for measuring different ranges of lipophilicity

***Method A**	
Methanol	50%
Phosphate buffer 50mM	50%
Flow	1 ml/min
Injection volume	10 µl
Sample preparation	PBS or DMSO
Sample concentration	10 µg/ml
Column	chromolith (100-4.6)

***Method B**	
Methanol	75%
MOPS buffer 50mM	25%
Flow	2 ml/min
Injection volume	10 µl
Sample preparation	PBS or DMSO
Sample concentration	10 µg/ml
Column	chromolith (100-4.6)

HPLC Preparation and Measurements

HPLC-grade methanol and buffer formulated in ddH_2O was used to prepare the eluting solvent, which was degassed immediately prior to the run in the automatic HPLC system, and delivered isocratically to the analytical column. All HPLC lines were purged for 10 minutes with mobile phases, and the injector was rinsed for 1 minute with ddH_2O. The method of choice entailed calibration for 10 minutes (in case of unstable UV baseline, the time of calibration increased) before start of measurements. 10 µl portions of the final dilution for all samples were injected into the HPLC system. To increase the confidence in the measurement, the retention times were determined in triplicate.

Evaluation of data

Calibration curve of standards

The retention time of an analyte to HPLC is described by the capacity factor k, as given by the expression in Eq. 1, where T_R is the retention time of the test substance, and t_0 is the dead-time, i.e. the average time a solvent molecule needs to pass the column. Uracil (standard 1) is an unretained organic substance that was used to measure the dead time in the system, from which the capacity factor of compounds was calculated (Eq. 1). The calibration curves were made by plotting Log k as a function of Log D for the reference substances (see Figure 9). The plot was made in Excel and Origin, using values of log k without altering or truncating the calculated number of decimals.

Test compounds

The mean capacity factor was calculated from the retention time for each sample, and the Log D determined by interpolation of associated calibration curve equation. An example of the calculations for three compounds measured with method A is shown in Table 2. Further data is found in “Appendix A: calibration curve data”.

Table 2: Examples of calculations from peak measurements to log k values

Compound	Avg T_R (min)	capacity factor*, k	Log k
Uracil (dead time)	1.639		
J1	3.591	1.19	0.1
J7	14.869	8.07	0.9
J9	9.148	4.58	0.7

Calculated from equation 1

Entering log k for J1 into method A regression equation would give a log D = 1.8. (See Table 11 for all test compound results).

4.2. Protein Binding

Procedures for making buffers

As described in “Procedures for making buffers” in chapter 4.1. “Lipophilicity”.

Equipment

Microcon protein centrifugal filters, 10 kDa
Shiseido CAPCELL PAK C18 MG 100 Å 5 µm, 250 x 4.6mm HPLC column
Binder heat cabinet
Bandelin Sonorex RK 102 H ultrasound bath
Heraeus Sepatech Biofuge 17RS centrifuge
Shimadzu Prominence-i LC-2030C HPLC
VWR vacuum gas pump
Thermo Scientific Orion Star A211 pH-meter
Eppendorf Safe-Lock microtubes
Screw vial for chromatography from Technolab as
Eppendorf Research Plus pipettes, 0-10 µl, 10-100 µl, 100-1000 µl and 0.5-5 ml

Chemicals

EDTA from Sigma Aldrich, ≥ 98.5%
Heparin from Sigma Aldrich, European Pharmacopoeia reference standard
Lansoprazole from Sigma Aldrich, ≥ 99.0%
PBS pH 7.4 (10X) from Gibco
Testosterone from Sigma, ≥ 99.0%
Warfarin from Fluka, analytical standard

4.2.1. Method

Calibration curve preparation

Prior to measuring protein binding, a calibration curve for each test compound had to be made. From the stock solution made for the lipophilicity studies (chapter 4.1.1.) a dilution series was made with PBS (Table 3).

Table 3: Dilution series for protein binding calibration curves

µg/ml		µl PBS
20	20 µl of stock (1 mg/ml)	980
10	500 µl of 20 µg/ml	500
5	500 µl of 10 µg/ml	500
1	200 µl of 5 µg/ml	800
0.1	100 µl of 1 µg/ml	900

All samples were diluted directly into HPLC vials and measured with method C described in Table 4. HPLC preparations and measurements were done in the same matter as described for lipophilicity studies in chapter 4.1.1. HPLC Preparation and Measurements.

Protein Binding Assay

To measure the protein binding of a compound, a known concentration was added to porcine plasma, which was then incubated, ultrafiltrated and measured with the HPLC system. The same stock solution as made for the lipophilicity studies were also used for protein binding (See chapter 4.1.1. sample preparations).

- For each compound three Eppendorf tubes were prepared with 1 ml porcine plasma and for each run one Eppendorf tube was prepared for standard 30 as an internal standard for the assay.
- 10 µl of a premade 1 mg/ml stock solution of each compound was added to the plasma. This gave a concentration of 10 µg compound per ml of plasma.
- All tubes were vortexed for 10 seconds.
- All tubes were incubated in 37 °C for 10 minutes.
- All tubes were flipped upside down 5 times.
- Microcon tubes were weighed for later reference.
- 150 µl aliquots of fluid was added to Microcon centrifuge filters and centrifuged at 13000 rpm for 20 minutes.
- Microcon tubes with the supernatant were weighed for later reference.
- Supernatant were thoroughly mixed by pipetting.
- 70 µl supernatant were mixed with 330 µl PBS, vortexed and measured by an HPLC method described below.

An HPLC method for protein binding was developed from lipophilicity method B, using the same criteria but with a different column and also a different flow rate. See Table 4 for method C parameters.

Table 4: Parameters of HPLC method C

*Method C	
Methanol	75%
MOPS buffer 50mM	25%
Flow	1 ml/min
Injection volume	10 µl
Sample preparation	PBS or DMSO
Column	Capcell pac (250-4.6)

HPLC preparations and measurements were done in the same matter as described for lipophilicity studies in chapter 4.1.1. HPLC Preparation and Measurements.

Evaluation of data

Calibration curve

The area under the curve (AUC) of the UV absorbance peak measured for each concentration of a compound was obtained by automatic or manual integration of the chromatogram; AUC correlates to the amount of compound, corrected for background absorbance. The calibration curves were made by plotting AUC as a function of concentration, and the plots were made in Excel and Origin, using values of concentration in µg/ml. (See Figure 11 as an example).

Test compounds

The concentration left in the supernatant after protein binding, was determined by AUC interpolation of associated calibration curve equation. An example is shown in Table 5.

Table 5: Example on test compound measurement after protein binding

	Average peak area	Calc conc from calibration curve (µg/ml)	Bound compound (%)	Std.dev (%)
Lansoprazole 10 µg/ml (27.07 µM)	1651	0.297 (0.80 µM)	97	0.62

Recovery of proteins

After centrifugation during the plasma protein binding assay, the filters were turned upside down, inserted to a new eppendorf tube and centrifuged for 3 minutes at 3861 rpm (per Microcon recommendation [31]). The fluid and proteins recovered was incubated in 150 µl of PBS, centrifuged over a new Microcon filter and free fraction from the second supernatant was measured by HPLC with the same method as earlier described.

5. Results and Discussion

Three screening methods were developed throughout this project, of which two were for lipophilicity within different ranges and one was for plasma protein binding. Some obstacles were encountered in the development phase, including equipment failure, and poor solubility of test compounds. There arose the consideration that efforts to develop a method general applicable for all test compounds was overly ambitious. Although not all functional groups are compatible with the present calibration curves, at least the present methods cover a broad range of compounds.

IUPAC names for all compounds are to be found in Appendix C: “General data concerning both lipophilicity and protein binding (Table 81).

5.1. Lipophilicity Results

Initial attempts were directed to creating a single generic method to accommodate all test compounds within the lipophilicity range from 0.5 to 5.4. The first aim was to obtain a stable calibration curve with simple aromatic test compounds bearing a range of functional groups typically present in drug molecules. At this point, the general utility of the calibration curve was challenged by increasingly complex, functionally diverse test compounds before testing the validity of the calibration with new drug molecules. However, this endeavour was hampered by increasingly impractical retention times for compounds with lipophilicity values 4 or higher. When residency times on the analytical column exceeded 30 min, axial diffusion of analyte lead to excessive peak broadening, which made difficult the detection and quantification of the UV absorption signal. Consequently, two types of analytical conditions were used, according to the lipophilicity of the test compound. Also, several compounds with log D lower than 0.5 eluted close to the dead volume measured with standard 1, such that it was not possible to obtain a reliable estimate of log k. One of the methods was optimized for Log D values in the range 0.5 to 3.5, and the other method was developed for compounds of Log D in the range 2.5 to 4.8. The details of the two methods are shown in Figure 9. Standard deviations of the log k values are shown with red error bars. See raw data in “Appendix A: Calibration Curve data”.

Method A

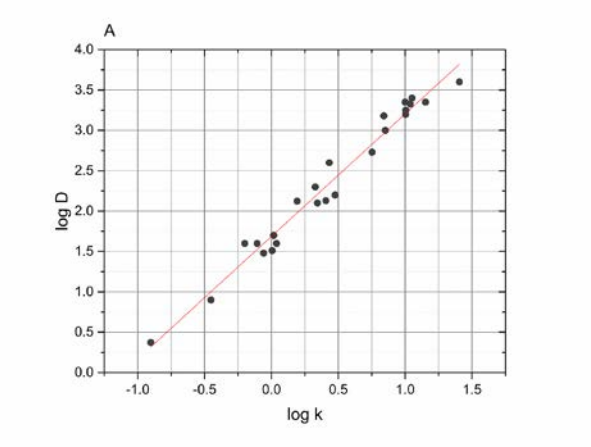

	Value	Standard Error
R-square	0.9727	
Intercept	1.6872	0.0381
Slope	1.5174	0.0530

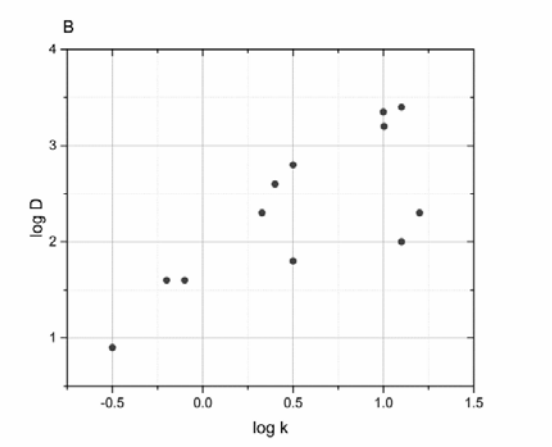

Method B

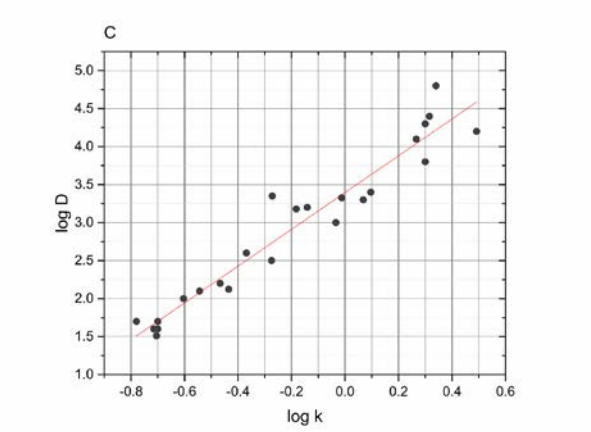

	Value	Standard Error
R-square	0.9483	
Intercept	3.3688	0.0525
Slope	2.4343	0.1181

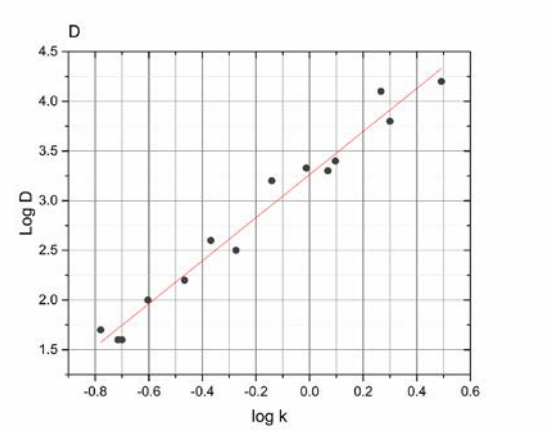

	Value	Standard Error
R-square	0.9719	
Intercept	3.2626	0.0460
Slope	2.1669	0.1020

Figure 9: Curve A: method A calibration curve with corresponding data. Curve B: An overview of spreading of commercial pharmaceuticals measured with method A. Curve C: Method B calibration curve with corresponding data. Curve D: A selection of commercial pharmaceuticals measured with method B.

Curve A in Figure 9 shows the calibration curve of Method A where all compounds fell within 0.2 log D values from literature which is a good accuracy for screening purposes and compared to literature variations and methods, it seems to be a quite accurate result in

general. Though method A did not show an as broad application as method B, since several commercial pharmaceuticals within the range of method A, still didn't elute or gave inconclusive data. Data can be found in Appendix A: "Calibration curve data". The calibration curve shows a good linearity, as the R^2 value is above 0.97. The intercept and slope standard errors are small (0.04 and 0.05 respectively. These deviations only change the second decimal number). (Method A regression equation can be seen in Eq. 2 below). And the reproducibility of the method from a day-to-day measurement of standard 1, showed a 0.1% standard deviation (Table 6).

Equation 2

$$y = 1.5174 * x + 1.6872$$

Table 6: Standard deviation of method A reproducibility measured with standard 1 and standard 16

	Average T_R (min)	Std.dev	Std.dev %
Standard 1	1.535	0.002	0.1
Standard 16	19.462	0.991	0.1

Curve B in Figure 9 shows two deviating branches when plotting method A measured commercial pharmaceuticals only. The three compounds forming the lower branch are standard 31, standard 33 and standard 38. These were discharged from the calibration curve and investigated as outliers (see "Aim for finding trends between lipophilicity and other chemical properties". Data can be found in Appendix A: "Calibration curve data"). The calibration curve for method B shows good linearity with an R^2 of almost 0.95 (curve C in Figure 9) albeit not as good as method A, which had $R^2 > 0.97$. (Data can be found in Appendix A: "Calibration Curve data".) The standards below method B cut-off area have been kept as this improved linearity to the curve. The intercept and slope standard errors (0.05 and 0.12 respectively) are somewhat high, especially the slope deviation, but they still not change Log D results by more than 0.1 Log D value at the most in either direction. (Method B regression equation can be seen in Eq. 3 below) A day-to-day comparison of the retention times with method B was done for standard 1 and standard 30 and they showed good reproducibility (Table 7).

Equation 3

$$y = 2.4343 * x + 3.3688$$

Table 7: Standard deviation of method B reproducibility measured with standard 1 and standard 30

	Average T_R (min)	Std.dev	Std.dev %
Standard 1	0.771	0.013	1.7
Standard 30	0.925	0.010	1.1

The method B calibration curve deviates more from literature than method A (standard 24 as high as 0.6), this could be due to complexity in the structure, molecular size, polar surface area (PSA) or other chemical properties that will be examined further. Deviations could also be from literature values deviating due to measurement or calculation methods. Literature values for certain compounds varied up to 0.6 log D values as well. Except for four other standards (whereas two were pharmaceuticals standard 25 and 29 which are quite similar compounds) with deviations of 0.3-0.4 all other standards had deviations below 0.2 log D values, amongst them standard 17, 19, 27, 28, 30, 31, 33, 37, 38 and 43 which are all established commercial pharmaceuticals. A TLC measurement was done with four compounds giving issues when measured with the HPLC, standard 37 and 43 as well as C4 and C5. Mobile phase from method B was used and standard 1 and 33 were used as comparison. For standard 37 and 43 as well as compound C4 the TLC results showed that they would be expected to elute quite late and also the peak would be waving out compared to fast eluting compounds. C5 did not drift through the chromatography paper, indicating that the compound could be stuck on the column.

Measuring standard 26 (log D 5.4) with method B gave more than 1 log D value deviation and standard 32 with log D of 5.8 did not show any results, so for log D above 4.8, this method does not fit. All compounds and their deviations can be seen in Table 39.

While a better R^2 value might have been achieved for the methods, the present aim was to obtain deviations as low as possible from literature lipophilicity values, for as many different compounds as possible. Therefore, it was necessary to include results for some standards that were not perfectly co-linear with the calibration curves, as could arise for a variety of reasons.

Although adding even more compounds to the general methods could have given a better regression coefficient for the curves, there was a mean standard deviation of only 0.1 for method A and 0.2 for method B (calculated from Table 38 and Table 40 in “Appendix A: Calibration curve data”). All standards except standard 24 met OECD`s recommendations explained in 3.6. “Statistics”. For better accuracy, it is necessary to narrow down the curve to compounds with the same functional group and size.

Curve D is a trimming of method B where an $R^2 > 0.97$ was achieved. This curve was from 14 of method B`s standards, whereas 9 of them were commercial pharmaceuticals. (Data can be found in Appendix A: “Calibration curve data”.) Amongst them were standard 25 and 29 who are highly similar to standard 28, still standard 28 had a 0.3 log D value different from

literature when using this curve. This cannot be explained by any chemical properties and checking up on literature, even though Gulyaeva measured this compound to be 4.3, Avdeef reports a log D value of 3.5. Hence, the measured result by this method of Log D 3.9 might just be correct. At least it was not possible to find a certain trend to the compounds that did get deviations of more than 0.2 Log D values with this curve (standard 24, 26, 27 and 28).

Log D values from literature for all standards are shown in Table 8, and the variance between some sources are further discussed below.

Table 8: Log D from literature, for 41 compounds (compound 21 was removed as no satisfying source of log D was found)

Compound	Log D	Ref
1	-1.1	[23]
2	0.9/0.5	[32-34]
3	0.4	[23, 33, 35]
4	1.5	[33, 36]
5	1.5	[37]
6	1.6	[32, 38]
7	1.7	[37]
8	2.1	[23]
9	2.1	[23]
10	2.3/2.5	[32, 33, 35, 39]
11	2.1	[37]
12	2.7	[33]
13	3.0	[30]
14	3.2	[30]
15	3.3	[23, 35]
16	3.3	[23, 35]
17	3.2/3.3	[32, 40]
18	3.4/ 3.3/3.2	[30, 32, 33, 38]
19	2.6	[41]
20	3.6	[42]
22	4.0	[32]
23	4.2	[23, 35]
24	4.8	[23, 32, 35]
25	3.8	[23, 34, 35]
26	5.4	[23, 32, 35]
27	4.4	[32, 35]
28	4.3	[32, 34]
29	3.6/4.2	[32, 34]
30	2.8/1.9/2.2	[35, 43]
31	2.5	[44]
32	5.8/4.2	[13, 34, 45]
33	2.0	[46]
34	0.8	[38]
35	2.6	[34]
36	0.4	[34]
37	4.1	[34]
38	1.7	[40]
39	0.8	[40]
40	1.6	[34]
41	3.4	[34]
42	1.6	[40]

All standards are described with product name and “International Union of Pure and Applied Chemistry” (IUPAC) name in “Appendix A: Lipophilicity”.

Literature values for several model compounds sometimes varied between different sources (Table 8). This could be due to different analytical methods and parameters; in the cases with discrepancy, the chosen values were from the references that reported on large libraries of compounds, and had used similar analysis parameters as the methods described here. Not all compounds that we wanted to use in the reference curve had literature reports citing their experimental Log D values. Below is a table showing the deviation from different sources for some of the compounds (Table 9).

Table 9: Deviations between different sources reporting log D values

Standard	Log D source 1	Log D source 2	Log D source 3	Log D average	Std.dev
2	0.9	0.5		0.7	0.2
10	2.3		2.5[1]	2.4	0.1
17	3.2		3.3[2]	3.3	0.0
18	3.3	3.4	3.2[1]	3.3	0.1
29	3.6	4.2		3.9	0.3
method	RP-HPLC	RP-HPLC	Other		

[1]shake-flask
[2] potentiometric titration

When measuring log D with for instance shake-flask method, it is difficult to withhold the same parameters for all samples, hence the method is not as suitable for screening purposes as an HPLC method. When inserting a group of samples in the automatic HPLC, all samples are treated the same regarding temperature, volumes, speed of injection and more.

Choice of method

To select between the two methods when preparing test compound, lipophilicity was predicted with the chemistry drawing software ChemDraw (www.camridgesoft.com). Method A was used for compounds with predicted log D ≤ 3.5, and method B was used for compounds with estimated Log D ≥ 2.5. When working with compounds of Log D falling in the overlap of these two ranges, an educated guess served to guide the decision. In case of poor water solubility, method B could be preferred due to the higher organic solvent composition of the mobile phase. Method B is quicker, but if method A is to be used for other compounds in the same group, decisions could be made according to practical considerations, i.e. in relation to the workflow.

If one specific library of tracers is to be analyzed, the prototype compound of the group should be tested with these methods to verify specificity. More compounds with functional groups resembling those of the library may need to be added, and trimming of the outliers in the calibration curve could give more specific results. Adding the internal standard of choice as a single point, the rest of the calibration curve is then adjusted according to the standard, to give the best possible measurement, slope and intercept for this specific compound. This entails keeping the standards with the most similar retention mechanisms to the standard, and omitting those causing deviations of the curve further away from the standard.

14 standards were measured with both methods (as well as with the trimmed version of method B) to compare their accuracy (Table 10). For all compounds with Log D less than 2.5, the percentage deviation between the methods were less than 5%, except for standard 30, which had a 7.4% deviation between method A and method B, whereas method A had the higher deviation compared to literature. For the compounds of log D in the overlap region of the methods, all deviations were below 10%, except for standard 19, which had a 17% deviation between the methods. In that case, method B underestimated the measurement relative to the literature value.

Table 10: Comparison of method A, method B and B trimmed method measuring 14 standards in the Log D range of 1.5 to 3.4

Standard	Log D	Method A Log D	Method B Log D	Method B trimmed Log D	% deviation between method A and method B	% deviation between method B and B trimmed
4	1.6	1.6	1.7	1.7	2.1	2.1
5	1.5	1.7	1.7		2.2	
6	1.6	1.8	1.7	1.7	4.3	0.1
7	1.7	1.7	1.7		2.4	
8	2.1	2.0	2.1		3.6	
11	2.1	2.2	2.3		4.6	
13	3.0	3.0	3.3		9.5	
14	3.2	3.0	3.0		1.0	
15	3.3	3.2	3.6	3.4	9.3	4.5
16	3.3	3.3	3.4	3.2	2.5	5.0
17	3.2	3.2	3.1	3.0	5.7	1.8
18	3.4	3.5	3.6	3.5	4.9	3.6
19	3.4	3.2	2.7		17.7	
30	2.2	2.4	2.3	2.3	7.4	1.5

Three groups of test compounds were run with the methods described. J4-J19 (See Table 81 in Appendix C) are structurally similar compounds with a calculated theoretical lipophilicity range of Log D = 3.3-5.0. The measured results ranged between Log D = 2.7-4.5, and both methods were used, as they fell in the overlap between methods.

L1-L19 is a group of highly similar compounds and they were synthesized during the course of this project. Results for the products tested for lipophilicity can be seen in Table 11 below, below, with specification of the particular method. Furthermore, seven commercial pharmaceuticals that are not part of the calibration curve, was measured (Table 12). Commercial names can be found in Appendix C and raw data can be found in Table 41.

Table 11: Results for test compounds analyzed with the two methods described above

Log D list Products synthesized by PET group	Method A	Method B
L2	3.1	
L3	2.7	
L4	3.8	
L5	3.4	
L6		1.7
L7	3.2	
L8	2.5	
L9	3.1	
L10	3.2	
L11		2.4
L12		2.4
L13		2.3
L14		2.3
L15		2.3
L16		2.3
L17		2.8
L18		1.7
L19		1.7
W1	3.7	
W3	2.7	
W4	3.8	
W5	3.8	
W6	2.8	
W7	4.0	
W8		3.1
W10		2.5
W11		3.2
W12		3.0
W13		2.7
W14	2.9	
W15		2.4
W16	3.0	
W17	3.5	
W18		2.4

J1	1.8	
J3		4.1
J4	3.3	
J5		3.0
J6		2.5
J7	3.1	
J8		2.9
J9	2.7	
J10	2.7	
J11		3.7
J12		3.7
J13		2.0
J14		4.0
J15		3.0
J16		4.0
J17		2.6
J18		3.7
J19		3.6

Table 12: Results for commercial pharmaceuticals analyzed with the two methods described above

Commercial pharmaceuticals	Method A	Method B
C1		2.9
C2	2.5[1]	
C3		2.7
C4	No eluting compound	2.9[2]
C5	No eluting compound	3.4[3]
C6	Not reproducible	4.2[4]
C7	Inconclusive	5.1[5]
C8	Not reproducible	4.4[6]

[1] Literature Log D value of 2.2 [43] [2]2.8 with trimmed version and literature value of 2.8 [34] [3] 3.2 with trimmed version [4]4.0 with trimmed version [5]4.8 with trimmed version [6]4.1 with trimmed version

Two of the commercial compounds had literature measured values for comparison with present methods; C2 measured with method A deviated by 0.3 log D units from the literature value, and C4 measured with method B deviated by 0.1 log D units from literature value, although the trimmed version of method B gave exactly the literature value. This shows the importance of choosing the right method for the compound to be tested.

For molecules acting on the CNS via passive diffusion through the BBB, a moderate lipophilicity within the range of Log P /Log D = 2-5 is considered on theoretical grounds to be optimal [12, 18, 25]. Some studies show even more stringent results, indicating poor brain penetration for compounds with lipophilicity exceeding Log D = 4.0 [47, 48], although this claim is on contrast with many successful brain radiotracers, N-butan-2-yl-1-(2-

chlorophenyl)-N-methylisoquinoline-3-carboxamide (Log D = 4.58), (5S)-5-(1-benzofuran-7-yl)-8-chloro-3-methyl-2,3,4,5-tetrahydro-1H-3-benzazepin-7-ol (Log D = 4.90) and 3R,5R)-5-(3-methoxy-phenyl)-3-((R)-1-phenyl-ethylamino)-1-(4-trifluoromethyl-phenyl)-pyrrolidin-2-one (Log D = 5.42) as examples [1]. The novel PET tracers measured during this project fell within a range of Log D = 1.7-4.1.

Aim for finding trends between lipophilicity and other chemical properties

Elution times of some compounds were troublesome to measure by HPLC, due either to absence of UV peaks, or extreme peak spreading, as can occur when there is persistent retention on the column, with as low elution. Of the simple aromatic model compounds in this series, alcohols in particular proved difficult to analyze. Phenol, estradiol and tiophenol were left out of the calibration curves as they failed to match the linear relationship between k and Log D. Phenol and tiophenol were excluded early in the process, while estradiol was tested several times when all compounds were measured together in one general calibration curve. Consequently, we retained estradiol in the standard group (standard 22). But when separating the two HPLC methods and aiming for the highest R^2 value for the regression line of the calibration curve, estradiol was removed from both method A and B due to its deviation from the regression line. Cl-benzene and aniline were likewise excluded from the calibration plots because of deviation from the regression lines (data not shown). Standard 37 (Trimipramine) was one of the troublesome pharmaceuticals that were retained on the list, despite failure to elute within 60 minutes.

Using all available standards and newly synthesized tracers, a library of 89 compounds were compiled with respect to their lipophilicity, molecular weight, molecular volume, polar surface area and molar refractivity, aiming to find a trend or an empirical mathematical function that could bring additional simplification for screening of tracers. Also, a comparison of compounds regarding their fraction of aliphatic versus aromatic carbons were investigated, as both PSA and MW change drastically as a function of the relative number of aliphatic and aromatic carbons in a molecular structure.

There were no trends to be found for the problematic compounds with respect to their type of carbon, except all were in the upper half of the aliphatic-to-aromatic range. However, the most aliphatic of all, testosterone, presented no problems for HPLC measurement. Thus, the aliphatic vs aromatic carbon ratio does not in itself fully explain why some compounds were harder to measure than others. In general, the test compounds measured are structurally complex, with many different functional groups, and so it is unlikely that any single parameter determines retention to RP-HPLC.

Although the linearity was somewhat scattered, there could be seen quite clear trends associating higher lipophilicity with higher molecular weight, molar refractivity and molecular volume. A slight trend of increasing lipophilicity with lower PSA could also be seen, but there was no evident association between molecular volume versus log D / PSA.

Commercial pharmaceuticals that fell out of linearity in method A, such as standard 31, 33 and 38, all have molar refractivity (M ref) above 10 m^3/mol. Some of the problematic pharmaceuticals in method B also showed high M ref, although also compounds with lower M ref also presented difficulties under measurement. There is some clustering of the outliers having high PSA values, but there are also outliers with low PSA, and other compounds with high PSA that fit well with the standard curve, so no simple relationship is evident. (Data used to make curves in Figure 10 can be found in Appendix A: «Data for comparison graphs in Figure 10»).

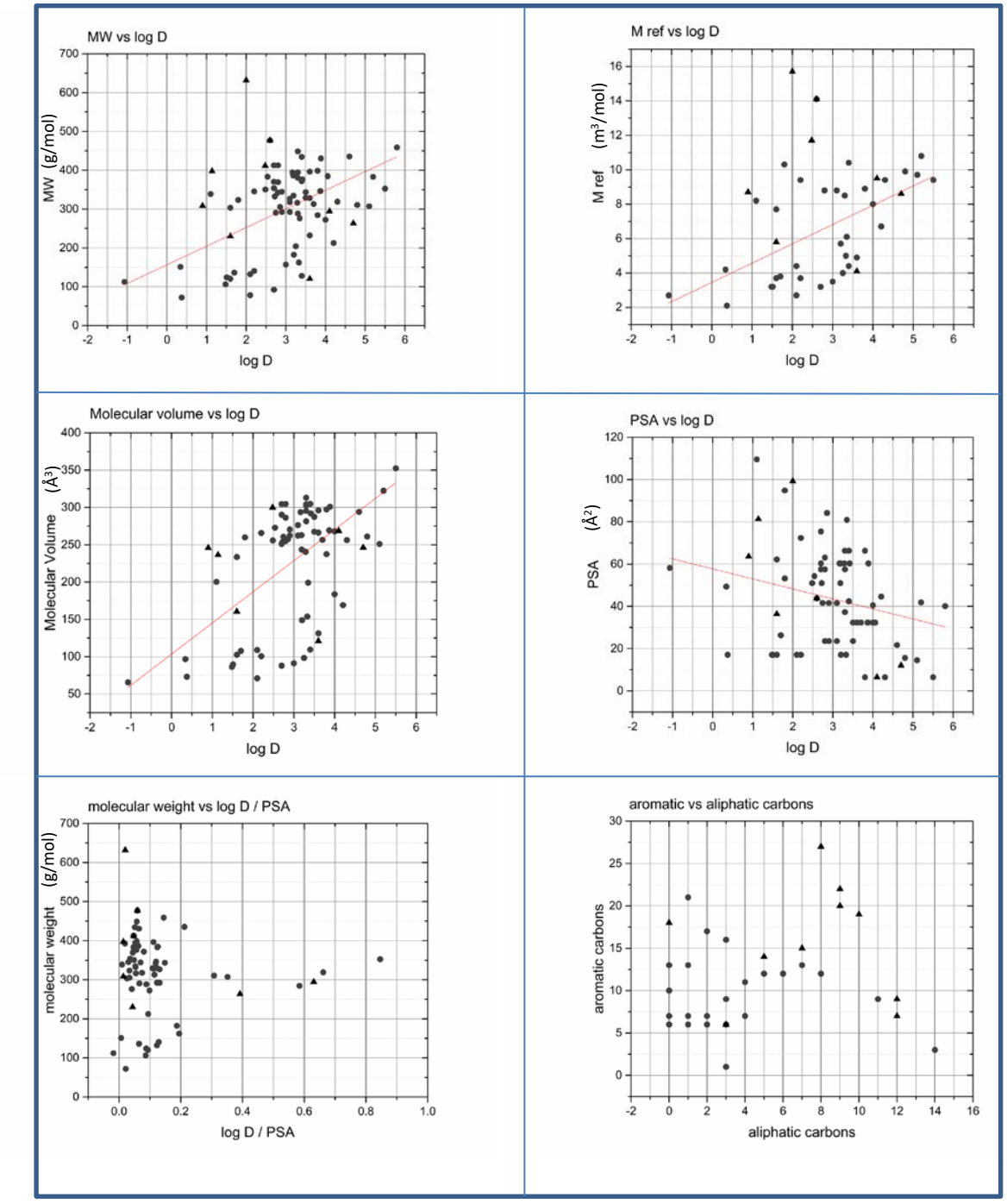

Figure 10: Aim for finding trends between lipophilicity and chemical properties like MW, molecular volume, M ref and PSA. Circles are standards measured with no problems occurring and triangles are compounds not part of the calibration curves due to problems during measurements.

To take the investigation one step further, an attempt was made to develop empirical mathematical functions for elucidating some factor that could adjust the results per chemical properties. An example of such a function could be;

Equation 4

$$\frac{PSA_{uracil}}{MW_{uracil}} = factor \times \frac{PSA_{compound}}{MW_{compound}} \times \log D$$

No such factor was identified, even though multiple regression analysis was done with linest function in excel as well. This approach was not exhaustively pursued as mathematical models do exist in literature.

Comparison of different computer programs

During the project, it became clear that some deviations were due to the mathematical programs and the number of decimal places used. For example, when inserting the same values from measurements, the logarithms in Excel and Origin gave slightly different intercept and slopes (see third row in first and second column as an example, Table 13) in the calibration curves. Obviously, this would also give rise to slight deviations in the results. A comparison was made between Excel and Origin spreadsheets, as these mathematical programs use different numbers of decimal places by default.

Both programs were adjusted to use ten decimal numbers when calculating, but still R_2 showed 0.5% decrease when inserting the same date from Excel to Origin. This meant having an R_2 value of 0.897 in Origin and 0.901 in Excel. Both rounds up or down to 0.90 and it does not give huge changes in the results, but it is obvious that the logarithms or the intra calculations are different in the two programs.

In addition, a comparison between four and ten decimal places was made for Excel to investigate what the difference in numbers would mean to the results. When working with only one decimal place in the results, it could appear that these deviations were as high as 0.1 Log D value, even though the highest real deviation of Log D using two decimal numbers was in the order of 0.03.

Table 13: Comparison between Excel and Origin with different amount of decimal numbers

Calibration curve made with 4 decimals (default) **Log D from calibration curve**	Origin comparison with 5 decimals (default) **Log D from calibration curve**	Excel comparison with 10 decimals **Log D from calibration curve**	**Compound**
2.8014x + 3.6443	2.73821x + 3.5857	y = 2.7616291818x + 3.6201399336	
2.0	2.0	2.0	**J13**
2.6	2.6	2.6	**W18**
3.3	3.2	3.3	**J5**

3.3	3.2	3.2	**W12**
3.1	3.0	3.1	**J8**
2.6	2.6	2.6	**W10**
2.7	2.6	2.7	**J6**
4.4	4.3	4.4	**J16**
3.3	3.2	3.3	**J14**
3.2	3.2	3.2	**J15**
3.4	3.4	3.4	**W11**
4.0	3.9	4.0	**J11**
2.7	2.7	2.7	**J17**
4.0	3.9	3.9	**J12**
4.1	4.0	4.0	**J18**
3.9	3.9	3.9	**J19**
4.4	4.4	4.4	**J3**
3.4	3.3	3.3	**W8**
2.9	2.9	2.9	**W13**
2.5	2.5	2.5	**W15**
2.8	2.8	2.8	**J2**
5.1	5.0	5.1	**Standard 29**
4.7	4.6	4.7	**Standard 24**
3.6	3.6	3.6	**Standard 23**

Michael Zavrel et. al. did a comparison between the several available calculation programs, including Excel version 2003 and Origin version 7.5 [49]. Both Excel and Origin uses algebraic parameter estimation, and provided very similar results, although there were up to 1% deviations from preset values between the two spreadsheets and the accuracy is higher in other programs, i.e. ModelMaker. Use of Excel is not to be recommended due to its low accuracy and limited statistical analysis. Zavrel found significant differences in the estimated parameter values between some programs, so deviations between log D values reported in the literature could partly result from the use of different spreadsheet programs.

Microsoft Support reports that Microsoft Excel only works to limited accuracy because it normally uses only 8-byte precision to represent numbers [50]. Although Excel can display 30 decimal places if necessary, its precision for a specified number is limited to 15 significant figures, with round off, truncation and binary storage. These properties are not reported for Origin, but any arithmetic calculation can suffer from error in precision.

Optimization

During the optimization of the lipophilicity analysis methods, concentration of the samples, concentration of organic solvent in the mobile phase, composition of mobile phase, injection volume, flow rate and sample preparation procedure were all varied systematically to optimize the method for the range of products to be tested. The analytical columns, sample concentration, mobile phases and buffers are presented in their own chapters below. Optimizing a single method for compounds over a wide range of Log D values proved difficult. The aim was to keep the test compound concentrations low to be sparing of valuable material. In the early phase of method development, concentrations as high as 1 mg/ml were measured to ensure sure that the compounds were eluting from the HPLC column as expected. The novel tracer ligands would not usually be measured at such high concentrations, but rather at 10 µg/ml, which gave adequate chromatographic peaks while not consuming much of the synthesized products. 20 µl, 10 µl and 5 µl sample volumes were injected to compare HPLC sensitivity. For many of the compounds, 5 µl portions proved sufficient, but when peak height was inadequate, 10 µl portions were used to obtain a better signal to noise ratio. All compounds gave sufficient peak height for 10 µl of 10 µg/ml solutions. This concentration was chosen as it was the lowest concentration that gave reproducible results (data not shown). The flow rate was adjusted according to the choice of column, aiming for the fastest method possible, while retaining good temporal separation between elution times relative to the to void time.

Sample preparation was initially done using pure methanol as solvent, but was changed to a mixture of methanol and water to ensure that evaporation of methanol wouldn't change the concentration of the stock solution. Despite these efforts, reproducibility was still inadequate, so the less volatile DMSO was used for stock solutions, with dilutions in DMSO or PBS according to solubility. DMSO freezes at 18 °C and the stock solution could also be stored in -80 °C [51].

Two methods were finalized for the measurement of lipophilicity. Method A (Table 3) was optimized for Log D values up to about 4, using 50/50 methanol/phosphate buffer and 1 ml /min flow. Method B (Table 1) was optimized for Log D values between 2.5 and 5.8, using 75/25 methanol/MOPS buffer and 2 ml /min flow. 10 µl was injected to a 10 cm chromolith analytical C-18 column. The calibration curves for these two methods are shown in chapter 4.1.1. "Calibration Curve".

The methods used for measuring retention time by HPLC are shown in Table 1. For some chemical groups, one method worked for a broader lipophilicity range, and therefore gave better results than would be obtained by switching between methods. Therefore, the ranges are indicative only. The use of the methods for the test compounds of unknown lipophilicity can be viewed in Table 11 in chapter 5.1. “Lipophilicity Results”.

When using all standards for both methods, R^2 values were fairly low due to the presence of a few outliers from the regression line. Some standards deviated between 2.6 to 3.0 Log D units from literature values when using all standards for method B, and were therefore not linear with the rest of the group of compounds. But as that method was for the high lipophilicity range, less lipophilic compounds were omitted to improve the linearity of the regression line for the range of interest. When recalculating the lipophilicity of the high lipophilicity compounds after deleting standards 2, 9 and 20, the deviations from literature values decreased to 0.0-0.6 Log D units. Standard 24 deviated by 0.6 from other literature measurements, but the compound was retained in the calibration curve due to its high lipophilicity.

Uncertainties due to amount of decimal numbers in log k and log D can be high. It was difficult to decide in significant numbers when collecting values from literature and making calibration curve out of these. Log D values were entered with one decimal and all calculations were done with ten decimals. Changing from one to ten decimals can differ a compounds log D value by 0.1, even log D units of 0.4 for the high lipophilicities (around log D 4). As we calculate in logarithmic scale, small changes can make high differences.

Buffers

According to literature there are two main options for composition of an HPLC buffer at pH 7.4: phosphate buffer and MOPS. Phosphate buffer gives a better match to physiological conditions [52] in terms of ionic strength. The physiological ionic strength in plasma lies between 100-200 mM KCl and/or NaCl. The ionic strength is a function of the total molar concentration and charge in the solution. However, there are some solubility limitations for some compounds in phosphate buffer. The saturated concentration at 0 °C is 2.50 M, but the recommended final buffer concentration is 10-15 mM. Phosphate is not very soluble when organic solvents are present at high concentration, which will make the mobile phase turbid. When higher buffer concentrations are required, MOPS is shown to be a good alternative. MOPS exhibits a high buffering capacity coupled to poor ion pair formation ability due to its zwitterionic nature and, thus it does not interact strongly either with solutes or the stationary phase [53]. Precipitation is an infrequent occurrence with MOPS as it is an organic salt, with a saturation concentration at 0 °C of 3.00 M. In aqueous solution MOPS is soluble to at least 33% (w/w), giving a clear solution. Table 14 shows an overview of the two buffers used.

Table 14: An overview of phosphate buffer and MOPS parameters, concentration, pH range and solubility

Buffer	Concentration used in experiments	pH range	pH used in experiment	Solubility
Phosphate	50 mM	7.3-7.5	7.4	4.30 g in 250 mL water
MOPS	50 mM	6.5-7.9	7.4	25 g in 50 mL water

Mobile Phases

Determination of the retention times with mobile phase of pure water or pure phosphate buffer are difficult or impossible to achieve. Therefore, organic phases must be added to the mobile phase [18]. The most widely used organic phases have been methanol and acetonitrile [18, 54]. Methanol was chosen as the organic component of the mobile phase, as it is well validated in literature. It is also desirable to get good hydrogen bonding with residual silanols on the stationary phase, as is the case with methanol. Indeed, methanol is the most suitable organic modifier for RP-HPLC, since it does not disturb the hydrogen bonding network of water. During equilibration, methanol forms a monolayer with the stationary phase and provides a hydrogen bonding capability in better agreement with n-octanol [53]. Like water, phosphate buffer was useful when running the analysis with low amounts of methanol, and with manual mixing of the mobile phase before pumping into the HPLC system. However, when the organic phase increased from 50% to 60%, or when the HPLC pump system mixed the mobile phase, there arose major problems with salt precipitation. Table 15 below shows the different mobile phases that were tested.

Table 15: Mobile phases tested throughout this project

Buffer	Organic phase	Mobile phase (aq/org)	Comments
Water	Methanol	10/90	no linear curve of samples
Water	Methanol	20/80	no linear curve of samples
Water	Methanol	25/75	double peaks and irregular peaks
Water	Methanol	40/60	Various retention times
Water	Methanol	50/50	problems with retention times and linearity
Phosphate	÷	100	no linear curve of samples
Phosphate	Methanol	50/50	used for method A
Phosphate	Methanol	40/60	problems with precipitation
MOPS	Methanol	25/75	used for method B and protein binding

MOPS buffer is considered as the buffer of choice for lipophilicity assessment by HPLC [32, 53] and was used for those products that needed methanol concentrations in excess of 50%. All standards and products with Log D values up to 5.4 eluted quickly and with good reproducibility using this buffer.

For the mobile phases containing only water in the aqueous phase, linear calibration curves were sometimes difficult to obtain, as several test compounds gave double peaks or irregular/serrated peaks. For the mobile phases with little or no organic component (0%, 10% and 20% methanol), the retention time for the compounds tended to decrease. Sample preparation was optimized with consideration of the evaporation of methanol, but the retention times still didn't match perfectly the expectations based upon lipophilicity differences between the compounds. With 50% methanol, some standards still fell out of linearity, i.e. standard 14 (benzophenone), which was particularly apt to deviate from the calibration curve. Some test compounds failed to elute within two hours, i.e. RO-04-5595. The zwitterion property of this compound could account for its very prolonged retention. Over all, some compounds showed very small and irregular UV peaks. In these cases, the methanol concentration was increased to 75%, which made flow rates as high as 2 ml/min due to the lower viscosity. However, retention times were highly unstable under these conditions. Some peaks eluted quite early, and therefore 60% methanol was tested at the same flow rate, so as to ensure separation from the void volume. The retention times still varied, especially for standard 22 ((8R,9S,13S,14S,17S)-13-methyl-7,8,9,11,12,13,14,15,16,17-decahydro-6H-cyclopenta[a]phenanthrene-3,17-diol) and standard 24 (1-([1,1'-biphenyl]-4-yl(phenyl)methyl)-1H-imidazole). The general method proved too slow for these compounds. The aim was to find a set of conditions for mobile phase, flow rate and analytical column that would give comparable retention times within a reasonable elution time, so the method would serve for rapid and valid screening. Solubility difficulties resulting in "permanent" retention of products on the column, the requirement for degassing the manual HPLC, and results deviating from the linear fittings, lead to discarding from consideration mobile phases with water, as described above. Some measurements were done with 100% phosphate buffer at pH 7.4. To ensure that the compounds weren't protonated at this pH; five compounds were tested at four different days (Table for curve A in Figure 11).

A curve standard	average capacity factor	St.dev.
9	0.948	0.064
12	1.548	0.109
13	1.703	0.116
14	1.267	0.096
18	2.283	0.192

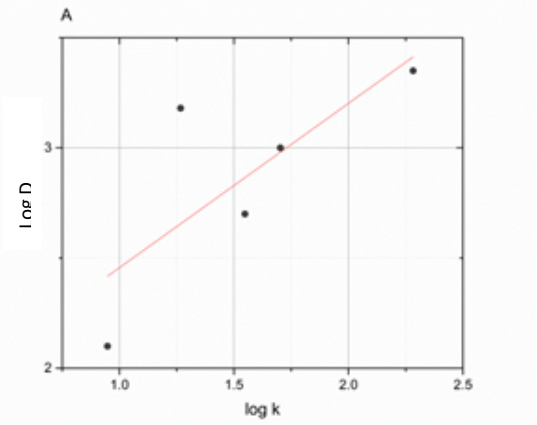

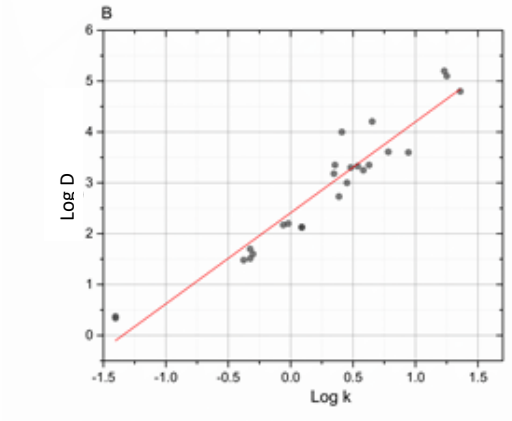

Curve B data

Equation	y = a + b*x		
Weight	No Weighting		
Residual Sum of Squares	3.46229		
Pearson's r	0.95667		
Adj. R-Square	0.91154		
		Value	Standard Error
Log D	Intercept	2.40996	0.0828
	Slope	1.79042	0.11362

Figure 11: Curve A showing results from using 100% phosphate buffer and standard deviation for day-to-day measurements. Curve B showing results from 60/40 methanol/phosphate buffer

The average retention times and standard deviations were good and the capacity factors were calculated, as shown in the table, but results deviated from the overall calibration curve (see curve A in Figure 11).

The relatively poor results with 100% phosphate buffer could be due to excessive retention on the column. As stated above it is difficult or impossible to elute certain compounds with water or buffer alone, so 60% methanol was added to the buffer to facilitate the elution. See curve B in Figure 11 showing the results for 60/40 methanol/ phosphate buffer.

The R^2 for the calibration curve B had a value above 0.9, which is sufficiently linear for the present purposes. Standard errors were 0.08 for the intercept and 0.11 for the slope. These values are admirably good, but it was important to see if equally good calibration curves could be obtained with lower retention times. When testing the 50/50 methanol/phosphate buffer mobile phase, the R^2 value increased to 0.97, and the standard errors decreased to 0.06 and 0.07 for the intercept and the slope respectively.

Columns

RP-HPLC is used to emulate the organic phase in octanol-water partitioning. From among a wide range of stationary phases available, C-18 silica gel columns are recommended for the estimation of drug lipophilicity at pH below 8 [18].

Several analytical columns were tested: µ-Bondapak C-18 300 x 4 mm, LiChrocart 250-4 HPLC-cartridge RP-18 (5 mm), and Chromolith Performance 100 x 4.6 mm. Among these the Chromolith column appeared to have superior properties for rapid analysis over a wide lipophilicity range. Using a chromolith column compared to other C-18 columns, made it possible to run higher flow rates with lower back pressures. Flow rates between 0.5-5 ml can be supported on the chromolith column as it contains a solid matric without particles, so it cannot be compressed. The appropriate pH range is 2-7.5.

HPLC setup and sample preparation

All test compounds have some solubility in water, and the choice between PBS and DMSO as solvent for sample preparation was made by trial and error. PBS was preferred as it is water-based and therefore more similar to conditions in vivo, and also because has less interference than DMSO in the UV-spectrum. DMSO was used if PBS failed to dissolve enough of a compound for valid measurement.

In the first instance, HPLC setup takes approximately 10 minutes, and in subsequent application, the parameters of flow rate and mobile phase composition can be copied. The same expedience applies when loading a batch of samples to be measured. There are no fixed rules for the time required to purge and rinse the system, but in general about 10 minutes` purge of each line is required when starting up the system or when changing mobile phases. Usually a 10 minutes' warmup phase is sufficient for obtaining a stable UV detector baseline and this can be done while the lines are being purged.

High throughput analyses are obtained using an automatic sample injector. This apparatus holds up to four trays of 54 wells each, giving the opportunity to run 216 samples in one session. The limiting factor is the time per analysis, which differs between samples and methods. Hence, the bottleneck of this automatic system is the amount of mobile phase required.

Another bottleneck in running many samples in one session is the need to manually inspect each chromatogram, to confirm the reliability of the automatic integration for the relevant UV peaks. This is especially true when the analyte concentration was fairly low or when there is any sample contamination. The retention time and area of each peak needs to be recorded, with segregation of the calibration data from test compound data. For quality control of a test compound, the workload can be smaller. However, quality control inspections are necessary, without placing undue reliance on the stability of the automatic system.

5.2. Protein Binding Results

A method for measuring plasma protein binding which is user friendly and requires few resources available was developed. This method is applicable for both manual and automatic HPLC systems. An automatic HPLC affords the opportunity to run a series of compounds in a row, without requiring the ongoing presence of the operator. The method was intended to entail the shortest possible time delay between incubation and measurement of free fraction, although though no specific tests were done on this parameter.

As a model, plasma obtained from pig blood was used to conduct the main part of the experiments. Use of human blood products, although perhaps preferable for the development of PET ligands, is problematic due to the risk of exposure to hepatitis and HIV virus. Furthermore, individual genetic difference in human plasma proteins may be a source of variance between batches. There are also some ethical constraints in using human blood, as consent must be given by the donor. Porcine blood plasma has a lower protein binding to certain drugs than human blood plasma, but can nonetheless be used to compare groups of tracers, as it seems that results for porcine and human plasma and/or serum are highly correlated [29, 55]. Homogenous porcine blood pooled from many animals is cheap and easy to obtain, and is thus a good alternative to human blood. To confirm its applicability, a comparison of binding properties for plasma obtained from pig and donated human blood was undertaken.

Figure 13 further down shows the method flow chart when six 15 ml tubes containing anticoagulants were used to collect pig blood. Three different anticoagulants (heparin, EDTA and warfarin) were used at concentrations in excess of those recommended in the literature [56-58]. Heparin was mistakenly added to a final concentration of 1000 IU/ml, which is probably ten-fold in excess of requirement. EDTA was added at a concentration of 35 mg for 15 ml blood, although 27 mg is reportedly sufficient. Warfarin was added to a final concentration of 40 µg in 15 ml blood, although 0.12 to 3 µg/ml is recommended.

Anticoagulants and blood were mixed thoroughly, and blood was then centrifuged at 4000 rpm for 15 to 20 minutes, to separate plasma from red blood cells. 4000 rpm was the highest speed for the clinical centrifuges and this low speed may have minimized damage to red blood cells.

The tubes with warfarin as anticoagulant did not separate as well as those with heparin or EDTA anticoagulant (See picture in Figure 12). Furthermore, the color differences showed that the warfarin plasma contained more red blood cells or hemoglobin than the others. Both whole blood and plasma were stored at -80 °C until use.

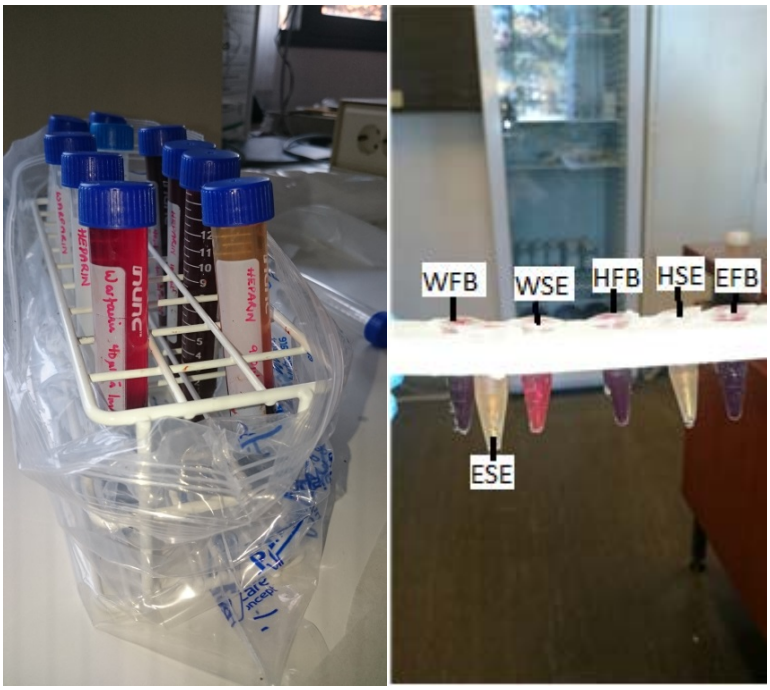

Figure 12: Tubes of warfarin and heparin after centrifugation to the left. Tubes of warfarin full blood (WFB), warfarin plasma (WSE), heparin full blood (HFB), heparin plasma (HSE), EDTA full blood (HFB) and EDTA plasma (HSE) after incubation are shown to the right

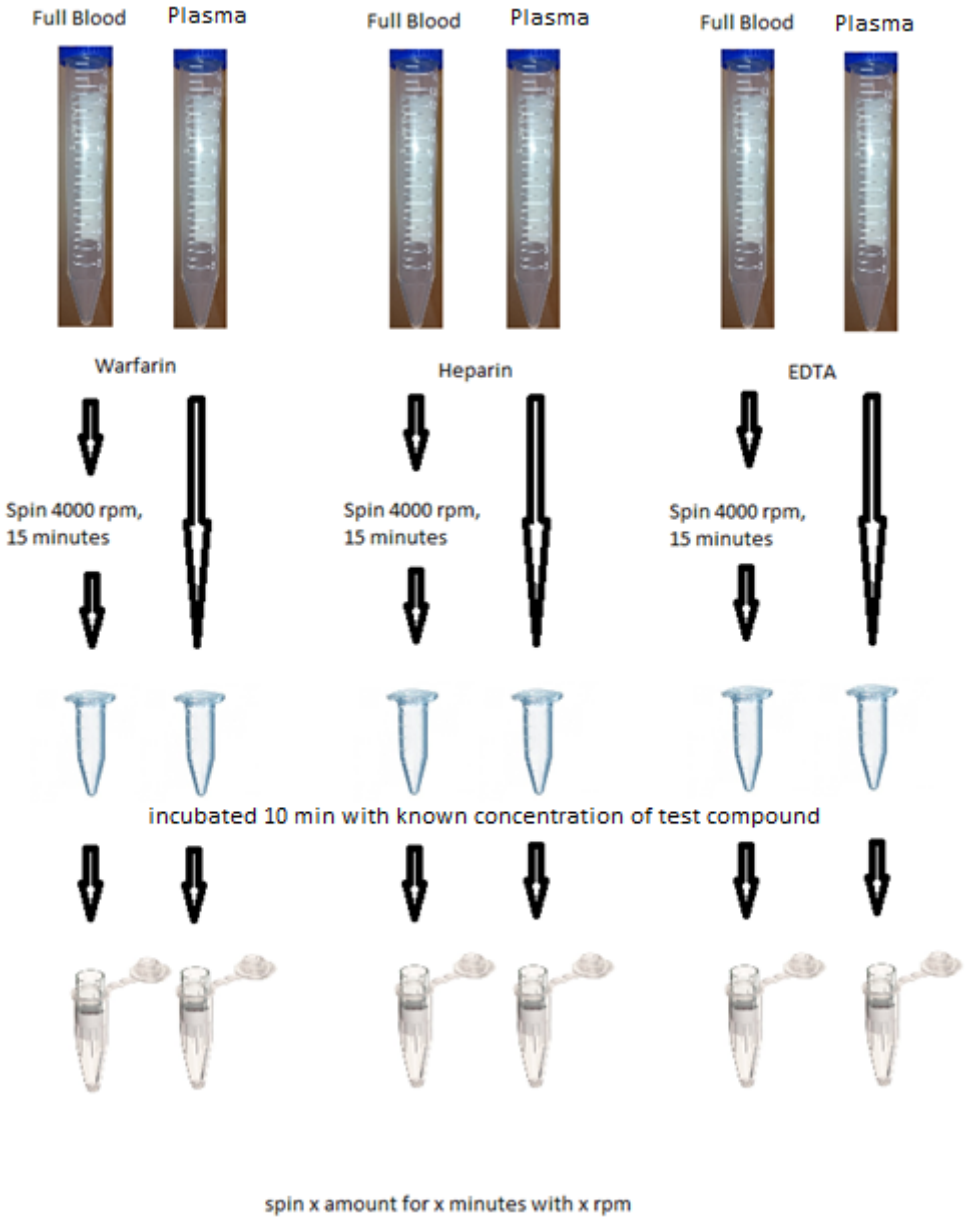

Figure 13: Flow chart over the initial protein binding method used

With an incubation of 200 µg/ml test compound in plasma, 5 µl samples of filtrate were sufficient to measure the free fraction on a manual HPLC. Since the automatic HPLC need a larger injectate volume, an optimization regarding dilution versus sample injection was done, aiming to afford a dilution as low as possible. To this end, tests were made to see the minimum necessary sample volume for reliable performance of the automatic HPLC. Starting with 1 ml volume, triplicates were measured with less and less volume available, until air bubbles were detected in the chromatogram. Volumes down to 300 µl gave good results, so it was decided to use 400 µl to have a margin of safety.

An optimization of the mobile phase was done, starting with method B as a model method (Table 16). Due to a spurious increase in the apparent test compound concentration during plasma protein binding, the methanol content of the mobile phase was decreased to ensure sure that warfarin did not elute with the void volume. Using 60% or 50% methanol and 40% or 50% MOPS buffer respectively, there were still some HPLC tests showing a spurious increase of warfarin concentration when measuring samples. The retention time variation of warfarin was at the most 0.019 minutes, which corresponds to a relative standard deviation of 0.005 min. There were changes of up to 0.5 minutes in retention time between the tests, but triplicate measurements within a run were stable. Experiments were done to eliminate problems arising from the use of plastic Eppendorf tubes and methanol in the samples. However, using PBS instead of methanol or adding both filtered and unfiltered samples to the Microcon centrifugal filter tubes, did not improve the results. When testing other test compounds, methanol content was decreased even further to 30% (while retaining MOPS buffer as the aquatic component of the mobile phase) to see if the results for these compounds would improve. Nonetheless, the calibration curves had R^2 values deemed unacceptably low.

Table 16: Mobile phases tested for protein binding

Buffer	Organic phase	Mobile phase (aq/org)	Comments
MOPS	Methanol	25/75	higher concentrations of Warfarin after protein binding
MOPS	Methanol	50/50	higher concentrations of Warfarin after protein binding
MOPS	Methanol	60/40	difficulties getting any readings
MOPS	Methanol	70/30	unstable readings for plasma

With concentrations as low as 0.01 µg/ml being tested it was necessary to slow down the retention. A Capcell pak C18 (100Å 5µm, 250mm x 4.6mm) column was successfully used with 1 ml/min flow and 10 µl injections. This is mentioned as method C (Table 4).

5.2.1. Calibration Curves for standards

To make a calibration curve for a single compound as in the context of protein binding determination is distinct from the general calibration curve for log k as described above. A single compound over a range of concentrations should give a linear result so long as sample preparation, solubility and equipment are standard. For most of the test compounds there arose no issues in making calibration curves, and such problems that did arise were related to solubility. Particular cases where solubility difficulties arose are discussed later.

As the different test compounds had various UV absorbance spectra, they would require different concentrations to fall within the range of detectability. To make this method as user-friendly as possible, we aimed for a concentration range that covered the detection limits, but without saturating the plasma protein binding sites. Concentrations in the range 0.01 µg/ml to 200 µg/ml (and in one test 700 µg/ml and 1000 µg/ml) were tested. Samples with the concentration 0.01 µg/ml gave up to 9% deviations in plasma protein binding, and were often close to background values. As tracer concentrations normally used in PET studies are generally in the low nanomolar range the calibration curves were generated for ligand concentrations ranging from 0.1 µg/ml and 20 µg/ml. Raw data for the concentration experiments can be found in Appendix B and graphs are presented under the subsections of each of the three standards tested, warfarin, testosterone and lansoprazole (literature values for the standards can be seen in Table 17.

Table 17: Protein binding standards and their literature values

Compound	Literature value for protein binding in human serum	Reference
Warfarin	99%	[59]
Testosterone	97-99%	[60]
Lansoprazole	97%	[61]

5.2.1.1. Warfarin

Several experiments were made to find a satisfactory calibration method applicable for the different compounds. The first warfarin calibration curve of concentration versus area under the curve measured with 254 nm wavelength (Curve A in Figure 14) was made with method B (Table 1).

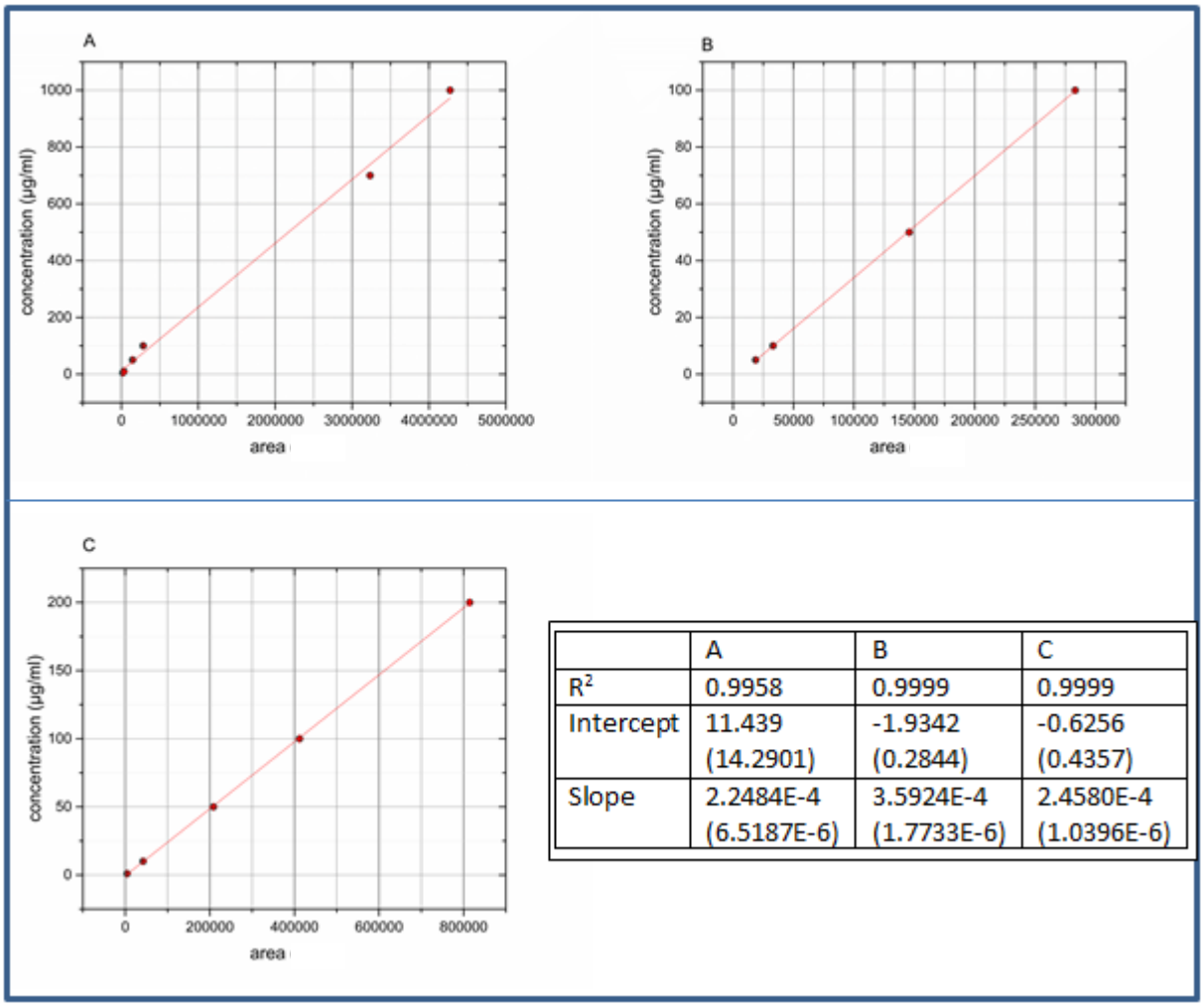

	A	B	C
R^2	0.9958	0.9999	0.9999
Intercept	11.439 (14.2901)	-1.9342 (0.2844)	-0.6256 (0.4357)
Slope	2.2484E-4 (6.5187E-6)	3.5924E-4 (1.7733E-6)	2.4580E-4 (1.0396E-6)

Figure 14: Warfarin calibration curves. A: Calibration curve 5 to 1000 µg/ml. B: Calibration curve outtake from curve A, 5-100 µg/ml. C: Calibration curve 1-200 µg/ml

The first warfarin calibration curve (A) had an acceptable R^2 value of 0.9958, even though standard errors (specifically for intercept) were high (intercept error of 14.2901 and slope error of 6.5187 E-4), and some discrepancies in the linearity were evident to inspection of the curve itself. The lower warfarin concentrations showed better linearity, with an R^2 value of 0.9999, and lower standard errors (Curve B). The partial concentration dependence of the calibration curve could be due to solubility issues or aspects of the instrumentation. To check the validity of this curve, a second warfarin calibration curve in the concentration range of 1-200 µg/ml was made (Curve C) in PBS according to method B (Table 1).

The results of an equal concentration reading between the two calibration curves would give a standard deviation of 1.9%, which is acceptable for the aim of these methods. In the protein binding chapters below, there arose some problems at higher warfarin concentration, so as alternatives, testosterone and lansoprazole were tested as internal standards instead of warfarin.

5.2.1.2. Testosterone

A calibration curve of testosterone was made in PBS (Figure 15 curve A) over a wide range of testosterone concentrations (1, 2.5, 25, 50, 100 and 200 µg/ml). Method C was then developed for calibration curves and protein binding assays. The method is explained in detail in Table 4.

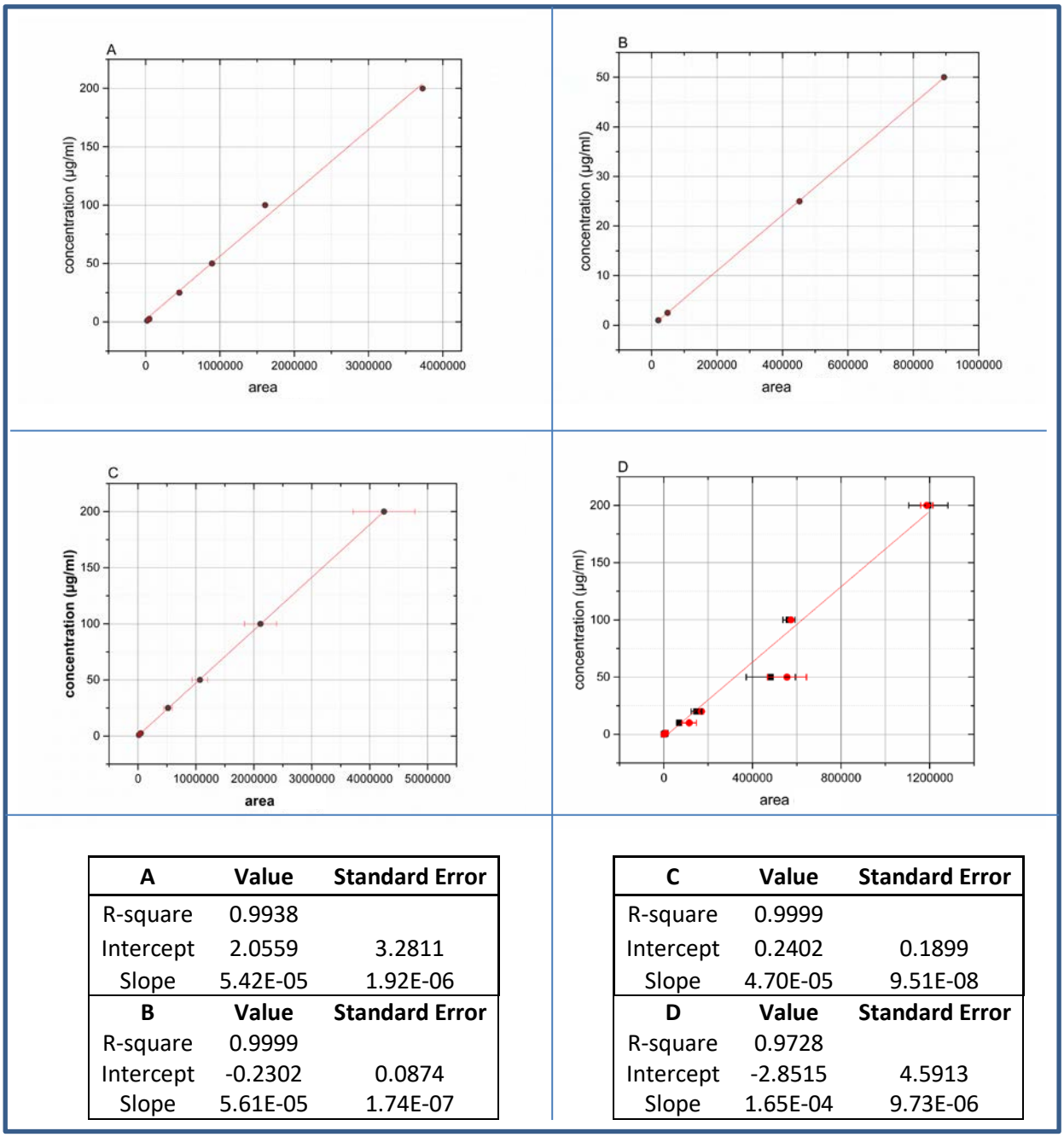

A	Value	Standard Error
R-square	0.9938	
Intercept	2.0559	3.2811
Slope	5.42E-05	1.92E-06

B	Value	Standard Error
R-square	0.9999	
Intercept	-0.2302	0.0874
Slope	5.61E-05	1.74E-07

C	Value	Standard Error
R-square	0.9999	
Intercept	0.2402	0.1899
Slope	4.70E-05	9.51E-08

D	Value	Standard Error
R-square	0.9728	
Intercept	-2.8515	4.5913
Slope	1.65E-04	9.73E-06

Figure 15: Testosterone calibration curves. Curve A: 1-200 µg/ml made with PBS. Curve B: Isolation of 1-50 µg/ml concentrations from curve A. Curve C: Second attempt on testosterone calibration curve 1-200 µg/ml with PBS. Curve D: Testosterone calibration curve made with DMSO. Table A-D shows statistics for each curve.

As with the first calibration curve for warfarin (Figure 14) the values of R^2 are acceptable, but the standard error for the intercept is high, and the 100 µg/ml and 200 µg/ml readings deviated from the regression line. When plotting only 1-50 µg/ml (Curve B) the linearity considerably increased. To validate the results for the testosterone calibration curve, the experiment was repeated with the same sample preparation, method and equipment (Curve C). Here, the R^2 value increased and standard errors of the trendline decreased, which shows high linearity and accuracy, although the standard errors of the measured areas increased considerably. The standard deviation between these two calibration curves was 8% when calculating the concentration result from an area of a 1,000,000 Au-min. The poor water solubility of testosterone [62] could be the reason for these deviations. A calibration curve was made (Curve D) where the stock solution was made in DMSO over a wide range of testosterone concentrations (0.01, 0.1, 0.5, 1.0, 10, 20, 50, 100 and 200 µg/ml), diluted with methanol to a concentration between 20-200 µg/ml and with water between 0.1-10 µg/ml. The calibration curve samples were run two times on the same day, to compare readings. The R^2 value was deemed a bit low, and the 50 µg/ml sample showed deviations both from the regression line and also between the two measurements.

A 20ug/ml sample was made from the same testosterone stock solution as used for the calibration curve and dilutions of this sample were made with water. The samples were measured and checked towards the calibration curve. As reported in Table 18 below, the calibration curve did not give accurate results, with substantial deviations at the low concentration end.

Table 18: Testosterone validation of calibration curve

Testosterone concentration (µM)	Calculated concentration (µM)
69	70
35	55
3.5	4.8
1.7	3.3
0.4	1.0

To ensure that these poor results didn't arise from the HPLC system or other equipment, the injection volume, the weights and the pipettes were all tested and calibrated, all of which showed good reproducibility and accurate results, as reported in "Appendix C: General data concerning both lipophilicity and protein binding" (Figure 27 and Table 82). The injection time was increased, but without improving the results. Since testosterone proved to be difficult to work with, apparently due to its low water solubility, it was decided not to proceed with this compound.

5.2.1.3. Lansoprazole

Stock solutions for a lansoprazole calibration curve were made in DMSO and stored at -86 °C. Before use, they were allowed to thaw to room temperature. Concentrations from 0.01 to 30 µg/ml (Figure 16) were weighed out and diluted with water, and then measured by method C (Table 4). Each sample was measured four times. The results showed no linear correlation. Several attempts had to be made before obtaining a satisfactory calibration curve for lansoprazole.

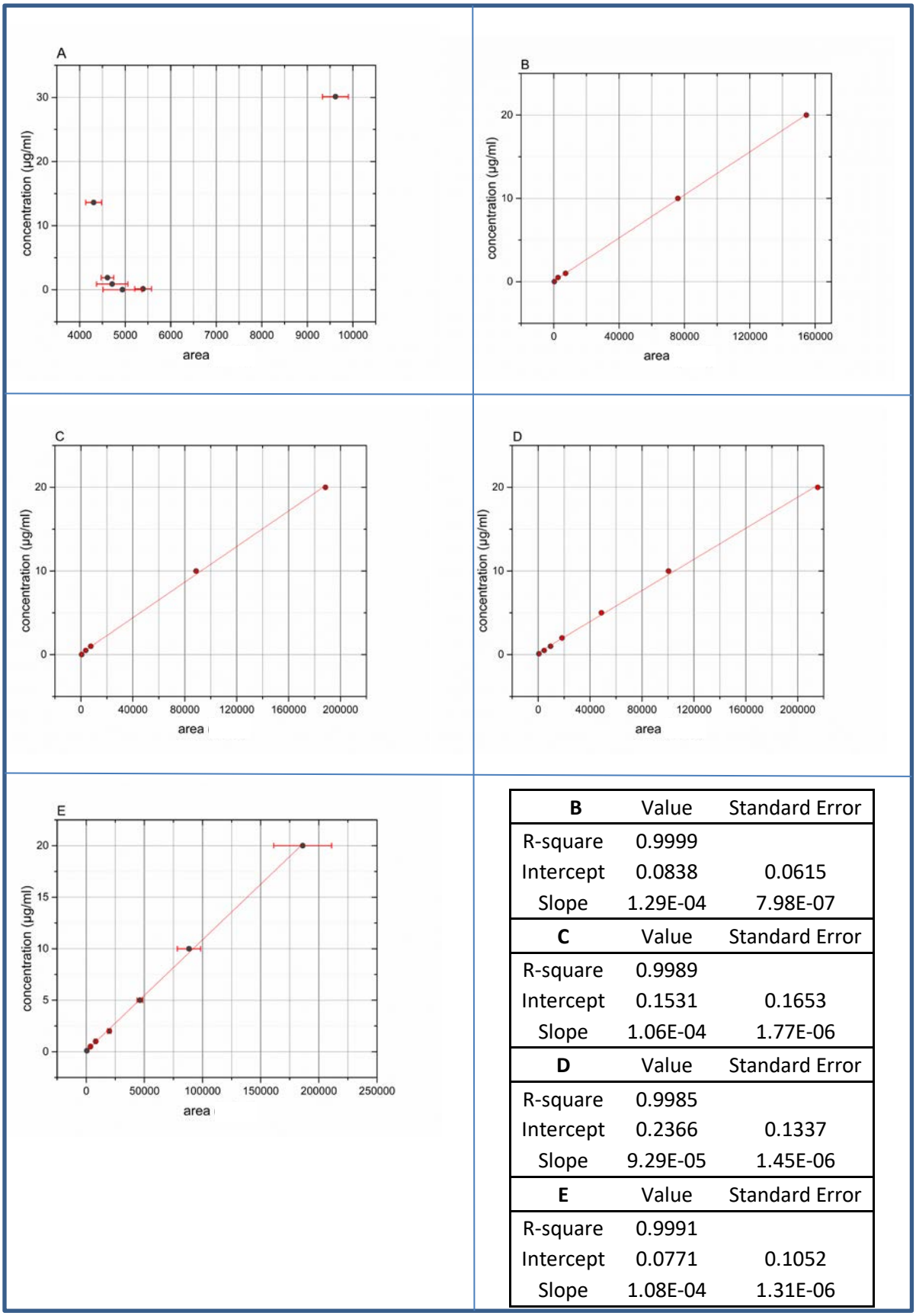

B	Value	Standard Error
R-square	0.9999	
Intercept	0.0838	0.0615
Slope	1.29E-04	7.98E-07
C	Value	Standard Error
R-square	0.9989	
Intercept	0.1531	0.1653
Slope	1.06E-04	1.77E-06
D	Value	Standard Error
R-square	0.9985	
Intercept	0.2366	0.1337
Slope	9.29E-05	1.45E-06
E	Value	Standard Error
R-square	0.9991	
Intercept	0.0771	0.1052
Slope	1.08E-04	1.31E-06

Figure 16: Calibration curve lansoprazole. Curve A: First attempt on lansoprazole calibration curve, no linearity. Curve B: Lansoprazole calibration curve 0.01-20 µg/ml, five points. Curve C: Repetition of experiment of curve B. Curve D: Lansoprazole calibration curve with seven points. Curve E: Average calibration curve from curve B, C and D.

The results from Curve A could be due to use of old solutions of lansoprazole, given that measurements below 10ug/ml were especially difficult to get good measurements for. A stock solution of lansoprazole made in DMSO should be stable for 2 weeks at 4 °C according to www.selleckchem.com. Therefore, a new calibration curve with fresh lansoprazole was made (Curve B) in the range of 0.01-20 µg/ml and method C was used. Concentrations < 0.1 µg/ml showed no measurable results. The five concentrations that were measurable showed good linear correlation, with an R^2 value of more than 0.999 and low standard errors for the intercept and the slope. The lowest concentration had readings that were indistinguishable from the blank. The calibration curve experiment was repeated to improve readings for 0.1 µg/ml (Curve C), although these readings could not be made in the repeat experiment either. Since the 0.1 µg/ ml did not show measurable results, this establishes a clear limit of the sensitivity of the assay. To compare the two lansoprazole calibration curves that were made, two samples were measured at concentrations of 2 µg/ ml and 5 µg/ml. See results in Table 19 below.

Table 19: Comparison of lansoprazole calibration curves

Calibration curve B	**µM**	**c_{calc}[1] / µM**	**% difference between conc and calc conc**	**Std. dev %**
Lansoprazole 2 µg/ml	5.4	6.6	18.2	0.29
Lansoprazole 5 µg/ml	13.5	13.0	3.7	0.27
Calibration curve C				
Lansoprazole 2 µg/ml	5.4	6.6	18.2	
Lansoprazole 5 µg/ml	13.5	13.0	3.7	

[1] c_{calc} = calculated activity from calibration curve

The two lansoprazole calibration curves show good reproducibility; although the difference between the theoretical and measured concentration is as high as 18%, this held only at the low end of the concentration range. Yet another calibration curve was made, and the calibration samples were allowed to stay in solution at 4 °C overnight, in order to test stability of the preparations. The blank readings of mobile phase without test compound were around 1000 Au-min in this experiment, which corresponds to the 0.1 µg/ml results. But as the samples remained stable, and as all the three lansoprazole calibration curves showed good linearity and low standard errors, an average of the three curves was used for further calculations when using lansoprazole as an internal standard (Curve E). The standard deviation for was 23% for 0.5 µg/ml and 13% for 20 µg/ml (Table 20). The standard deviations for the lower concentrations are somewhat high, but as the calibration curve is intended for protein binding of known concentrations, and is only used for screening purposes, this was deemed adequate for the present purposes. If 10 µl of a standard solution of 10 µg/ml is added to 1 ml plasma and 1% free fraction is to be measured, the concentration would be 0.1 µg/ml, whereas a 10% free fraction would give 1 µg/ml. These expected concentrations fall in the range of sensitivity of the method.

Table 20: Data for final calibration curve of lansoprazole

Lansoprazole (µM)	Average peak area	Std.dev	Std.dev %
0.3	569	0.00	0
1.4	3633	825	23
2.7	8129	1004	12
5.4	19,870	1483	7
13.5	46,227	2482	5
27.1	88,364	9981	11
54.2	186,138	24,877	13

The final calibration curve for lansoprazole had an R^2 value > 0.999, and standard errors of 0.1 for the intercept and 10^{-6} for the slope.

5.2.2. Calibration curves of test compounds

Calibration curves were made by dilutions from highest to lowest concentration with five final concentrations points (0.1, 1, 5, 10 and 20 µg/ml) and 92% of the R^2 values of used calibration curves were 0.99 or higher, whereas 100% of the used R^2 values were 0.98 or higher.

Calibration curves were made accordingly to OECD guidelines 117 [30]. Automatic integration of the peaks was in most cases deemed adequate, but at low drug concentrations and in specific cases with tailing or overlap, manual integration was done. Figure 17 illustrates the quantitation of concentration and present comments on manual versus automatic integration.

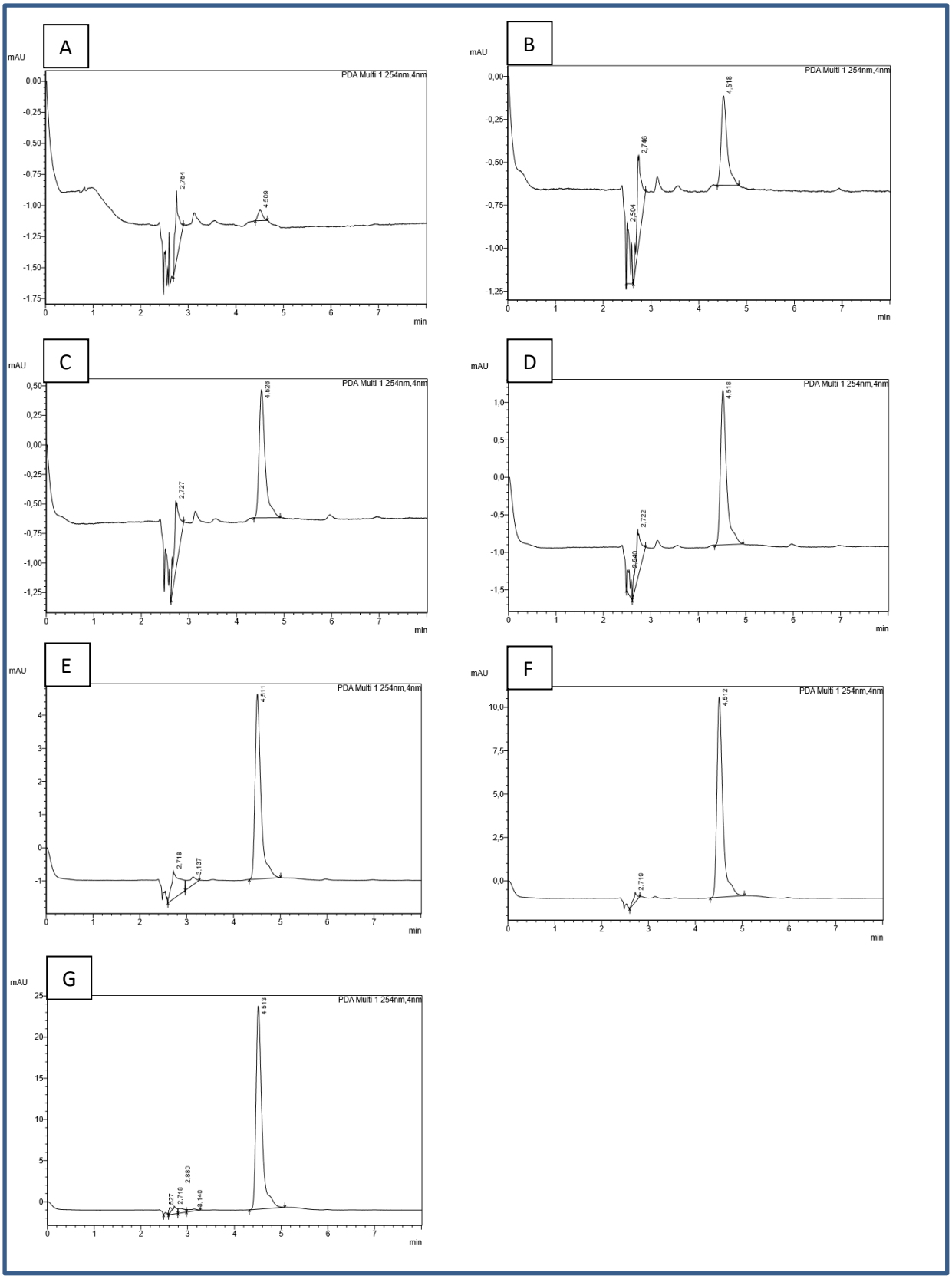

Figure 17: HPLC chromatograms. A: Lansoprazole 0.1 µg/ml manually integrated. B: Lansoprazole 0.5 µg/ml manually integrated. C: Lansoprazole 1 µg/ml automatically integrated. D: Lansoprazole 2 µg/ml automatically integrated. E: Lansoprazole 5 µg/ml automatically integrated. F: Lansoprazole 10 µg/ml automatically integrated. G: Lansoprazole 20 µg/ml automatically integrated

The calibration curve for L12 is shown as an example in Figure 18, being the compound with the highest R^2 value. Some of the other compounds are discussed below with regard to other aspects of the calibration curve development, and the remainder of the calibration curve data are presented in Appendix B: "Raw data tracer protein binding" as LINEST data, a statistical array from Excel). The intercept of calibration plats was not forced to zero, as background signal of the UV detector could deviate the intercept in one direction of the other. Strictly speaking, this detector background is expected to be stable, and hence should be seen as the true zero point. The measured areas for the lowest concentrations will tend towards a slightly overestimation when baseline is not set. This means that some misattributed area in a peak is added according to the position of the baseline above or below the zero value. The overall very high R^2 values indicated that there should nonetheless be high accuracy in the linearity for the calibration curves of most compounds. Any imprecision would derive from the assay itself, whereas several points of the experiment could deviate from expectation. These deviations could be due to the quality of the plasma used, particular concentrations during sample preparation, incubation, centrifugation and filtration, and finally dilution of the sample prior to HPLC measurement. The internal standard (standard 30) showed a standard deviation of 1.98 µg/ml (2.1%), which would indicate that a result between 95-99% is to be expected for a compound with exactly 97% protein binding.

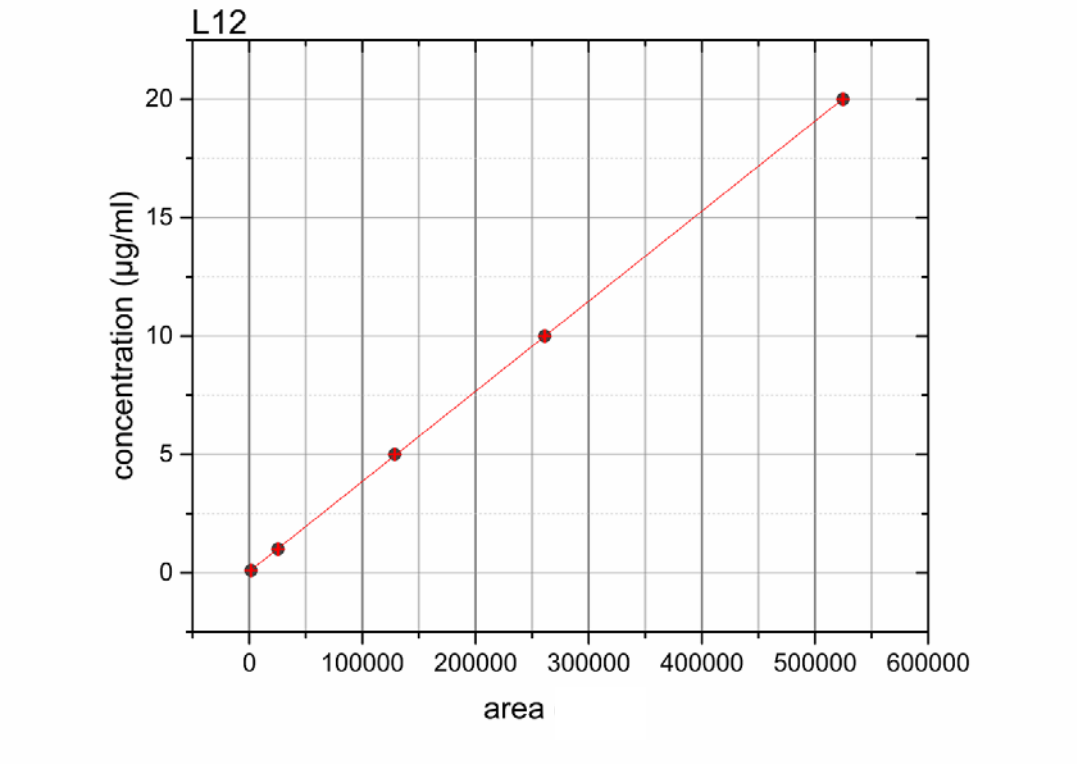

Figure 18: Protein binding calibration curve of L12 with red error marks. Highest regression number of protein binding test compounds

For all the compounds that were measured for plasma protein binding, a linear least squares curve fitting routine called linest was used that produces uncertainty estimates for the fitted parameters (slope and intercept). All the "linest data" can be seen in Appendix B: "Raw data tracer protein binding". Table 21 is presented as an example to explain the data for the case of test compound W1.

Table 21: W1 Raw data and statistics

Average peak area	Conc (µg/ml)	Linest data		% uncertainty slope	% uncertainty intercept
307	0.1	2.015E-04	4.556E-01		
3178	1	6.960E-06	3.431E-01	3.5	75.3
18496	5	9.964E-01	5.617E-01		
48893	10	8.382E+02	3.000E+00		
96973	20	2.644E+02	9.464E-01		

The linest data outlined in grey has the following meaning (Table 22)

Table 22: Linest data explanation

slope	intercept
+/-	+/-
R^2	s(y)
F	degrees of freedom
regression	residual ss

The first row presents the slope and the intercept of the calibration curve, with the standard deviation in the second row. From these numbers, the percentage uncertainty of the slope and intercept is calculated. The first value in the third row is the regression coefficient, R^2. The F reported in row four is the Fisher F- statistic, which is the ratio of the variance in the data explained by the linear model divided by the variance unexplained by the model. The F-statistic is calculated from the regression sum of squares and the residual sum of squares in row five. The residual sum of squares is the sum of the squared residuals. The R^2 value, which is calculated from the sum of the squared deviations, is used for evaluating the models, although it is only a rough indicator of the goodness of fit.

Compound L4 has an uncertainty in its intercept of -611.7% (Table 23), which corresponds to a deviation of the intercept between -0.3 and 0.2, which is not significantly further from the zero-intercept seen for other curves. The results for the 20 µg/ml concentration are not present, as there were some inconsistencies in the measured results, despite several attempts. This single concentration results deviated enormously from linearity, dragging the

R^2 value down to 0.78. Removing this point increased the uncertainty of the intercept by 50%, but decreased the uncertainty of the slope (the more salient parameter) by more than 80% (Table 24). The inconsistencies for this instance could be due to solubility issues, but as the concentrations that will be measured after plasma protein binding occurs in trace amounts, it was decided to use this calibration curve only with four points. In any event, no unbound fraction was detectable for this compound.

Table 23: L4 raw data and statistics

Average peak area	Conc (µg/ml)	Linest data		% uncertainty slope	% uncertainty intercept
296	0.1	2.103E-04	-4.856E-02		
4319	1	1.108E-05	2.970E-01	5.3	-611.7
26336	5	9.945E-01	4.109E-01		
46519	10	3.605E+02	2.000E+00		
		6.087E+01	3.377E-01		

Table 24: L4 raw data when keeping values for 20 µg/ml measurements

Average peak area	Conc (µg/ml)	Linest data		% uncertainty slope	% uncertainty intercept
296	0.1	3.233E-04	-8.381E-01		
4319	1	9.761E-05	3.117E+00	30.2	-372.0
26336	5	7.852E-01	4.358E+00		
46519	10	1.097E+01	3.000E+00		
47158	20	2.084E+02	5.699E+01		

The compound L11 has an uncertainty in the intercept of 237%. This is equal to the intercept varying between -0.2 and 0.5, which is close enough to zero compared to other curves (Table 25).

Table 25: L11 raw data and statistics

Average peak area	Conc (µg/ml)	Linest data		% uncertainty slope	% uncertainty intercept
636	0.1	7.763E-05	1.544E-01		
7666	1	2.795E-06	3.651E-01	3.6	236.5
58378	5	9.961E-01	5.854E-01		
137677	10	7.713E+02	3.000E+00		
250708	20	2.643E+02	1.028E+00		

For compound L16, the point for 20 µg/ml was removed from the calibration curve to quickly test if its omission would have a significant impact on the regression results. Even though the

curve data improved substantially with inclusion of the higher concentration, it gave no change in the overall plasma protein binding result for compound L16 (Table 26).

Table 26: L16 raw data and statistics

Average peak area	Conc (µg/ml)	Linest data		% uncertainty slope	% uncertainty intercept
2173	0.1	3.147E-05	1.202E-01		
28541	1	1.947E-07	6.293E-02	0.6	52.3
150439	5	9.999E-01	1.008E-01		
314343	10	2.613E+04	3.000E+00		
632693	20	2.653E+02	3.046E-02		

After seeing that several of the L-group compounds had to be reformulated or made up with DMSO instead of PBS due to solubility problems, all samples from this group were dissolved in pure DMSO only. PBS is however the first choice of solvent, since using DMSO tends to result in broader peaks being detected by UV, which increases the risk of contamination of the signal by other compounds.

5.2.3. Method Development

Internal standard

The first attempts for internal standard quantitation were made with warfarin, as it could be used in a primary role as clotting inhibitor. The calibration curves of warfarin were successfully developed, but due to influences from hormone factors, it proved impossible to use warfarin as internal standard with this method. However, warfarin was only tested at the high concentration of 200 µg/ml, it cannot be certain that it would not have served as internal standard at some lower concentration. As alternates to warfarin, testosterone and lansoprazole were also tested for this purpose. Testosterone has insufficient solubility in aqueous buffer, and earlier studies on the binding of testosterone to plasma show that the plasma concentration of testosterone is influenced by estrogen and the age and general state of health of the test subject [63]. The influence of these factors did not favor the use of testosterone as internal standard. Consequently, testosterone recovery was not measured at lower concentrations.

Lansoprazole showed a good stability and reproducibility as an internal standard; there were no solubility difficulties in the lower ranges of concentration, and no effects of hormone levels are reported. It might present difficulties for working with higher concentrations, as the solubility for lansoprazole in plasma is 0.4 mg/ml. The measured bound fraction is compatible with literature values and this at a concentration too low to cause saturation of binding sites. The matrix experiment explained in chapter 4.2.4. showed no influence of the dilution of plasma compared to direct addition to whole plasma. The only change observed was when the lansoprazole concentration was as low as 1 µg/ml, where the deviations in UV peaks were already very high. All in all, lansoprazole showed a robustness that led to its selection as the preferred internal standard for the plasma protein binding method.

Below is explained the method development of protein binding for the three compounds tested as internal standard.

Protein Binding of Warfarin

The initial testing of plasma protein binding assay was done with warfarin. Warfarin proved to present some difficulties for the method developed, and a number of other compounds were therefore tested in the method optimization, discussed later. The experiments done with whole blood were done with warfarin only. Initially a comparison between full blood and plasma was planned, to distinguish clearly binding to plasma proteins and whole red blood cells. However, subsequent efforts focused more exclusively on the blood plasma, except for one additional experiment explained later. The centrifugation/ultrafiltration procedure described above was used in conjunction with both manual and automatic HPLC. The results for both systems indicated that the concentration of the warfarin somehow had

increased after protein binding. There was no indication that the addition of heparin or EDTA interfered with the protein binding. Results from two attempts of protein binding with warfarin are shown in Table 27 below.

Table 27: Protein binding of warfarin in blood and plasma

Protein binding of warfarin 200 µg/ml 0.65 mM	Average peak area	Cal. curve DMSO (mM)	Cal. curve PBS (mM)
Warfarin/pig blood	13,422,733	9.82	10.70
2nd attempt	11,857,483	7.73	9.45
Warfarin/pig plasma	3,294,617	2.44	2.63
2nd attempt	3,167,433	2.09	2.53
Heparin/pig blood	7,335,783	5.39	5.85
2nd attempt	8,825,983	5.76	7.03
Heparin/pig plasma	2,530,383	1.88	2.02
2nd attempt	2,669,583	1.77	2.13
EDTA/pig blood	9,581,483	7.02	7.64
2nd attempt	13,430,033	8.75	10.71
EDTA/pig plasma	3,320,217	2.46	2.65
2nd attempt	3,039,167	2.01	9.45

Both experiments of warfarin protein binding showed the same trend of "increasing" concentrations, as seen in the table above. After adding 200 µg/ml warfarin to blood and plasma aliquots, the warfarin concentration in the supernatant after filtration was measured to be 500 µg/ml and above 3000 µg/ml unbound fraction, as calculated from calibration curves made with both DMSO and PBS.

Whole blood and plasma were weighed before and after filtered centrifugation of the plasma, to determine the total amount of plasma passing through the filter. In addition, this procedure could give an indication if some contaminant from the filter membrane could give rise to chromatographic peaks interfering with the HPLC analysis. Table 28 shows the percentage of the full blood or plasma that came through the filters as supernatant carrying the unbound fraction during the first warfarin experiment, and how much of the filtrate was captured and thus possibly bound to proteins.

Table 28: Weights before and after centrifugation/filtration of the first warfarin experiment

	150 µl Plasma (mg)	Epp.tube (mg)	After spin (mg)	Super-natant (mg)	% super-natant	% proteins	% protein and RBC
WFB	146.2	903.2	946.2	43.0	29		71
WSE	145.6	902.8	978.9	76.1	52	48	
HFB	157.1	907.4	955.7	48.3	31		69
HSE	144.8	902.1	980.3	78.2	54	46	
EFB	151.9	902.4	943.0	40.6	27		73
ESE	147.4	898.3	977.3	79.0	54	46	

It was necessary to determine the source of the seemingly increasing warfarin concentration. An experiment was done to test if the increase could be due to contamination from lipophilic compounds released from the filter membrane during centrifugation (Table 29). In this test, warfarin was dissolved in mobile phase and divided between two eppendorf tubes. One tube was filtrated, and the other not. The mobile phase contained 50% methanol to ensure that there was sufficient retention to resolve any additional UV absorbing compounds in the chromatogram. 200 µg/ml warfarin was added to 1 ml of mobile phase the results showing that only the filtered sample showed an apparent increased in warfarin concentration (row 4 and 5 in table below), even though there was no indication of the presence of a second compound (i.e. no increase in peak width).

Table 29: Trouble shooting of warfarin plasma protein binding method. Tests of filtration, mobile phase and stepwise measurements

All samples made up to 200 µg/ml (0.65 mM) warfarin and run with described protein binding method, if no otherwise specified	50_50 MOPS/ MeOH µM	After 8 days in 4 °C µM	PBS/ Microcon tubes only µM	40_60 MOPS/ MeOH µM
PBS	682	642		636
filtered/centrifuged	961[1]		617	
not filtered/centrifuged	571[1]		646	
PBS measured directly	630/636			
PBS after incubation	636/636			
PBS after filtration	701/698			
HSE with 200 µg/ml warfarin	65	62		26

[1]dissolved in mobile phase

To eliminate methanol and Eppendorf tubes as sources of error, warfarin was measured in parallel in PBS (filtered or unfiltered), but after only being placed in Microcon tubes for the same amount of time (row 4-5 in Table 29). This experiment did not indicate any addition of

the warfarin signal after filtration, but (as expected) some amount was lost during the filtration. If any UV absorbing material was being released from the filter, this means that it was being dissolved and released by the organic phase.

A comparison between HPLC with 50% and 40% methanol mobile phase was done at this point, measuring ultrafiltrates of PBS with and without addition of warfarin as well as plasma with and without warfarin (row 3 and 9 in Table 29 shows the PBS with warfarin addition and the plasma with warfarin addition). The blank samples showed that there was a stable baseline and no interference to be seen from either PBS or plasma (not shown). The results from the 50% methanol mobile phase were close to expected results, but the apparent concentration still increased when running PBS through the filters and showed pretty high values of free fraction compared to literature values for plasma. With 10% less methanol in the mobile phase the concentration of unbound warfarin decreased by 7% in PBS and by 60% in plasma. The samples were retested after 8 days' storage at 4 °C, which showed a minor warfarin concentration of free fraction decrease of about 5 %. The first and third rows (of Table 29 show results for the same warfarin concentration measured with the same parameters, but at different days, showing a deviation of 16.2%. However, when measuring the same sample twice, the reproducibility and precision were both found to be above 98%, indicating that the method and the equipment are reliable.

To investigate further where warfarin concentrations changed in the assay, two samples were measured with removal of aliquots before and after incubation, and after filtration (row 6-8 Table 29). The minimal concentration difference (< 1%) after filtration shows that the sample preparation is reproducible, but once again the apparent increase of warfarin concentrations can be seen. Retention time (T_R) variation was no more than 0.019 minutes, with a standard deviation of 0.005 minutes. From a starting volume of 150 µl PBS only 90-100 µl went through the filter, and still there was an apparent concentration increase in both samples after filtration.

The method was scrutinized step by step to look for mathematical or sample preparation errors that could explain the apparent increase of warfarin concentration. The pipettes were tested as well as analytical balances and other equipment (see Table 82 in Appendix C). Calibrations of some instruments showed a bit of uncertainty, but neither alone nor together could these uncertainties explain the increase of warfarin concentration. In the next step, other test compounds were tested to examine if a peak co-eluting with warfarin could be discerned after filtration/centrifugation of other standards. No indications of this were found.

Protein Binding of Testosterone

Testosterone was chosen as a test compound to determine if the difficulties encountered in the previous section were due to inherent properties of warfarin. The mean value of the unbound fraction for testosterone in human plasma is 2% [64].

The first test with testosterone was performed by adding stock solution to a final concentration of 200 µg/ml of the compound to pig plasma. Table 30 shows the experimental results from the protein binding assay with plain PBS, PBS along with testosterone, plain pig plasma and pig plasma along with testosterone (rows 3 and 5). No measureable peak was detected with plain PBS or plasma, so these are omitted from the table. Only 5% of the testosterone in PBS was detected by HPLC. As PBS contains no proteins, this suggests that the testosterone either failed to dissolve or was adsorbed by the tubes or filter materials. As testosterone is known to be poorly soluble in water, we only performed one further test to investigate whether the centrifugal step could explain the loss.

Table 30: Protein binding results of testosterone

All samples with testosterone 693 µM	Conc µM	Unbound fraction %
PBS 1	10.39	5.19
PBS 2	15.28	7.88
Porcine plasma 1	0.49	0.24
Porcine plasma 2	0.57	0.29
PBS not centrifuged 2	19.94	10.28

In the second experiment, a PBS sample with testosterone was not centrifuged, but analyzed otherwise as the plasma samples. Results from these measurements indicate a 2% loss of testosterone in the filtration step (Table 30), which is insufficient to account for the overall loss, as only 7% of the testosterone added to PBS was measured in the free fraction.

Due to apparent solubility issues for testosterone, it was decided to try a third compound as internal standard for the plasma protein binding assays.

Protein Binding of Lansoprazole

Concentration dependent plasma protein binding was measured for lansoprazole to investigate if saturable, reversible or irreversible binding may confound the results. Incubation with dilution of plasma was attempted to determine if the matrix influenced the protein binding (Table 31). The test compound was added to plasma to a final concentration of 20 µg/ml and then diluted by addition of pig plasma to 10 µg/ml and 1 µg/ml. There was no clear peak at the expected HPLC elution position of lansoprazole, suggesting that the 1

µg/ml sample was too dilute to be quantified by these methods (Chromatograms can be seen in Appendix B: "Lansoprazole".) For the sake of comparison, the same test was replicated without diluting the plasma, but rather upon direct addition of the test compound from a high concentration solution of lansoprazole (1 mg/ml made from stock solution on the day of experiment; see "Direct addition" columns in the table below). To select optimal concentrations for protein binding assays, a third experiment was done at final concentrations of 5 µg/ml, 15 µg/ml and 30 µg/ml (see "Direct addition 2" in Table 31).

Table 31: Lansoprazole protein binding with and without plasma dilution

Lansoprazole	Plasma dilution		Direct addition		Direct addition 2	
µM	% bound	% std.dev	% bound	% std.dev	% bound	% std.dev
81					90	5.42
54	97	0.58	97	0.79		
40					90	0.80
27	97	0.83	97	0.62	90	2.28
13.5					84	47.40
2.7	83	3.71	79	3.22		

Having established lansoprazole as a valid internal standard for the method, other compounds were tested for protein binding using the method described above. These test compounds were primarily synthesized by the PET-group in the University of Oslo as potential tracers for PET imaging. The test compounds and their plasma protein binding are presented in in chapter 5: "Results and Discussion".

As noted above, it is difficult to obtain human blood or plasma for routine binding studies. However, we were able to undertake a small-scale comparison of the binding of lansoprazole and four test compounds in pig plasma and human serum, derived from the experimenter's own blood. Results of this test are presented in chapter 5.2.4. "Results".

Concentration

Although the percentage of bound compound differs by 7% between the measurements in Table 31, lansoprazole in the concentration range 10-30 µg/ml gives the same plasma protein binding fraction in porcine plasma, indicating lack of saturation. This can also be seen graphically in Figure 19, where all lansoprazole protein binding experiments have been assembled. Concentrations of 1, 5, 10, 15, 20 and 30 µg/ml are plotted towards the percentage of bound fraction. The two lowest percentage bound fractions measured from 10 and 20 µg/ml in this graph are derived from the two first experiments, where plasma samples were diluted after adding test compounds. As such, they do not depict reproducibility of the method, but show a concentration range with constant free fraction. At 1 µg/ml the deviations were huge, such that bound fractions of 20-80% were estimated. Thus, these concentrations are too low for use as internal standard with this method.

Incubating with a standard concentration as low as 1 µg/ml, when only 3% free fraction is expected, gives unstable results. Since the concentration of 30 µg/ml was tested only once, it is difficult to say if the high deviation is due to saturation of protein binding, or due to error in that experiment. Though it is preferable to keep concentration as low as possible, to fall into the range for tracers, a standard concentration of 10 µg/ml was selected for routine use.

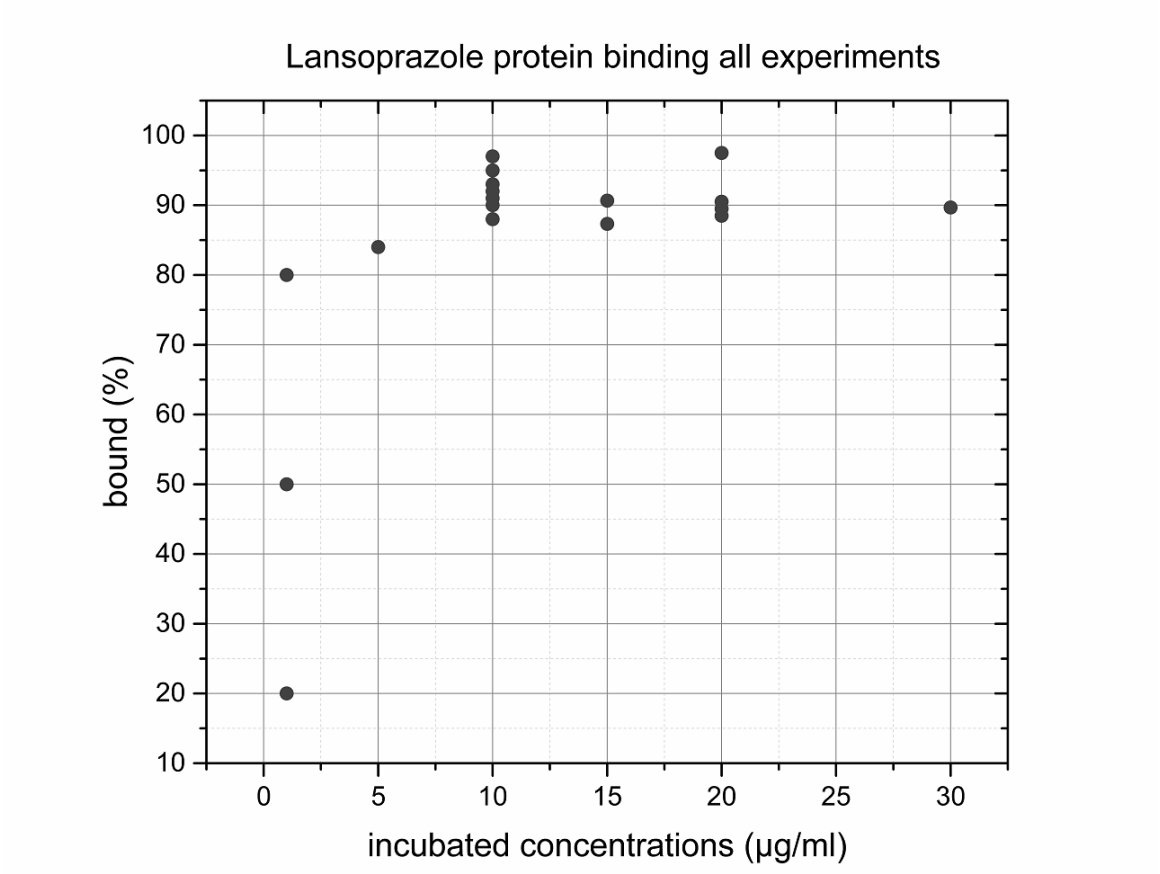

Figure 19: All lansoprazole protein binding measurements with different concentrations

From concentration in the range 10-30 µg/ml relationship plateaued, and 10 µg/ml was chosen as the standard incubation concentration, i.e. well within the tracer range, but high enough to afford stable measurements by RP-HPLC with UV detection. A comparison between 10 and 20 µg/ml is shown in Table 32 where the average bound compound differed by 1 %. For 1 µg/ml incubations, the relative standard deviation was 22 %, which is unusably high.

Table 32: Comparison of 10 µg/ml (27 µM) and 20 µg/ml (54 µM) lansoprazole incubation to protein binding

Concentration (µM)	% average bound	Std.dev.
27	94.5	3
54	93.2	4

The concentration data for lansoprazole was plotted into a spreadsheet and analyzed by a saturation fit algorithm (GraphPad Prism 7.03). This gave (with an R^2 of 0.995) K_D of 3520 µM and B_{max} of 3269 µM.

Temperature

After adding the test compound to the blood or plasma, samples were incubated in a water bath with a temperature of 37 °C, preferably. It proved difficult to hold a stable temperature in the ultrasound bath (Bandelin Sonorex RK 102 H) used for the incubations. The range of temperature within one incubation period could differ as much as 10 °C, and the range between tests was up to 19 °C (Table 33). The standard deviation of three samples of lansoprazole measured after incubation in a difference of 10 °C within 10 minutes was no more than 0.8, which is in this case 10%. According to Table 33 there are no indications that incubation at 25°C would alter the unbound fraction compared to incubation at 44 °C. For the last few experiments, a heating cabinet was available, in which the temperature was held stable at 37 °C. However, not enough tests were done in this condition to ascertain if incubation in the heating cabinet would have given systematically more stable results, although results of three tests do not support an important effect of temperature.

Table 33: Parameters of protein binding and their influence on the unbound fraction result of lansoprazole. Numbers in brackets are number of restarts of the centrifuge

	% unbound fraction	Incubation	% throughput of filter	# minutes centrifugation
		water bath 25-35°C		
Day 1	7		84	20
add wash	9		115	27 (2)
add 2. wash	8		109	17
Day 2	7			16
	8			16
	8			16
		water bath		
Day 3	8.5	36-44°C	92	16
		water bath		
Day 4	7.5	31-38°C	99	18
		water bath		
Day 5	7	38-40°C	99	20
		water bath		
Day 6	8.9	30-37°C	98	20 (2)
Day 7	7	water bath 37°C	95	19 (2)
Day 8	6.3	heating cabinet	78	15
Day 9	9.3	heating cabinet	81	20 (4)
	9.7	heating cabinet	89	20 (4)

Centrifugation

Volume of fluid and the centrifuge parameters were optimized by trial and error on a Biofuge 17RS centrifuge. As the filters could hold up to 500 µl plasma, this volume was first tested. At 5000 rpm for 5 minutes, four of six filters broke, and the two intact ones did not have enough supernatant to measure. Lower sample volumes and higher speed of centrifugation were tested, and the optimal condition was 13000 rpm for 20 minutes. After 20 minutes, there was no further increase in the supernatant volume (due to occlusion of the filter membranes). There was some tendency of the centrifuge to overheat, so effect of centrifuge time between 15 and 20 minutes was tested (Table 33). The experiments shown in the table are for centrifugation times of 15 to 27 minutes, and also report if the centrifuge overheated and had to be cooled down and restarted (number of times in brackets). The experiment with 15 minutes of centrifugation had a low volume throughput of 78% and the low unbound fraction of 6.5%. This only shows that there is a limit of the range that these parameters can change without altering results. However, there was no indications that centrifugation in the range 16-27 minutes of centrifuging, or the necessity to cool and restart biased the measured unbound fraction.

The column in Table 33 called “% throughput” shows the percentage weight of applied plasma that passed through the filter during centrifugation. As the highest throughput shows 115%, there is an indication of up 15% deviation in the weight that was applied. Throughputs between 85-115% could be considered to be fully centrifuged. The unbound fraction of an experiment with only 81% throughput was still over 9%, which is in the upper part of the range of results. One outlier experiment had only 78% throughput and 6.3% unbound fraction. These results could indicate that a minimum of 80% throughput would be advisable. Prior to and after the filtered spinning, the centrifuge tubes were weighed without the filters, for determining the mass of protein-free plasma available in the tube. After centrifugation, as little as 70 µl would be available. Due to this low volume (already more than four times dilution was necessary for automatic HPLC analysis), the tubes were not vortexed, but a pipette was used to mix the fluid properly before injection to the HPLC.

Only one test was done with throughput below 80%, but there are no indications that percentage throughput as low as 78% would interfere with the unbound fraction, as the measured unbound fraction was higher in the triplicate test with 76 % throughout than in the cases with higher throughput.

Washing the filter would give a higher concentration of unbound fraction, but as further tests of this approach were not done, it is uncertain if this would better emulate the in vivo environment. One experiment was done recovering the proteins after lansoprazole protein binding, whereas the proteins were incubated with 150 µl of buffer and filtrated once more. The results of 5% unbound fraction indicates reversible binding of the compound and adding more volume to the filter in the aim of washing, would then interfere with the equilibrium.

When discussing the experiments with lansoprazole, results are comparable to literature results, in which the washing step was left out.

Reproducibility

To assess reproducibility of the method, a triplicate experiment of lansoprazole was done (Table 34). The standard deviation of the mean free fraction between the triplicates was 3.57%.

Table 34: Reproducibility of lansoprazole protein binding

	% unbound fraction	% std.dev
Lansoprazole 1	7	0.08
Lansoprazole 2	8	0.40
Lansoprazole 3	8	0.13

Out of six measurement of lansoprazole binding to pig plasma protein, the mean percentage bound was 94.5% with a standard deviation of 1.98%. Data and chromatograms are presented in “Appendix B: Raw data tracer protein binding” and “Appendix B: Lansoprazole”.

5.2.4. Results

Standard 30 (lansoprazole) was selected for use as internal standard for the plasma protein binding method, and for validation a similar compound (L20, astemizole) was also measured. These two commercial drugs were tested to compare with literature values of their free fractions (Table 35). Standards 30 and L20 both have literature values of 97% bound (presented value for L20 was 96.7%) in human plasma, and we know that binding in porcine plasma is only a few percent lower. The mean protein binding of lansoprazole in porcine plasma with the developed method was 95% and the mean protein binding of L20 was 94%. This has a closer relation to findings in human serum reported by Eldredge found with compound MS-325 when comparing human serum to porcine plasma [29, 55]. (Table 35 shows the protein binding results for standard 30, L20 and the test compounds synthesized by the PET group at UiO). The plasma protein method developed was made for screening purposes only, and the results are reported to one decimal place of precision.

One additional experiment was done using porcine full blood and the protein binding of standard 30 was measured for three samples injected in triplicates. The result for the experiment showed a protein binding of 97%, which is an increase of 3% from plasma protein binding of 94% measured during the same experiment (Raw data can be seen in Table 80 in Appendix B). This was expected as there would be some binding of compound to

red blood cells as well, though a standard deviation of 34% was seen and further experiments would need to be done to state any conclusions.

Table 35 shows the compounds that were chosen for further experiments with porcine plasma (Raw data can be seen in Table 76 and Table 77 in Appendix B). W1 and W5 were the compounds in the W-group that had shown the best affinity and selectivity values to κ and δ opioid receptors in brain. These tracers showed better selectivity to μ and were also easier to label with ^{18}F compared to other compounds in the group. Within the L-group, the K_D and selectivity data showed that L9 was the best option for vivo experiments. It had better selectivity for binding to τ protein, and had lower K_D values compared to other members of the group.

Table 35: Results for protein binding of newly synthesized tracers

	% protein binding human blood from literature	% protein binding pig blood measurements	% protein binding human blood measurements	Log D measured
standard				
30	97	94.5[!]	97	2.8
C2		77		2.5
L2		93		3.2
L3		91		2.7
L4		100		3.9
L5		96		3.4
L6		94		2.7
L7		87	95*	3.3
L8		91	91	2.5
L9		96	100	3.2
L10		87	92	3.2
L11		100		3.4
L12		98		3.3
L13		98		3.3
L14		76		3.3
L15		95		3.3
L16		90		3.3
L17		100		3.8
L18		96		2.8
L19		97		2.7
Std. 31		100		2.5
Std. 32	96.7	94		5.8
W1		89		3.7
W5		70		3.9
C1		81		3.5
C3		90		2.7
C5		100		3.4

*single point measurement [!]Full blood measurement: 97%

As introduced in chapter 3.5. “Protein binding” an 8% difference has been found for protein binding to human serum as compared to porcine plasma. To make a direct comparison with porcine plasma, human serum was used in the protein binding method with some of the test compounds and standard 30 (Table 35). The standard deviation of standard 30 was 0.1% (All raw data can be seen in Table 78 and Table 79 in Appendix B). Standard 30, and test compounds L8, L9 and L10 were measured in triplicate. Due to limited supply of human serum, L7 was measured only once. Except for L7, the binding of the compounds was 0-5% higher in human serum compared to porcine plasma. The human serum protein binding of standard 30 matched literature values for human serum. L9 and L10 bound 4% and 5% respectively higher to human serum than to pig plasma, and L10 also tended to have higher protein binding than L8 in human serum, binding of L10 was lower than L8 in human serum. These deviations can be explained given the overall 10% standard deviation for standard 30 using this protein binding method. More experiments would be necessary to draw strong conclusions from this study, but present data show a consistently higher binding in human plasma, as reported in the literature.

The compounds tested with porcine plasma had a lipophilicity value in the range of 2.5-3.9 (except L20, which is a commercial drug with lipophilicity of 5.8 and a 94% protein binding in porcine plasma). It may be that there were not enough highly lipophilic compounds to confirm the prediction that high lipophilicity predicts higher protein binding, but as W1, W5 and L9 had lipophilicity in the range of 3.2-3.9, even though their plasma protein binding ranges from 70 to 96%, there are no immediate indications that lower protein binding is necessary for a good PET radiotracer. The lowest protein binding value in the measured group was 70% and the highest was 100%, and both compounds have log D = 3.9. Thus, lipophilicity is not the sole determinant of free fraction.

The polar surface area of the test compounds was in the range of 51-66 $Å^2$. There were no clear trends in the relationships between protein binding and lipophilicity with polar surface area, molecular weight or molecular volume. See 3D graphs (Figure 20, Figure 21 and Figure 22).

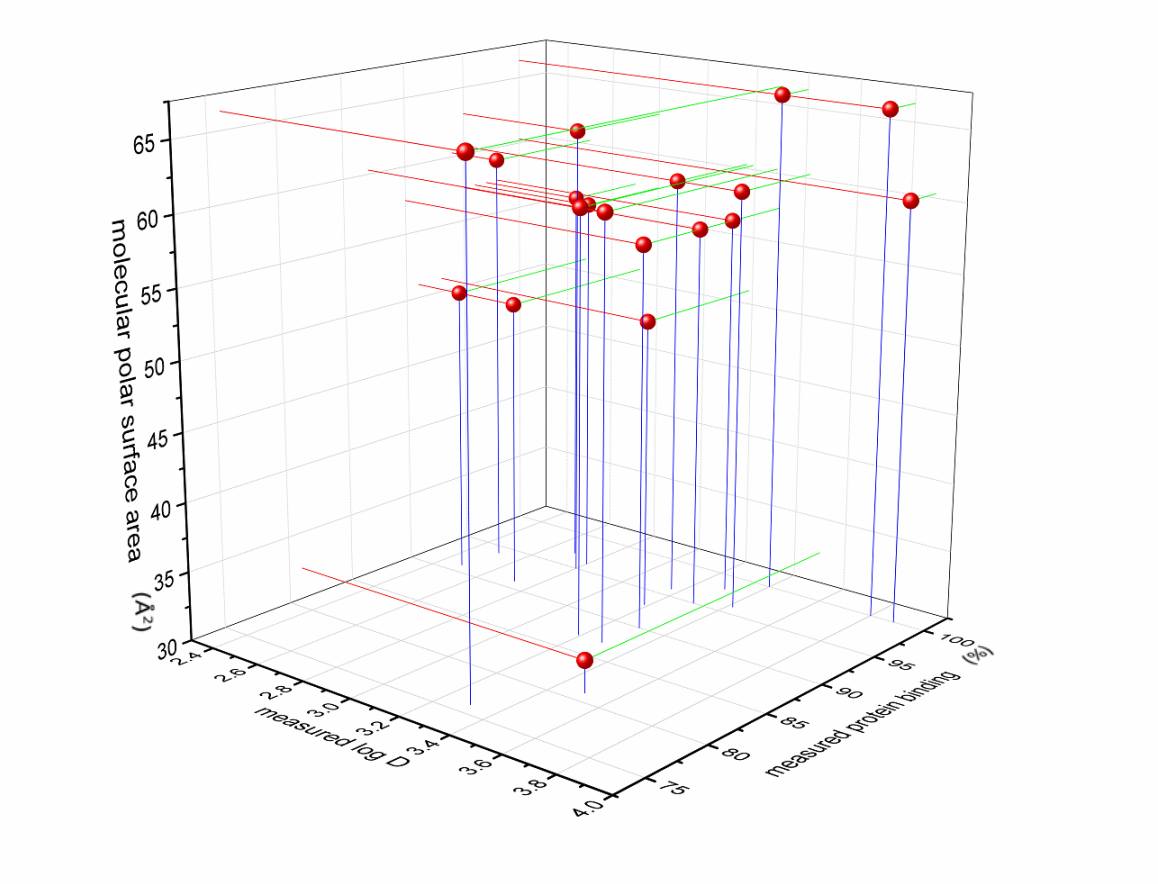

Figure 20: Log D vs Protein Binding vs Polar Surface Area

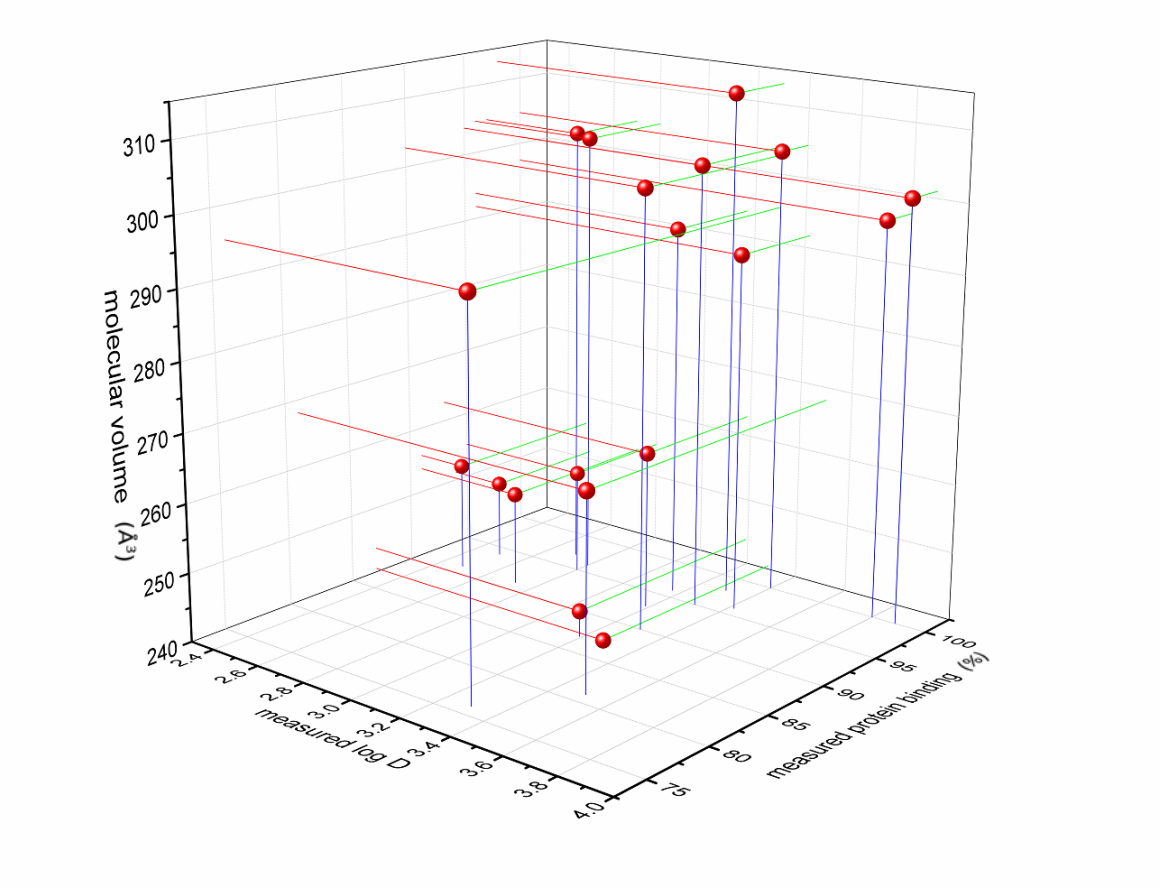

Figure 21: Log D vs Protein Binding vs Molecular Volume

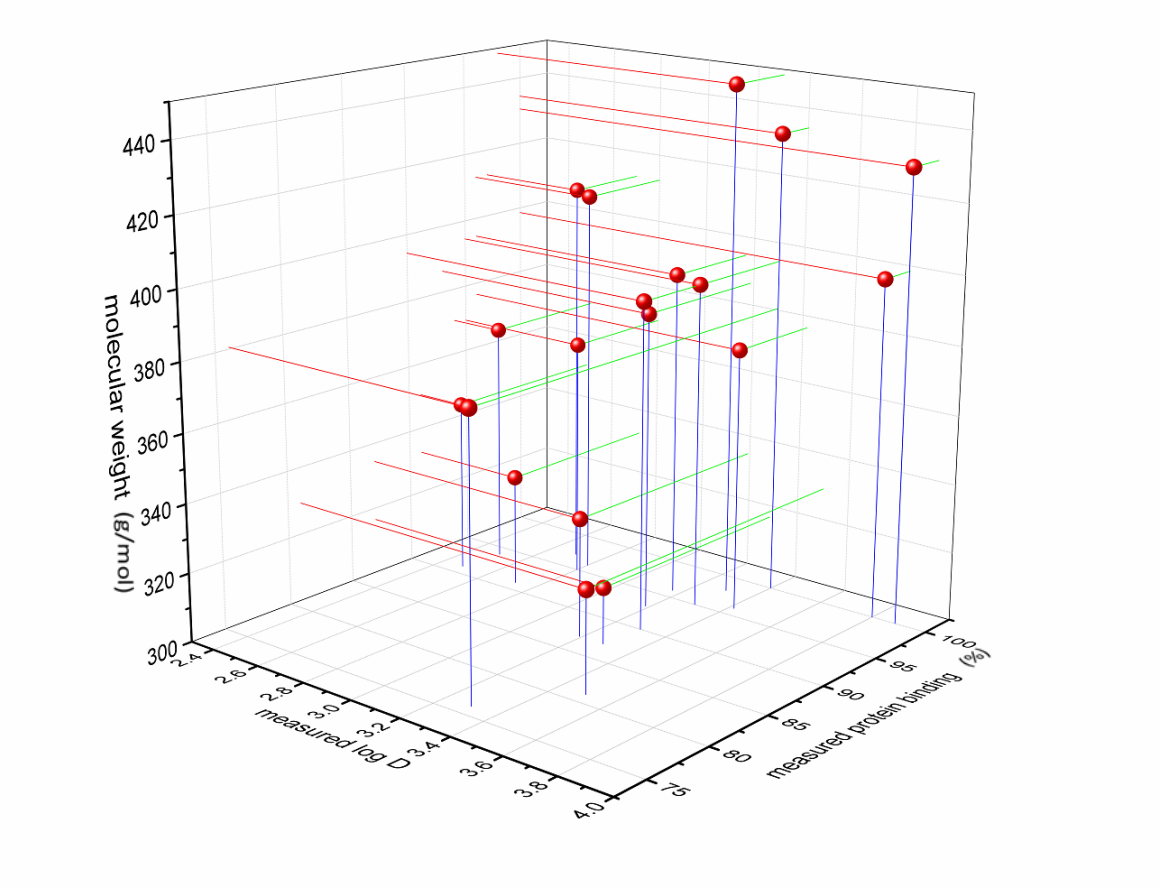

Figure 22: Log D vs Protein Binding vs Molecular Weight

5.3. Significant numbers, errors and retention times

When working with numerical results extending over a range of magnitudes up to 10^9, the number of decimal places can bias the calibration curve equation and hence the results of measurements. When calculating the log D values based on Log k, ten decimal places were used from the equation.

The HPLC retention time changes slightly between experiments (about 2-3% at the most during protein binding assays of warfarin) between the experiments, but remained close within the same experiment and for triplicate measurements of the same sample.

Solubility proved to be a challenge both in lipophilicity measurements and for protein binding measurements. Literature values were not always obtained, and several attempts had to be made to dissolve some of the compounds. Two compounds had to be excluded as neither PBS nor DMSO dissolved them. To test other solvents would require further validation of the protein binding conditions.

6 Conclusions

The aim of this project was to optimize screening methods for tracer development. Two lipophilicity measurement methods and one protein binding method were developed. The HPLC-methods developed show good reproducibility and provide the means to rapidly measure the Log D-value and the protein binding of a broad range of compounds, with sensitivity sufficient for low ligand concentrations. As these methods together comprise branches of the same main assay, it is possible to acquire a large set of data for a group of compounds within a single working day. When synthesizing a new compound, product purity needs to be tested. Using these lipophilicity methods for serves an incidental purity check, and lipophilicity results are given in the same reading. The stock solution made for the purity/lipophilicity test can be used for quantitation of the protein binding without significant changes in buffer systems or hardware.

Several two and three-parameter comparisons were done, aiming to establish a correlation between these properties and tissue uptake distribution, without any major correlations to be found between lipophilicity and plasma protein binding. There were some correlations between MW, PSA and Molecular volume compared to lipophilicity, but no clear trends making the screening of tracers easier. These calculations could not substitute the methods described at this point. To find functions for tracer screening, all aspects discussed should be embedded into a more complex mathematical model. For further investigations, in vivo data should also be compared to the in vitro data obtained during this project.

Conventionally, plasma protein binding is done after separation of the red blood cells. More tests could have been done to distinguish red blood cell and plasma concentrations, and the results could then have been used in other model systems. The plasma protein binding method here described in fact gives only the free fraction, but is not informative about the nature of the binding site. The theory is that the compounds bind to the proteins in the plasma (and red blood cells), and that upon centrifugation through the Microcon filters, only the unbound fraction remains in the measured supernatant. If added the test compound to whole blood prior to separation of plasma, the extent of portioning between plasma and red blood cells might be ascertained.

References

1. Pike, V.W., *PET radiotracers: crossing the blood–brain barrier and surviving metabolism.* Trends in Pharmacological Sciences, 2009. **30**(8): p. 431-440.
2. Sokoloff, L., Reivich, M., Kennedy, C., Des Rosiers, M.H., Patlak, C.S., Pettigrew, K.D., Sakurada, O. and Shinohara, M., *Deoxyglucose-C-14 Method for Measurement Of Local Cerebral Glucose-Utilization - Theory, Procedure, And Normal Values In Conscious And Anesthetized Albino-Rat.* Journal of Neurochemistry, 1977. **28**(5): p. 897-916.
3. Tietze, K.J., *Chapter 5 - Review of Laboratory and Diagnostic Tests*, in *Clinical Skills for Pharmacists (Third Edition)*. 2012, Mosby: Saint Louis. p. 86-122.
4. Shanij, J., Wolf, W., Schlesinger, T., Atkins, H.L., Bradley-Moore, P.R., Casella, V., Fowler, J.S., Greenberg, D., Ido, T., Lambrecht, R.M., MacGregor, R., Mantescu, C., Neirinckx, R., Som, P., Wolf, A.P., Wodinsky, I. and Meaney, K., *Distribution of 18F-5-Fluorouracil in tumor-bearing mice and rats.* International Journal of Nuclear Medicine and Biology, 1978. **5**(1): p. 19-28.
5. Hamacher, K., H.H. Coenen, and G. Stöcklin, *Efficient stereospecific synthesis of no-carrier-added 2-18F-fluoro-2-deoxy-D-glucose using aminopolyether supported nucleophilic substitution.* Journal of nuclear medicine : official publication, Society of Nuclear Medicine, 1986. **27**(2): p. 235.
6. Gunn, R.N., Slifstein, M., Searle, G.E. and Price, J.C., *Quantitative imaging of protein targets in the human brain with PET.* Phys Med Biol, 2015. **60**(22): p. R363-411.
7. Chan, L.M.S., S. Lowes, and B.H. Hirst, *The ABCs of drug transport in intestine and liver: efflux proteins limiting drug absorption and bioavailability.* European Journal of Pharmaceutical Sciences, 2004. **21**(1): p. 25-51.
8. Dhawan, B., Cesselin, F., Raghubir, R., Reisine, T., Bradley, P.B., Portoghese, P.S. and Hamon, M., *International Union of Pharmacology. XII. Classification of opioid receptors.* Pharmacological Reviews, 1996. **48**(4): p. 567-592.
9. Anna, J., F. Jakub, and J. Tomasz, *Opioid Receptors and their Ligands.* Current Topics in Medicinal Chemistry, 2004. **4**(1): p. 1-17.
10. Paolinelli, R., Corada, M., Orsenigo, F. and Dejana, E., *The molecular basis of the blood brain barrier differentiation and maintenance. Is it still a mystery?* Pharmacol. Res., 2011. **63**(3): p. 165-171.
11. Abbott, N.J., Patabendige, A.A.K., Dolman, D.E.M., Yusof, S.R. and Begley, D.J.., *Structure and function of the blood-brain barrier.* Neurobiol. Dis., 2010. **37**(1): p. 13-25.
12. Pardridge, W.M., *Blood-brain barrier delivery.* Drug Discov Today, 2007. **12**(1-2): p. 54-61.
13. Di, L. and E.H. Kerns. *Methods for assessing blood-brain barrier penetration in drug discovery*. 2012. John Wiley & Sons, Inc.
14. Pardridge, W.M., *Brain Drug Targeting: The Future of Brain Drug Development*. 2001: Cambridge University Press. 320 pp.
15. Liu, X., Tu, M., Kelly, R.S., Chen, C. and Smith, B.J., *Development of a computational approach to predict blood-brain barrier permeability.* Drug Metab. Dispos., 2004. **32**(1): p. 132-139.
16. Ohtsuki, S. and T. Terasaki, *Contribution of Carrier-Mediated Transport Systems to the Blood-Brain Barrier as a Supporting and Protecting Interface for the Brain; Importance for CNS Drug Discovery and Development.* Pharm. Res., 2007. **24**(9): p. 1745-1758.
17. Summerfield, S.G., Read, K., Begley, D.J., Obradovic, T., Hidalgo, I.J., Coggon, S., Lewis, A.V., Porter, R.A. and Jeffrey, P., *Central nervous system drug disposition: the relationship between in situ brain permeability and brain free fraction.* J. Pharmacol. Exp. Ther., 2007. **322**(1): p. 205-213.
18. Rutkowska, E., K. Pajak, and K. Jozwiak, *Lipophilicity-methods of determination and its role in medicinal chemistry.* Acta Pol. Pharm., 2013. **70**(1): p. 3-18.

19. Jones, D.R., Hall, S.D., Jackson, E.K., Branch, R.A. and Wilkinson, G.R., *Brain uptake of benzodiazepines: effects of lipophilicity and plasma protein binding.* J. Pharmacol. Exp. Ther., 1988. **245**(3): p. 816-22.
20. Dishino, D.D., Welch, M.J., Kilbourn, M.R. and Raichle, M.E., *Relationship between lipophilicity and brain extraction of C-11-labeled radiopharmaceuticals.* J Nucl Med, 1983. **24**(11): p. 1030-8.
21. Li, A.P., *Screening for human ADME/Tox drug properties in drug discovery.* Drug Discovery Today, 2001. **6**(7): p. 357-366.
22. Kerns, E.H., *High throughput physicochemical profiling for drug discovery.* J. Pharm. Sci., 2001. **90**(11): p. 1838-1858.
23. C.Hansch, A.L., D.Hoekman. *Exploring QSAR: Hydrophobic, Electronic, and Steric Constants*. 1995 [cited 2016 19.12.16].
24. Leeson, P.D. and B. Springthorpe, *The influence of drug-like concepts on decision-making in medicinal chemistry.* Nat. Rev. Drug Discovery, 2007. **6**(11): p. 881-890.
25. Waterhouse, R.N., *Determination of lipophilicity and its use as a predictor of blood-brain barrier penetration of molecular imaging agents.* Mol Imaging Biol, 2003. **5**(6): p. 376-89.
26. Tanaka, H. and K. Mizojiri, *Drug-protein binding and blood-brain barrier permeability.* J. Pharmacol. Exp. Ther., 1999. **288**(3): p. 912-918.
27. Lin, T.H. and J.H. Lin, *Effects of protein binding and experimental disease states on brain uptake of benzodiazepines in rats.* J. Pharmacol. Exp. Ther., 1990. **253**(1): p. 45-50.
28. Bohnert, T. and L.-S. Gan, *Plasma protein binding: From discovery to development.* Journal of Pharmaceutical Sciences, 2013. **102**(9): p. 2953-2994.
29. Eldredge, H.B., Spiller, M., Chasse, J.M., Greenwood, M.T. and Caravan, P., *Species dependence on plasma protein binding and relaxivity of the gadolinium-based MRI contrast agent MS-325.* Investigative radiology, 2006. **41**(3): p. 229.
30. OECD, *Test No. 117: Partition Coefficient (n-octanol/water), HPLC Method*. OECD Publishing.
31. Millipore, M., *User guide Microcon® Centrifugal Filter Devices*, in *PR04305*. 2013, Merck Millipore Ltd.
32. Lombardo, F., Shalaeva, M.Y., Tupper, K.a. and Gao, F., *ElogDoct: A Tool for Lipophilicity Determination in Drug Discovery. 2. Basic and Neutral Compounds.* Journal of Medicinal Chemistry, 2001. **44**(15): p. 2490-2497.
33. Sangster, J. *Octanol-Water Partition Coefficients of Simple Organic Compounds*. 1989 [cited 2016 19.12.16].
34. Gulyaeva, N., Zaslavsky, A., Lechner, P., Chlenov, M., McConnell, O., Chait, A., Kipnis, V. and Zaslavsky, B., *Relative hydrophobicity and lipophilicity of drugs measured by aqueous two-phase partitioning, octanol-buffer partitioning and HPLC. A simple model for predicting blood-brain distribution.* European Journal of Medicinal Chemistry, 2003. **38**(4): p. 391-396.
35. Lab, V.-M. *Lansoprazole*. 2016 [cited 2016 19.12.16].
36. Willighagen, E.L., Denissen, H.M. Wehrens, R. and Buydens, L.M., *On the Use of 1H and 13C 1D NMR Spectra as QSPR Descriptors.* Journal of Chemical Information and Modeling, 2006. **46**(2): p. 487-494.
37. Kar, S., Harding, A.P., Roy, K. and Popelier, P.L., *QSAR with quantum topological molecular similarity indices: toxicity of aromatic aldehydes to Tetrahymena pyriformis.* SAR and QSAR in Environmental Research, 2010. **21**(1-2): p. 149-168.
38. Andrés, A., Rosés, M., Ràfols, C., Bosch, E., Espinosa, S., Segarra, V. and Huerta, J.M., *Setup and validation of shake-flask procedures for the determination of partition coefficients (log D) from low drug amounts.* European Journal of Pharmaceutical Sciences, 2015. **76**: p. 181-191
39. S Bharate, S., V. Kumar, and R. A Vishwakarma, *Determining partition coefficient (Log P), distribution coefficient (Log D) and ionization constant (pKa) in early drug discovery.* Combinatorial chemistry & high throughput screening, 2016. **19**(6): p. 461-469.
40. Avdeef, A., *Octanol–Water Partitioning*, in *Absorption and Drug Development*. 2012, John Wiley & Sons, Inc. p. 174-219.

41. Nakashima, S., Yamamoto, K., Arai, Y. and Ikeda, Y., *Impact of Physicochemical Profiling for Rational Approach on Drug Discovery.* Chemical and Pharmaceutical Bulletin, 2013. **61**(12): p. 1228-1238.
42. Medicine, T.-U.N.L.o., https://chem.nlm.nih.gov/chemidplus/name/4-ethyltoluene. 2016.
43. Shao, X., Carpenter, G.M., Desmond, T.J., Sherman, P., Quesada, C.A., Fawaz, M., Brooks, A.F., Kilbourn, M.R., Albin, R.L., Frey, K.A. and Scott, P.J.H., *Evaluation of [11C]N-Methyl Lansoprazole as a Radiopharmaceutical for PET Imaging of Tau Neurofibrillary Tangles.* ACS Medicinal Chemistry Letters, 2012. **3**(11): p. 936-941.
44. Hooker, J.M., Kim, S.W., Reibel, A.T., Alexoff, D., Xu, Y. and Shea, C., *Evaluation of [11C]metergoline as a PET radiotracer for 5HTR in nonhuman primates.* Bioorganic & Medicinal Chemistry, 2010. **18**(22): p. 7739-7745.
45. Di, L., Kerns, E.H., Bezar, I.F., Petusky, S.L. and Huang, Y., *Comparison of blood-brain barrier permeability assays: in situ brain perfusion, MDR1-MDCKII and PAMPA-BBB.* J. Pharm. Sci., 2009. **98**(6): p. 1980-1991.
46. Chen, C., Wu, D., Guo, Z., Xie, Q., Reinhart, G.J., Madan, A., Wen, J., Chen, T., Huang, C.Q., Chen, M., Chen, Y., Tucci, F.C., Rowbottom, M., Pontillo, J., Zhu, Y.F., Wade, W., Saunders, J., Bozigian, H. and Struthers, R.S., *Discovery of sodium R-(+)-4-{2-5-(2-fluoro-3-methoxyphenyl)-3-(2-fluoro-6-trifluoromethylbenzyl)-4-methyl-2,6-dioxo-3,6-dihydro-2H-pyrimidin-1-yl-1-phenylethylamino}butyrate (elagolix), a potent and orally available nonpeptide antagonist of the human gonadotropin-releasing hormone receptor.* Journal of medicinal chemistry, 2008. **51**(23): p. 7478.
47. Van de Waterbeemd, H., D.A. Smith, and B.C. Jones, *Lipophilicity in PK design: methyl, ethyl, futile.* J. Comput.-Aided Mol. Des., 2001. **15**(3): p. 273-286.
48. Poulin, P. and F.-P. Theil, *Prediction of pharmacokinetics prior to in vivo studies.: II. Generic physiologically based pharmacokinetic models of drug disposition.* J. Pharm. Sci., 2002. **91**(5): p. 1358-1370.
49. Zavrel, M., K. Kochanowski, and A.C. Spiess, *Comparison of different approaches and computer programs for progress curve analysis of enzyme kinetics.* Engineering in Life Sciences, 2010. **10**(3): p. 191-200.
50. Support, M. *Floating-point arithmetic may give inaccurate results in Excel*. 2010.
51. Ashe, C.G. *Safety Data Sheet Dimethyl Sulfoxide (DMSO)*. 2016 [cited 2016.
52. Platts, J.A., Oldfield, S.P., Reif, M.M., Palmucci, A., Gabano, E. and Osella, D., *The RP-HPLC measurement and QSPR analysis of log P o/w values of several Pt(II) complexes.* Journal of Inorganic Biochemistry, 2006. **100**(7): p. 1199-1207.
53. Giaginis, C. and A. Tsantili‐Kakoulidou, *Current State of the Art in HPLC Methodology for Lipophilicity Assessment of Basic Drugs. A Review.* Journal of Liquid Chromatography & Related Technologies, 2007. **31**(1): p. 79-96.
54. Valko, K., *Application of high-performance liquid chromatography based measurements of lipophilicity to model biological distribution.* J. Chromatogr. A, 2004. **1037**(1-2): p. 299-310.
55. Sondeen, L.J., de Guzman, R., Amy Polykratis, I., Dale Prince, M., Hernandez, O., Cap, A.P., Dubick, M.A., *Comparison between human and porcine thromboelastograph parameters in response to ex-vivo changes to platelets, plasma, and red blood cells.* Blood Coagulation & Fibrinolysis, 2013. **24**(8): p. 818-829.
56. Schoultz, B.W., Hjørnevik, T. Reed, B.J., Marton, J., Coello, C.S., Willoch, F. and Henriksen, G., *Synthesis and evaluation of three structurally related ^{18}F-labeled orvinols of different intrinsic activities: 6-O-^{18}Ffluoroethyl-diprenorphine (^{18}FFDPN), 6-O-^{18}Ffluoroethyl-buprenorphine (^{18}FFBPN), and 6-O-^{18}Ffluoroethyl-phenethyl-orvinol (^{18}FFPEO).* Journal of medicinal chemistry, 2014. **57**(12): p. 5464.
57. Arzoumanian, L. *Tech Talk; The BD Technical Services Department receivesmany questions about our products.* 2002 [cited 2016 26.12.16]; Tech Talk new bulletin for www.bd.com].
58. Alliance, N.B.C. *Blood Clot Treatment Anticoagulants: Treatment of Blood Clots*. [webpage.org] 2014 April 2014 [cited 2016 27.12.16].

59. Mullokandov E., A.J., Szalkiewicz A., Babayeva M. , *Protein Binding Drug Interaction between Warfarin and Tizoxanide in Human Plasma.* Austin Journal of Pharmacology and Theraperutics, 2014.
60. Shlomo Melmed, K.S.P., P. Reed Larsen, Henry M. Kronenberg, *Williams textbook of endocrinology*. 2016, Elsevier Health Sciences.
61. Thomson, *Drug Information for the Health Care Professional*. 2004.
62. Aldrich, S. *Cat. No. T1500TESTOSTERONE--DEA SCHEDULE III*. 2016 [cited 2016 08.01.16]; Product information data sheet].
63. Vermeulen, A. and L. Verdonck, *Studies on the binding of testosterone to human plasma.* Steroids, 1968. **11**(5): p. 609-635.
64. Södergard, R., Bäckström, T, Shanbhag, V. and Carstensen, H., *Calculation of free and bound fractions of testosterone and estradiol-17 beta to human plasma proteins at body temperature.* Journal of Steroid Biochemistry, 1982. **16**(6): p. 801-810.

Appendix A: Lipophilicity

Data from method development of lipophilicity measurements

Table 36 shows the standards product names and their associated IUPAC names.

Table 36: The standards product names and associated IUPAC names, standard 21 was withdrawn due to unsure literature data

Std. no.	Standard names	IUPAC names
1	Uracil	pyrimidine-2,4(1H,3H)-dione
2	Acetaminophen	N-(4-hydroxyphenyl)acetamide
3	2-Butanone	butan-2-one
4	Benzaldehyde	Benzaldehyde
5	4-Fluorobenzaldehyde	4-fluorobenzaldehyde
6	Acetophenone	Acetophenone
7	Anisaldehyde	4-methoxybenzaldehyde
8	Trans-cinnamaldehyde	trans-cinnamaldehyde
9	Benzene	Benzene
10	Omeprazole	5-methoxy-2-(((4-methoxy-3,5-dimethyl-pyridin-2-yl)methyl)sulfinyl)-1H-benzo[d]imidazole
11	4-Chlorobenzaldehyde	4-chlorobenzaldehyde
12	Toluene	Toluene
13	Brombenzene	Brombenzene
14	Benzophenone	Benzophenone
15	Iodobenzene	Iodobenzene
16	4-Tertbutylbenzaldehyde	4-(tert-butyl)benzaldehyde
17	Testosterone	(8R,9S,10R,13S,14S,17S)-17-hydroxy-10,13-dimethyl-1,2,6,7,8,9,10,11,12,13,14,15,16,17-tetradecahydro-3H-cyclopenta[a]phenanthren-3-one
18	Naphthalene	Naphthalene
19	Flutamide	N-(4-nitro-3-(trifluoromethyl)phenyl)isobutyramide
20	4-Ethyltoluene	4-ethyltoluene
21	2-Iodoethylbenzene	2-iodoethylbenzene
22	Estradiol	(8R,9S,13S,14S,17S)-13-methyl-7,8,9,11,12,13,14,15,16,17-decahydro-6H-cyclopenta[a]phenanthrene-3,17-diol
23	2-Hydroxybenzaldehyde phenylhydrazone	(E)-2-((2-phenylhydrazineylidene)methyl)phenol
24	Bifonazole	1-([1,1'-biphenyl]-4-yl(phenyl)methyl)-1H-

		imidazole
25	Promethazine	N,N-dimethyl-1-(10H-phenothiazin-10-yl)propan-2-amine
26	Tolnaftate	O-(naphthalen-2-yl) methyl(m-tolyl)carbamothioate
27	Loratadin	ethyl 4-(8-chloro-5,6-dihydro-11H-benzo[5,6]cyclohepta-[1,2-b]pyridin-11-ylidene)piperidine-1-carboxylate
28	Chlorpromazine	3-(2-chloro-10H-phenothiazin-10-yl)-N,N-dimethylpropan-1-amine
29	Triflupromazine	N,N-dimethyl-3-(2-(trifluoromethyl)-10H-phenothiazin-10-yl)propan-1-amine
30	Lansoprazole	2-(((3-methyl-4-(2,2,2-trifluoroethoxy)-pyridin-2-yl)methyl)sulfinyl)-1H-benzo[d]imidazole
31	Altanserin	3-(2-(4-(4-fluorobenzoyl)piperidin-1-yl)ethyl)-2-thioxo-2,3-dihydroquinazolin-4(1H)-one
32	Astemizole	1-(4-fluorobenzyl)-N-(1-(4-methoxyphenethyl)piperidin-4-yl)-1H-benzo[d]imidazol-2-amine
33	Elagolix	(R)-4-((2-(5-(2-fluoro-3-methoxyphenyl)-3-(2-fluoro-6-(trifluoromethyl)benzyl)-4-methyl-2,6-dioxo-3,6-dihydropyrimidin-1(2H)-yl)-1-phenylethyl)amino)butanoic acid
34	Warfarin	4-hydroxy-3-(3-oxo-1-phenylbutyl)-2H-chromen-2-one
35	Naloxone	17-Allyl-4,5alpha-epoxy-3,14-dihydroxymorphinan-6-one hydrochloride
36	Tyrosine	L-tyrosine
37	Trimipramine	3-(10,11-dihydro-5H-dibenzo[b,f]azepin-5-yl)-N,N,2-trimethylpropan-1-amine
38	Dexamethasone	(8S,9R,10S,11S,13S,14S,16R,17R)-9-fluoro-11,17-dihydroxy-17-(2-hydroxyacetyl)-10,13,16-trimethyl-6,7,8,9,10,11,12,13,14,15,16,17-dodecahydro-3H-cyclopenta[a]phenanthren-3-one
39	Chlorthalidone	2-chloro-5-(1-hydroxy-3-oxoisoindolin-1-yl)benzenesulfonamide
40	Clonidine	N-(2,6-dichlorophenyl)-4,5-dihydro-1H-imidazol-2-amine
41	Trazodone	2-(3-(4-(3-chlorophenyl)piperazin-1-yl)propyl)-[1,2,4]triazolo[4,3-a]pyridin-3(2H)-one
42	Flumazenil	ethyl 8-fluoro-5-methyl-6-oxo-5,6-dihydro-4H-benzo[f]imidazo[1,5-a][1,4]diazepine-3-carboxylate
43	Loperamide	4-[4-(4-Chlorophenyl)-4-hydroxypiperidin-1-yl]-

		N,N-dimethyl-2,2-diphenylbutanamide
44	Trifluoperazine	1010-[3-(4-methylpiperazin-1-yl)propyl]-2-(trifluoromethyl)phenothiazine
45	Diprenorphine	(5α,7α)-17-(Cyclopropylmethyl)- 4,5-epoxy-18,19-dihydro- 3-hydroxy- 6-methoxy- α,α-dimethyl- 6,14-ethenomorphinan- 7-methanol
C1	AH-7921	3,4-dichloro-N-((1-(dimethylamino)cyclohexyl)methyl)benzamide
C2	N-methyl lansoprazole	1-methyl-2-(((3-methyl-4-(2,2,2-trifluoroethoxy)pyridin-2-yl)methyl)sulfinyl)-1H-benzo[d]imidazole
C3	RO-04-5595	1-[2-(4-Chlorophenyl)ethyl]-1,2,3,4-tetrahydro-6-methoxy-2-methyl-7-isoquinolinol
C4	Protriptyline	3-(5H-dibenzo[a,d][7]annulen-5-yl)-N-methylpropan-1-amine
C5	PR04	N-4-Fluorobut-2-yn-1-yl-2ss-carbo-[^{11}C]methoxy-3ss-phenyltropane
C6	WAY 207024	6-[[4-[2-(4-tert-butylphenyl)-1H-benzimidazol-4-yl]piperazin-1-yl]methyl]quinoxaline
C7	AG 045572	5-[5,6,7,8-Tetrahydro-3,5,5,8,8-pentamethyl-2-naphthalenyl-methyl]-N-(2,4,6-trimethoxyphenyl)-2-furancarboxamide
C8	GBR 12909 dihydrochloride	1-[2-[*Bis*-(4-fluorophenyl)methoxy]ethyl]-4-(3-phenylpropyl)piperazine dihydrochloride

C1-C3 are compounds measured with the two methods without using them in the calibration curves. C1 and C3 did not show any literature results. Results are shown in Table 11.

Calibration curve data

The data to make the calibration curve for method A is shown in Table 37 and Table 38.

Table 37: Data for making calibration curve with method A, 26 compounds. Red compounds were discharged due to lack of linearity

Standard	Peak T_R (min)	Average peak T_R (min)	Capacity factor, k	Std.dev peak	Log D
1	1.621	1.621	0.00	0.000	-1.1
	1.621				
	1.621				
2	1.717	1.721	0.06	0.006	0.5
	1.728				
	1.717				
3	1.824	1.817	0.12	0.006	0.4
	1.813				
	1.813				
4	3.040	3.036	0.87	0.006	1.6
	3.040				
	3.029				
5	3.264	3.253	1.01	0.011	1.5
	3.243				
	3.253				
6	3.392	3.392	1.09	0.000	1.6
	3.392				
	3.392				
7	3.307	3.307	1.04	0.000	1.7
	3.307				
	3.307				
8	4.139	4.139	1.55	0.000	2.1
	4.139				
	4.139				
9	5.760	5.753	2.55	0.006	2.1
	5.749				
	5.749				
10	5.067	5.067	2.13	0.000	2.3
	5.067				
	5.067				
11	5.195	5.184	2.20	0.011	2.1
	5.184				
	5.173				
12	10.773	10.780	5.65	0.013	2.7
	10.773				
	10.795				

13	13.120	13.106	7.09	0.012	3.0
	13.099				
	13.099				
14	12.843	12.829	6.91	0.016	3.2
	12.832				
	12.811				
15	18.005	18.044	10.13	0.038	3.3
	18.080				
	18.048				
16	19.339	19.175	10.83	0.511	3.3
	19.584				
	18.603				
17	17.963	17.956	10.08	0.022	3.3
	17.931				
	17.973				
18	24.629	24.618	14.19	0.049	3.4
	24.661				
	24.565				
19	17.803	17.724	9.93	0.145	2.6
	17.813				
	17.557				
20	42.795	43.079	25.58	0.247	3.6
	43.243				
	43.200				
21	37.451	37.579	22.18	0.111	3.6
	37.632				
	37.653				
23	33.163	34.564	20.32	1.263	4.2
	35.616				
	34.912				
30	6.117	6.135	2.99	0.016	2.8
	6.140				
	6.148				
34	2.075	2.076	0.35	0.002	0.9
	2.078				
	2.074				
35	5.682	5.699	2.71	0.042	2.6
	5.747				
	5.668				
40	2.746	2.737	0.78	0.009	1.6
	2.736				
	2.729				
41	19.029	18.847	11.26	0.159	3.4
	18.778				
	18.734				

Standard 1 was only used for dead time calculations and standard 2, 19 and 23 was dropped to get higher R^2 value for method A.

Table 38 shows calculated log k for the standards of method A and their deviations from literature.

Table 38: Calculations from retention time to k-factor and comparison between literature log D and the measured result obtained from the calibration curve for method A

Log k	Log D	Compound	Calculated log D from curve	Deviation from literature
-0.9	0.4	2	0.3	0.1
-0.5	0.9	34	1.0	-0.1
-0.1	1.5	4	1.6	-0.1
0.0	1.5	5	1.7	-0.2
0.0	1.6	6	1.8	-0.2
-0.2	1.6	42	1.4	0.2
-0.1	1.6	40	1.6	0.0
0.0	1.7	7	1.7	0.0
0.2	2.1	8	2.0	0.1
0.4	2.1	9	2.3	-0.2
0.3	2.3	10	2.2	0.1
0.4	2.6	35	2.4	0.2
0.3	2.1	11	2.2	-0.1
1.1	3.4	41	3.3	0.1
0.8	2.7	12	2.8	-0.1
0.5	2.8	30	2.4	-0.2
0.9	3.0	13	3.0	0.0
0.8	3.2	14	3.0	0.2
1.0	3.3	15	3.2	0.0

1.0	3.3	16	3.3	0.0
1.0	3.2	17	3.2	0.0
1.2	3.4	18	3.5	-0.1
1.4	3.6	20	3.8	-0.2

The data for method B calibration curve is shown in Table 39 and Table 40.

Table 39: Data for making calibration curve with method B, standards in red were discharged from calibration curve

Standard	Peak T_R (min)	Average peak T_R (min)	Capacity factor, k	Std.dev peak	Log D
1	0.811	0.811	0.00	0.000	-1.1
	0.811				
	0.811				
2	0.821	0.821	0.01	0.000	0.5
	0.821				
	0.821				
3	0.853	0.850	0.05	0.006	0.4
	0.853				
	0.843				
4	0.971	0.967	0.19	0.006	1.6
	0.960				
	0.971				
5	0.971	0.971	0.20	0.000	1.5
	0.971				
	0.971				
6	0.981	0.981	0.21	0.000	1.6
	0.981				
	0.981				
7	0.971	0.967	0.19	0.006	1.7
	0.960				
	0.971				
8	1.103	1.043	0.29	0.052	2.1
	1.013				
	1.013				
9	1.227	1.227	0.51	0.000	2.1
	1.227				
	1.227				
10	0.992	0.992	0.22	0.000	2.3
	0.992				
	0.992				
11	1.109	1.109	0.37	0.000	2.1
	1.109				
	1.109				

12	1.515	1.518	0.87	0.006	2.7
	1.525				
	1.515				
13	1.568	1.561	0.92	0.012	3.0
	1.568				
	1.547				
14	1.344	1.344	0.66	0.000	3.2
	1.344				
	1.344				
15	1.760	1.760	1.17	0.000	3.3
	1.760				
	1.760				
16	1.600	1.600	0.97	0.000	3.3
	1.600				
	1.600				
17	1.397	1.397	0.72	0.000	3.3
	1.397				
	1.397				
18	1.824	1.824	1.25	0.011	3.4
	1.835				
	1.813				
19	1.280	1.245	0.53	0.031	3.4
	1.227				
	1.227				
20	2.667	2.667	2.29	0.000	3.6
	2.667				
	2.667				
21	2.165	1.821	1.22	0.587	3.6
	2.155				
	1.144				
23	1.589	1.593	0.94	0.006	4.2
	1.589				
	1.600				
24	2.624	2.620	2.19	0.006	4.8
	2.624				
	2.613				
25	3.232	3.331	3.05	0.090	3.8
	3.349				
	3.413				
26	3.008	2.997	2.65	0.018	5.1
	3.008				
	2.976				
27	2.517	2.521	2.07	0.006	5.2
	2.528				
	2.517				
28	2.688	2.713	2.30	0.027	5.4

	2.709				
	2.741				
29	3.371	3.371	3.10	0.022	5.5
	3.392				
	3.349				
30	1.088	1.088	0.34	0.001	2.2
	1.089				
	1.088				
31	1.242	1.242	0.53	0.001	2.5
	1.243				
	1.241				
33	1.012	1.013	0.25	0.001	0.8
	1.013				
	1.014				
37	2.269	2.262	1.85	0.007	4.1
	2.260				
	2.256				
38	0.926	0.926	0.17	0.001	1.7
	0.927				
	0.926				
43	1.135	1.134	0.43	0.001	2.6
	1.134				
	1.134				

Table 40: Calculations from retention time to k-factor and comparison between literature log D and the measured result obtained from the calibration curve for method B

Log k	Log D	Compound	Calculated log D from calibration curve	Deviation from literature
-0.7	1.6	4	1.7	0.1
-0.7	1.5	5	1.7	0.2
-0.7	1.6	6	1.7	0.1
-0.8	1.7	38	1.5	-0.2
-0.7	1.7	7	1.7	0.0
-0.6	2.0	33	1.9	-0.1
-0.5	2.1	8	2.1	0.0
-0.4	2.1	11	2.3	0.2
-0.3	2.5	31	2.7	0.2
-0.4	2.6	43	2.5	-0.1
-0.5	2.2	30	2.3	0.1
0.0	3.0	13	3.3	0.3
-0.2	3.2	14	3.0	-0.2
0.1	3.3	15	3.6	0.2
0.0	3.3	16	3.4	0.0
-0.1	3.2	17	3.1	-0.1
0.1	3.4	18	3.6	0.2
-0.3	3.4	19	2.7	0.1
0.3	3.8	25	4.1	0.3
0.3	4.1	37	4.0	-0.1
0.3	4.3	28	4.1	-0.2
0.3	4.8	24	4.2	-0.6
0.3	4.4	27	4.2	-0.2
0.5	4.2	29	4.6	0.4

Lipophilicity measurements raw data

The table below shows raw data for all lipophilicity measurements. The results are divided between the two methods by colour.

Table 41: Raw data for lipophilicity measurements

Compound	T_R (min)	Std. dev. (min)	Log k	Log D
L2	16.658	0.027	1.0	3.1
L3	9.237	0.022	0.7	2.7
L4	43.605	0.075	1.4	3.8
L5	22.709	0.251	1.1	3.4
L6	0.945	0.001	-0.7	1.7
L7	19.065	0.219	1.0	3.2
L8	6.990	0.027	0.5	2.5
L9	16.202	0.049	1.0	3.1
L10	16.779	0.032	1.0	3.2
L11	1.111	0.001	-0.4	2.4
L12	1.090	0.001	-0.4	2.4
L13	1.083	0.001	-0.4	2.3
L14	1.077	0.001	-0.4	2.3
L15	1.080	0.001	-0.4	2.3
L16	1.069	0.001	-0.4	2.3
L17	1.254	0.001	-0.2	2.8
L18	0.956	0.002	-0.7	1.7
L19	0.951	0.000	-0.7	1.7
W1	34.759	1.346	1.3	3.7
W3	9.593	0.512	0.7	2.7
W4	42.848	1.770	1.4	3.8
W5	43.15	0.432	1.4	3.8
W6	10.962	0.016	0.8	2.8
W7	55.876	1.216	1.5	4.0
W8	1.454	0.016	-0.1	3.1
W10	1.173	0.000	-0.4	2.5
W11	1.486	0.012	-0.1	3.2
W12	1.419	0.000	-0.1	3.0
W13	1.266	0.006	-0.3	2.7
W14	12.08	0.301	0.8	2.9
W15	1.131	0.000	-0.4	2.4
W16	14.432	0.139	0.9	3.0
W17	28.135	0.713	1.2	3.5
W18	1.166	0.006	-0.4	2.4
J1	3.591	0.038	0.1	1.8

J3	2.382	0.016	0.3	4.1
J4	20.299	0.105	1.1	3.3
J5	1.429	0.000	-0.1	3.0
J6	1.184	0.000	-0.3	2.5
J7	14.869	0.022	0.9	3.1
J8	1.344	0.000	-0.2	2.9
J9	9.148	0.098	0.7	2.7
J10	9.241	0.153	0.7	2.7
J11	1.909	0.000	0.1	3.7
J12	1.881	0.006	0.1	3.7
J13	1.042	0.031	-0.6	2.0
J14	1.422	0.006	-0.1	4.0
J15	1.402	0.006	-0.1	3.0
J16	2.322	0.006	0.3	4.0
J17	1.195	0.000	-0.3	2.6
J18	1.955	0.016	0.1	3.7
J19	1.831	0.006	0.1	3.6
C1	1.300	0.001	-0.7	2.9
C2	7.438	0.006	0.6	2.5
C3	1.237	0.000	-0.3	2.7
C4	0.638	0.01	-0.2	2.9
C5	1.590	0.021	0.0	3.4

method A
method B

Data for comparison graphs in Figure 10

Data for all trend curves for comparison between compounds properties in Figure 10 is shown in Table 42.

Table 42: Chemical properties for comparison trend curves

Compounds	Measured log D	Molecular volume ($Å^3$)	Molecular polar surface area ($Å^2$)	Molecular weight (g/mol)	M ref (m^3/mol)
Lansoprazole	2.8	255.1	63.1	369.4	8.8
Uracil	-1.1	65.7	58.2	112.1	2.7
Acetaminophen	0.3	96.8	49.3	151.2	4.2
2-butanone	0.4	73.1	17.1	72.1	2.1
Benzaldehyde	1.5	86.4	17.1	106.1	3.2
4-fluorobenzaldehyde	1.5	89.6	17.1	124.1	3.2
Acetophenone	1.6	102.6	17.1	120.2	3.7
Anisaldehyde	1.7	107.9	26.3	136.2	3.8
trans-Cinnamaldehyde	2.1	108.9	17.1	132.2	4.4
Benzene	2.1	71.1		78.1	2.7
Omeprazole	2.2	265.8	72.3	345.4	9.4
4-chlorobenzaldehyde	2.2	100.7	17.1	140.6	3.7
Toluene	2.7	87.9		92.1	3.2
Brombenzene	3.0	91.1		157.0	3.5
Benzophenone	3.2	148.9	17.1	182.2	5.7
Iodobenzene	3.3	98.3		204.0	4.0
4-tertbutylbenzaldehyde	3.3	153.8	17.1	162.2	5.0
Testosterone	3.3	281.4	37.3	288.4	8.5
Naphtalene	3.4	109.5		128.0	4.4
Flutamide	3.4	199.2	80.9	276.2	6.1
4-ethyltoluene	3.6	120.8		120.2	4.1
2-iodoethylbenzene	3.6	131.2		232.1	4.9
Estradiol	4.0	183.7	40.5	272.4	8.0
2-hydroxybenzaldehyde phenylhydrazone	4.2	169.1	44.6	212.3	6.7
Bifonazole	4.8	261.1	15.6	310.4	9.9
Tolnaftate	5.1	251.1	14.5	307.4	9.7
Loratadine	5.2	322.4	41.9	382.9	10.8
Triflupromazine	5.5	352.4	6.5	352.4	9.4
Promethazine	3.8	237.4	6.5	284.4	8.9
Chlorpromazine	4.3	256.3	6.5	318.9	9.4
LANSO 01	3.2	262.9	51.0	386.4	
LANSO 02	2.7	253.6	51.0	332.4	
LANSO 03	3.9	301.0	60.3	430.5	

LANSO 04	3.4	291.8	60.3	376.5	
LANSO 05	2.7	251.2	60.3	370.3	
LANSO 06	3.3	240.5	60.3	316.4	
LANSO 07	2.5	255.7	51.0	350.4	
LANSO 08	3.2	293.8	60.3	394.5	
LANSO 09	3.2	243.7	60.3	334.4	
LANSO 10	3.4	304.7	66.3	434.4	
LANSO 11-1	3.3	313.0	57.5	448.5	
LANSO 11-2	3.3	313.0	57.5	448.5	
LANSO 12	3.3	295.2	66.3	380.5	
LANSO 13-1	3.3	304.0	57.5	394.5	
LANSO 13-2	3.3	302.8	57.5	394.5	
LANSO 14	3.8	297.4	66.3	398.5	
LANSO 15-1	2.8	304.7	57.5	412.5	
LANSO 15-2	2.7	304.6	57.5	412.5	
LANSO-methyl	2.5	272.9	54.3	383.4	
Astemizole	5.8		40.1	458.6	
AH-7921	4.0	268.1	32.3	329.3	
WR-01	3.7	256.6	32.3	312.8	
WR-02		270.3	84.2	339.8	
WR-03	2.7	260.6	41.6	290.4	
WR-04	3.9	269.5	32.3	346.4	
WR-05	3.9	269.1	32.3	346.4	
WR-06	2.9	257.4	84.2	305.4	
WR-07	4.1		32.3	384.5	
WR-08	3.5	267.4	32.3	329.3	
WR-09		303.2	23.6	375.3	
WR-10	2.9	270.4	41.6	344.4	
WR-11	3.6	296.1	32.3	396.4	
WR-12	3.5	287.4	23.6	343.3	
WR-13	3.1	276.5	23.6	326.8	
WR-14	2.9	262.3	23.6	292.4	
WR-15	2.7	290.2	75.4	353.8	
WR-16	3.1	262.3	23.6	292.4	
WR-17	3.6	266.3	32.3	328.4	
WR-18	2.8	286.3	23.6	342.4	
WR-19		282.2	84.2	373.4	
WR-20		281.9	32.3	400.3	
Santosh	1.8	259.9	53.2	323.4	
Gaute (GG 1-04F)	4.6	294.1	21.7	435.3	
RO-04	3.1	262.4	41.5	317.8	8.8
Dexamethasone	1.8		94.8	392.5	10.3
Chlorthalidone	1.1	200.2	109.5	338.8	8.2
PR04		281.8	26.3	330.4	
BPN		230.2	48.8	308.3	9.6
Warfarin	0.9	245.9	63.6	308.3	8.7

Elagolix	2.0		99.2	631.6	15.7
Altanserin	2.48	299.8	52,7	411.5	11.7
Gavestinel	1.14	236.3	81.3	397.2	
Flumazenil	1.6	233.6	62.2	303.3	7.7
Protriptyline	4.7	246.3	12	263.4	8.6
Loperamide	2.6		43.8	477	14.1
Clonidine hydrochloride	1.6	160.4	36.4	230.1	5.8
Trazodone	3.4	304.9	42.4	371.9	10.4
Trimipramine solution	4.1	268.6	6.5	294.4	9.5
Naloxone	2.6		43.8	477	14.1

Appendix B: Protein Binding

Data from method development for protein binding

Warfarin

Table 43 and Table 44 show the raw data for the calibration curves of warfarin in Figure 14.

Table 43: Raw data for concentration test in calibration curve A of Warfarin in Figure 14

Warfarin concentration	T_R (min)	Peak area
3243 µM	0.833	4270575
	0.832	4273548
	0.834	4279194
2270 µM	0.831	3232621
	0.831	3233169
	0.831	3236768
324 µM	0.843	283057
	0.843	283077
	0.843	283353
162 µM	0.841	145758
	0.845	146144
	0.843	145497
32 µM	0.844	33165
	0.844	33185
	0.844	33097
16 µM	0.841	18733
	0.841	18721
	0.842	18737

Table 44: Raw data for warfarin calibration curve B of conc 1-200 µg/ml (3.24-648.66 µM) in Figure 14

Warfarin concentration	T_R (min)	Peak area
648.66 µM	1.293	812323
	1.293	815557
	1.292	815059
324.33 µM	1.292	411181
	1.295	411642
	1.292	412828
162.16 µM	1.294	208738
	1.295	208336
	1.296	208967
32.43 µM	1.296	42181
	1.296	42170
	1.298	42202
3.24 µM	1.300	4327
	1.298	4342
	1.299	4325

Testosterone

Table 45, Table 46 and Table 47 shows raw data for testosterone calibration curves Figure 15.

Table 45: Raw data for testosterone calibration curve A and B

Testosterone concentration	T_R (min)	Peak area
693.43 µM	6.902	3734907
	6.909	3732590
	6.908	3719799
346.72 µM	6.935	1611114
	6.938	1612401
	6.941	1600228
173.36 µM	6.937	893641
	6.936	893613
	6.932	894409
86.68 µM	6.927	453892
	6.930	451677
	6.934	450826
8.67 µM	6.914	48587
	6.920	49046
	6.925	48619
3.47 µM	6.916	20521
	6.180	20519
	6.920	20629

Table 46: Raw data for testosterone calibration curve C

Testosterone concentration	T_R (min)	Peak area
693.43 µM	6.867	3604286
	6.877	4904246
	6.879	4232729
346.72 µM	6.869	1810797
	6.880	2483637
	6.882	2048359
173.36 µM	6.864	905537
	6.878	1237555
	6.881	1063420
86.68 µM	6.861	429015
	6.877	614571
	6.883	513796
8.67 µM	6.849	38897
	6.875	58341
	6.883	47330
3.47 µM	6.845	14184
	6.878	19953
	6.885	16896

Table 47: Raw data for testosterone calibration curve D

Testosterone concentration	T_R (min)	1: Peak area	2: Peak area
693.43 µM	6.902	1153944	1198221
	6.909	1110290	1148875
	6.908	1316047	1213436
346.72 µM	6.936	548162	573746
	6.938	543363	575101
	6.941	602341	572321
173.36 µM	6.937	326094	431552
	6.936	548587	615335
	6.932	572939	620383
69.34 µM	6.927	123222	182001
	6.930	139110	161967
	6.934	179034	165194
34.67 µM	6.914	70736	69740
	6.920	69408	129906
	6.925	68606	143778
3.47 µM	6.916	8530	7344
	6.180	8284	8733
	6.920	8676	8257
1.73 µM	6.890	4322	4511
	6.889	4710	4684
	6.887	4289	4301
0.35 µM	6.874	967	1109
	6.879	1011	2911
	6.882	1470	1782
0.03 µM	6.935	260	821
	6.944	236	540
	6.932	200	492

Lansoprazole

Raw data for lansoprazole calibration curves can be seen in Table 48, Table 49, Table 50 and Table 51 for Figure 16 curve A to D respectively.

Table 48: Raw data for lansoprazole calibration curve Figure 16 curve A

Lansoprazole	T_R (min)	Peak area
54 µM	4.343	9539
	4.347	9259
	4.343	10054
	4.347	9616
27.07 µM	4.339	4413
	4.343	4447
	4.339	4059
	4.345	4502
2.71 µM	4.340	4593
	4.337	4611
	4.337	4627
	4.342	4292
1.35 µM	4.334	5041
	4.341	4939
	4.341	4163
	4.334	4623
3.0E-3 µM	4.331	5436
	4.333	5198
	4.336	5546
	4.339	5083
3.0E-6 µM	4.330	5347
	4.329	4929
	4.329	4542
	4.927	4210

Table 49: Raw data for lansoprazole calibration curve Figure 16 curve B

Lansoprazole	T_R (min)	Peak area
54.15 µM	4.498	182635
	4.499	183487
	4.497	183345
27.07 µM	4.490	81917
	4.497	81979
	4.497	82155
2.71 µM	4.500	8127
	4.500	8059
	4.502	8129
1.35 µM	4.497	2543
	4.498	2515
	4.494	2518
3.0E-3 µM	4.677	310
	4.677	320
	4.680	344

Table 50: Raw data for lansoprazole calibration curve Figure 16 curve C

Lansoprazole	T_R (min)	Peak area
mobile phase	4.357	915
54.15 µM	4.573	187881
	4.574	187845
	4.571	189529
mobile phase	4.311	927
27.07 µM	4.573	88525
	4.574	88746
	4.580	88844
mobile phase	4.320	892
2.71 µM	4.589	7555
	4.590	7638
	4.597	7712
mobile phase	4.349	877
1.35 µM	4.592	3810
	4.589	3685
	4.590	3690
mobile phase	4.332	896
mobile phase	4.356	937
0.027 µM	4.392	529
	4.372	552
	4.358	617
mobile phase	4.341	793
	4.341	868

Table 51: Raw data lansoprazole calibration curve Figure 16 curve D

Lansoprazole	T_R (min)	Peak area
mobile phase	n/a	n/a
0.27 µM	4.509	570
	4.511	577
	4.512	559
mobile phase	4.285	1107
1.35 µM	4.518	4508
	4.511	4627
	4.512	4641
mobile phase	4.284	1137
2.71 µM	4.526	9562
	4.523	9500
	4.522	9521
mobile phase	4.294	938
5.41 µM	4.518	18276
	4.515	18646
	4.516	18239
mobile phase	4.301	1055
13.54 µM	4.511	49048
	4.515	48658
	4.517	48422
mobile phase	4.294	1157
27.07 µM	4.512	100733
	4.513	100384
	4.515	100126
mobile phase	4.301	1099
54.15 µM	4.513	215946
	4.515	215145
	4.517	215113

Chromatograms for concentrations 1 µg/ml and 10 µg/ml in experiment from Table 31; dilutions by plasma, can be seen below (Figure 23).

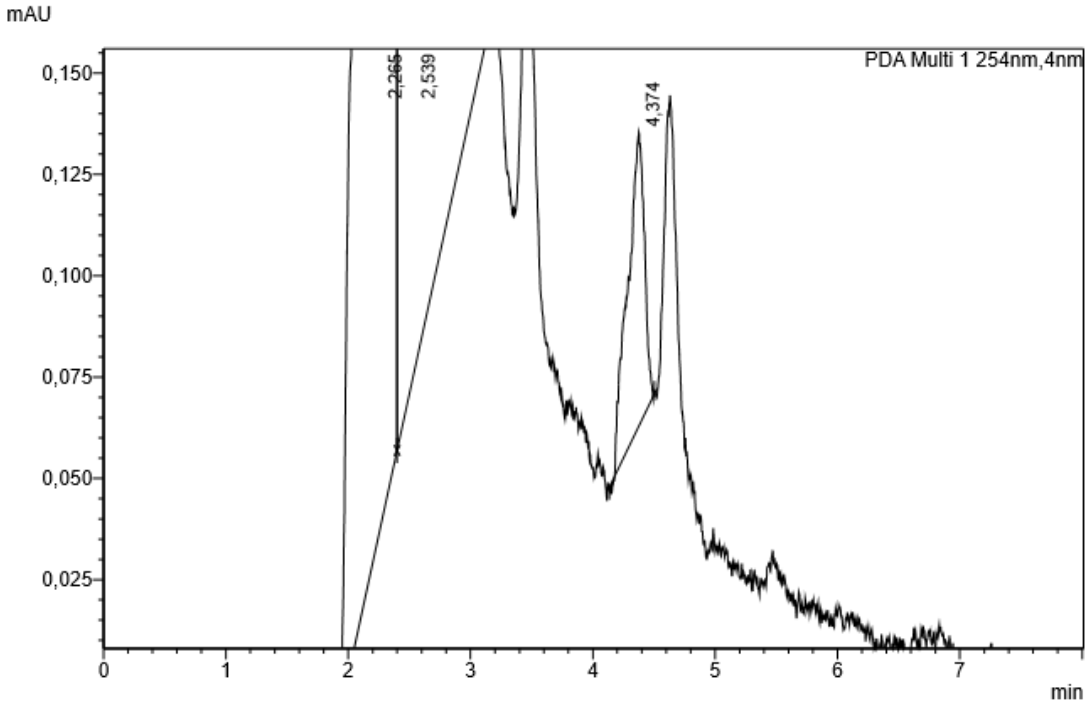

Figure 23: HPLC chromatogram of lansoprazole protein binding, 1 µg/ml plasma diluted. Lansoprazole being the peak at 4.374 minutes.

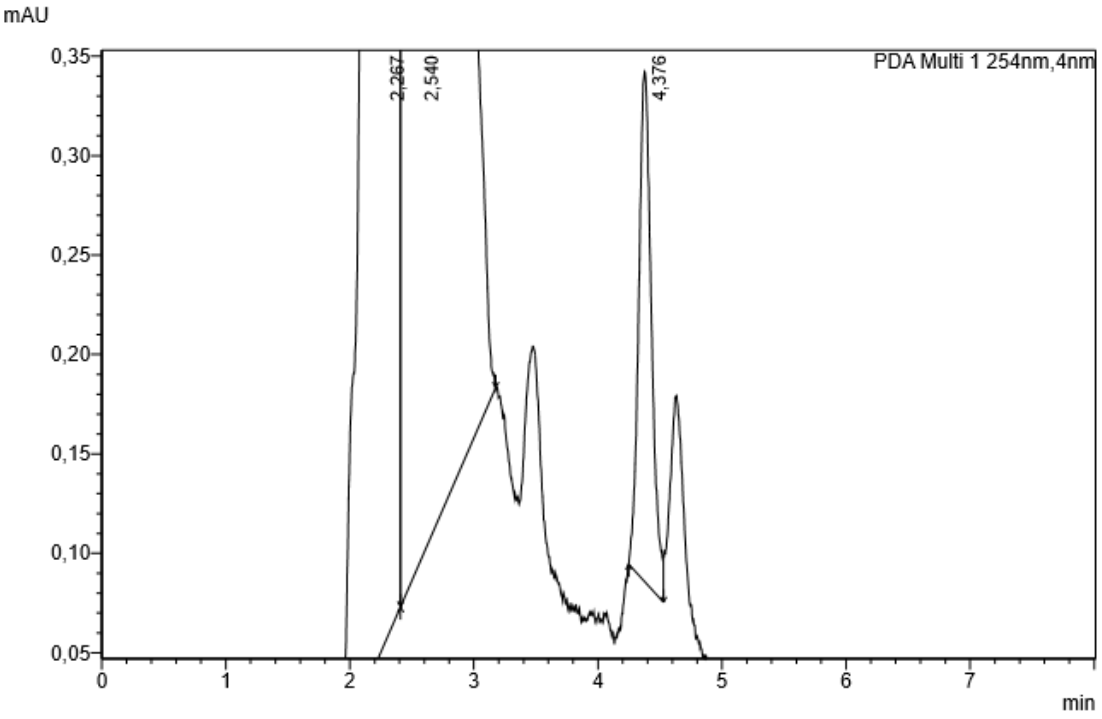

Figure 24: HPLC chromatogram of lansoprazole protein binding, 10 µg/ml plasma diluted. Lansoprazole being the peak at 4.376 minutes.

Chromatograms for concentrations 1 µg/ml (2.71 µM)and 10 µg/ml (27.07 µM) in experiment from Table 31, undiluted, can be seen below (Figure 25 and Figure 26).

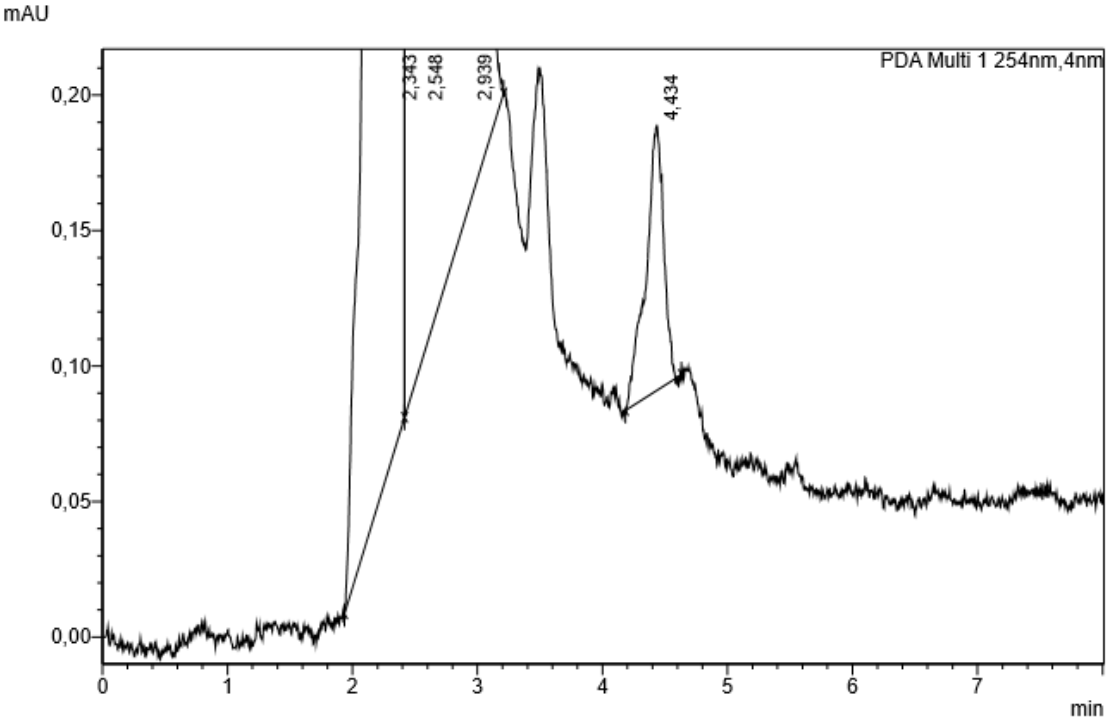

Figure 25: HPLC chromatogram of lansoprazole protein binding, 1 µg/ml (2.71 µM), undiluted addition of test compound. Lansoprazole being the peak at 4.434 minutes.

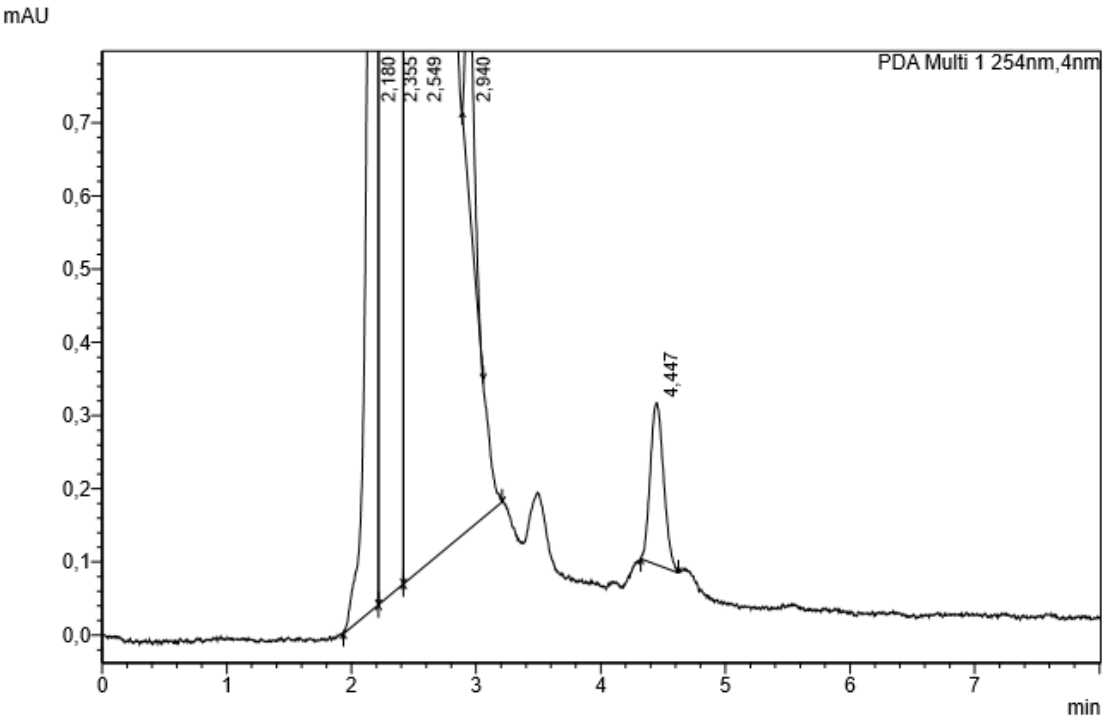

Figure 26: HPLC chromatogram of lansoprazole protein binding, 10 µg/ml (27.07 µM), and undiluted addition of test compound. Lansoprazole being the peak at 4.447 minutes.

Raw data tracer protein binding calibration curves

Raw data and LINEST statistics for the protein binding experiments are to be found in the Tables below (Table 53 to Table 75). All areas are the average peak area under the curve for the specific compound.

Table 52: Lansoprazole raw data and statistics

Average area	Conc (µg/ml)	Linest data		% uncertainty slope	% uncertainty intercept
348	0.01	1.292E-04	8.376E-02		
2579	0.5	7.974E-07	6.149E-02	0.6	73.4
7223	1	9.999E-01	1.074E-01		
75973	10	2.623E+04	3.000E+00		
154593	20	3.026E+02	3.461E-02		

Table 53: L1 raw data and statistics

Average area	Conc (µg/ml)	Linest data		% uncertainty slope	% uncertainty intercept
780	0.1	9.447E-05	3.324E-01		
7723	1	1.764E-06	1.871E-01	1.9	56.3
46005	5	9.990E-01	3.039E-01		
100028	10	2.869E+03	3.000E+00		
209983	20	2.651E+02	2.772E-01		

Table 54: L2 raw data and statistics

Average area	Conc (µg/ml)	Linest data		% uncertainty slope	% uncertainty intercept
640	0.1	9.733E-05	5.254E-01		
6714	1	3.192E-06	3.242E-01	3.3	61.7
41008	5	9.968E-01	5.334E-01		
92213	10	9.296E+02	3.000E+00		
203348	20	2.645E+02	8.536E-01		

Table 55: L3 raw data and statistics

Average area	Conc (µg/ml)	Linest data		% uncertainty slope	% uncertainty intercept
1062	0.1	7.805E-05	2.358E-01		
10774	1	1.205E-06	1.557E-01	1.5	66.0
58458	5	9.993E-01	2.514E-01		
121761	10	4.197E+03	3.000E+00		
255339	20	2.652E+02	1.895E-01		

Table 56: L4 raw data and statistics

Average area	Conc (µg/ml)	Linest data		% uncertainty slope	% uncertainty intercept
			-4.856E-02		
296	0.1	2.103E-04			
4319	1	1.108E-05	2.970E-01	5.3	-611.7
26336	5	9.945E-01	4.109E-01		
46519	10	3.605E+02	2.000E+00		
		6.087E+01	3.377E-01		

Table 57: L5 raw data and statistics

Average area	Conc (µg/ml)	Linest data		% uncertainty slope	% uncertainty intercept
852	0.1	8.135E-05	1.273E-01		
9387	1	1.771E-06	2.213E-01	2.2	173.8
56334	5	9.986E-01	3.545E-01		
127349	10	2.109E+03	3.000E+00		
242009	20	2.650E+02	3.770E-01		

Table 58: L6 raw data and statistics

Average area	Conc (µg/ml)	Linest data		% uncertainty slope	% uncertainty intercept
1278	0.1	5.782E-05	4.553E-01		
13344	1	1.953E-06	3.355E-01	3.4	73.7
72176	5	9.966E-01	5.494E-01		
154027	10	8.762E+02	3.000E+00		
344107	20	2.645E+02	9.054E-01		

Table 59: L7 raw data and statistics

Average area	Conc (µg/ml)	Linest data		% uncertainty slope	% uncertainty intercept
1867	0.1	3.358E-05	2.813E-01		
24164	1	5.783E-07	1.732E-01	1.7	61.6
133340	5	9.991E-01	2.804E-01		
281117	10	3.373E+03	3.000E+00		
592527	20	2.651E+02	2.358E-01		

Table 60: L8 raw data and statistics

Average area	Conc (µg/ml)	Linest data		% uncertainty slope	% uncertainty intercept
861	0.1	9.056E-05	3.817E-01		
7944	1	2.072E-06	2.285E-01	2.3	59.9
45795	5	9.984E-01	3.724E-01		
104452	10	1.911E+03	3.000E+00		
218515	20	2.650E+02	4.159E-01		

Table 61: L9 raw data and statistics

Average area	Conc (µg/ml)	Linest data		% uncertainty slope	% uncertainty intercept
1015	0.1	1.265E-04	-4.048E-01		
7491	1	9.709E-06	8.061E-01	7.7	-199.1
44656	5	9.826E-01	1.239E+00		
95808	10	1.697E+02	3.000E+00		
152438	20	2.608E+02	4.609E+00		

Table 62: L10 raw data and statistics

Average area	Conc (µg/ml)	Linest data		% uncertainty slope	% uncertainty intercept
1721	0.1	3.273E-05	6.403E-01		
21039	1	1.395E-06	4.179E-01	4.3	65.3
107876	5	9.946E-01	6.926E-01		
273059	10	5.502E+02	3.000E+00		
601598	20	2.639E+02	1.439E+00		

L11 is shown and commented in chapter 5.2. “Protein binding results”.

Table 63: L11 raw data and statistics

Average area	Conc (µg/ml)	Linest data		% uncertainty slope	% uncertainty intercept
636	0.1	7.763E-05	1.544E-01		
7666	1	2.795E-06	3.651E-01	3.6	236.5
58378	5	9.961E-01	5.854E-01		
137677	10	7.713E+02	3.000E+00		
250708	20	2.643E+02	1.028E+00		

Table 64: L12 raw data and statistics

Average area	Conc (µg/ml)	Linest data		% uncertainty slope	% uncertainty intercept
780	0.1	6.487E-05	8.495E-02		
14258	1	1.659E-07	2.609E-02	0.3	30.7
75342	5	1.000E+00	4.167E-02		
152133	10	1.528E+05	3.000E+00		
307476	20	2.654E+02	5.210E-03		

Table 65: L13 raw data and statistics

Average area	Conc (µg/ml)	Linest data		%	%
1728	0.1	3.804E-05	5.402E-02	uncertainty slope	uncertainty intercept
25578	1	8.884E-08	2.387E-02	0.2	44.2
128627	5	1.000E+00	3.805E-02		
261220	10	1.833E+05	3.000E+00		
524821	20	2.654E+02	4.343E-03		

Table 66: L14 raw data and statistics

Average area	Conc (µg/ml)	Linest data		%	%
1501	0.1	4.167E-05	8.912E-01	uncertainty slope	uncertainty intercept
15355	1	1.769E-06	4.572E-01	4.2	51.3
92376	5	9.964E-01	6.021E-01		
205451	10	5.552E+02	2.000E+00		
465183	20	2.013E+02	7.251E-01		

Table 67: L15 raw data and statistics

Average area	Conc (µg/ml)	Linest data		%	%
		4.476E-05	6.508E-01	uncertainty slope	uncertainty intercept
16094	1	1.263E-06	3.093E-01	2.8	47.5
91608	5	9.984E-01	4.007E-01		
202162	10	1.256E+03	2.000E+00		
436238	20	2.017E+02	3.212E-01		

Table 68: L16 raw data and statistics

Average area	Conc (µg/ml)	Linest data		%	%
2173	0,1	3.147E-05	1.202E-01	uncertainty slope	uncertainty intercept
28541	1	1.947E-07	6.293E-02	0.6	52.3
150439	5	9.999E-01	1.008E-01		
314343	10	2.613E+04	3.000E+00		
632693	20	2.653E+02	3.046E-02		

Table 69: L17 raw data and statistics

Average area	Conc (µg/ml)	Linest data		%	%
1309	0.1	5.117E-05	1.236E-01	uncertainty slope	uncertainty intercept
17537	1	2.965E-07	5.894E-02	0.6	47.7
93461	5	9.999E-01	9.440E-02		
191541	10	2.978E+04	3.000E+00		
389608	20	2.653E+02	2.673E-02		

Table 70: L18 raw data and statistics

Average area	Conc (µg/ml)	Linest data		%	%
1912	0.1	5.770E-05	-1.734E-02	uncertainty slope	uncertainty intercept
15698	1	3.657E-07	6.509E-02	0.6	-375.4
89070	5	9.999E-01	1.032E-01		
174409	10	2.489E+04	3.000E+00		
346060	20	2.653E+02	3.198E-02		

Table 71: L19 raw data and statistics

Average area	Conc (µg/ml)	Linest data		%	%
2825	0.1	3.511E-05	-8.520E-02	uncertainty slope	uncertainty intercept
27531	1	3.639E-07	1.069E-01	1.0	-125.5
151425	5	9.997E-01	1.688E-01		
288922	10	9.307E+03	3.000E+00		
569670	20	2.653E+02	8.551E-02		

Table 72: L20 raw data and statistics

Average area	Conc (µg/ml)	Linest data		%	%
216	0.1	1.718E-04	9.840E-01	uncertainty slope	uncertainty intercept
2693	1	1.100E-05	6.117E-01	6.4	62.2
18300	5	9.879E-01	1.036E+00		
46361	10	2.441E+02	3.000E+00		
113922	20	2.621E+02	3.222E+00		

Table 73: W1 raw data and statistics

Average area	Conc (µg/ml)	Linest data		%	%
307	0.1	2.015E-04	4.556E-01	uncertainty slope	uncertainty intercept
3178	1	6.960E-06	3.431E-01	3.5	75.3
18496	5	9.964E-01	5.617E-01		
48893	10	8.382E+02	3.000E+00		
96973	20	2.644E+02	9.464E-01		

Table 74: W5 raw data and statistics

Average area	Conc (µg/ml)	Linest data		%	%
598	0.1	2.268E-04	2.293E-01	uncertainty slope	uncertainty intercept
3585	1	3.739E-06	1.664E-01	1.6	72.6
19426	5	9.992E-01	2.685E-01		
42927	10	3.679E+03	3.000E+00		
87612	20	2.652E+02	2.162E-01		

Table 75: W21 raw data and statistics

Average area	Conc (µg/ml)	Linest data		%	%
1159	0.1	7.672E-05	9.699E-02	**uncertainty slope**	**uncertainty intercept**
11204	1	3.083E-07	4.094E-02	0.4	42.2
63518	5	1.000E+00	6.546E-02		
128524	10	6.192E+04	3.000E+00		
259809	20	2.654E+02	1.286E-02		

Raw data tracer protein binding assay

Porcine plasma protein binding raw data can be seen in Table 76 and Table 77.

Table 76: Raw data for protein binding assay of tracers and standards

	T_R (min)	Peak Area	Concentration calculated from associated calibration curve (µg/ml)	Unbound Fraction (%)	Average Unbound (%)	Std. dev (%)	Bound (%)
Std. 30	4.435	4926	0.6	6.1			
	4.426	5407	0.7	6.6	6.3	3.7	93.7
	4.426	4983	0.6	6.2			
C3	5.230	1188	1.0	9.8			
	5.243	1193	1.0	9.8	9.6	2.2	90.4
	5.223	1127	0.9	9.3			
Std. 31	8.039	1655	0.3	2.8			
	7.971	1254	0.3	2.6	2.6	7.0	97.4
	7.919	778	0.2	2.4			
L2	5.813	1681	0.7	6.9			
	5.852	1834	0.7	7.0	7.0	1.0	99.0
	5.862	1839	0.7	7.0			
L3	5.355	9334	1.0	9.6			
	5.351	8566	0.9	9.0	9.4	2.8	97.2
	5.354	9245	1.0	9.6			
L4	0	0	0.0	0.0	0.0	0.0	100.0
L5	7.381	3047	0.4	3.8			
	7.401	3393	0.4	4.0	3.8	3.5	96.5
	7.419	3041	0.4	3.7			
L6	4.781	1903	0.6	5.7			
	4.780	2258	0.6	5.9	5.8	1.0	100.0
	4.785	2151	0.6	5.8			
L7	6.399	27698	1.2	12.1			
	6.391	30844	1.3	13.2	12.5	4.0	96.0
	6.408	28113	1.2	12.3			
L8	4.285	5816	0.9	9.1			
	4.284	5536	0.9	8.8	9.0	4.0	96.0
	4.284	5720	0.9	9.0			
L9	6.001	5110	0.7	6.5			
	5.952	5250	0.7	6.6	6.6	1.4	98.6
	5.982	5280	0.7	6.7			
L10	5.605	20341	1.3	13.1			
	5.612	21577	1.4	13.5	13.5	2.4	97.6
	5.609	22798	1.4	13.9			
L11	0	0	0.0	0.0	0.0	0.0	100.0

L12	6.241	2032	0.2	2.2			
	6.240	2225	0.2	2.3	2.2	2.3	97.7
	6.164	2159	0.2	2.3			
L13	5.988	3465	0.2	1.9			
	5.984	4097	0.2	2.1	2.0	5.1	94.9
	5.999	3654	0.2	1.9			
L14	6.117	2159	0.5	23.3			
	6.080	2362	0.5	24.2	0.4	1.9	76.1
	6.044	2291	0.5	24.3			
L15	5.823	21445	2.3	4.9			
	5.821	22332	2.4	5.0	0.1	1.1	95.0
	5.825	22402	2.4	5.0			
L16	5.556	29997	1.1	10.6			
	5.525	29191	1.0	10.4	0.3	3.3	89.7
	5.544	27442	1.0	9.8			
L17	0	0	0.0	0.0			
	0	0	0.0	0.0	0.0	0.0	100
	0	0	0.0	0.0			
L18	4.576	7251	0.4	4.0			
	4.581	7425	0.4	4.1	0.1	1.2	95.9
	4.578	7939	0.4	4.4			
L19	4.461	11838	0.3	3.3			
	4.464	11178	0.3	3.1	0.1	4.1	96.9
	4.465	10980	0.3	3.0			
Std. 32	8.678	943	1.1	5.7			
	8.702	886	1.1	5.7	5.7	0.3	94.3
	8.534	910	1.1	5.7			
C2	4.280	19715	2.2	21.9			
	4.282	20719	2.3	22.9	22.7	2.3	77.3
	4.283	21012	2.3	23.2			
C1	5.423	21832	1.8	17.7			
	5.417	25613	2.1	20.6	19.1	6.2	80.9
	5.409	23510	1.9	19.0			
C5	0	0	0	0	0	0	100.0
WR-01	4.351	8778	2.2	11.1			
	4.351	8901	2.2	11.2	11.3	2	88.7
	4.351	9292	2.2	11.6			
WR-05	4.712	12532	3.1	30.7			
	4.708	11616	2.9	28.6	29.5	3	70.5
	4.716	11908	2.9	29.3			

Table 77: Centrifugal data for the compounds where this was measured

	Weight of supernatant* (g)	Corresponding volume (µl)	Throughput filter (%)
Std. 30	0.0989	148.4	98.9
	0.0782	117.3	78.2
	0.0923	138.5	92.3
C3	0.0744	111.6	74.4
	0.0805	120.8	80.5
	0.0815	122.3	81.5
Std. 31	0.0844	126.6	84.4
	0.0812	121.8	81.2
	0.0921	138.2	92.1
L2	0.0964	144.6	96.4
	0.1010	151.5	101.0
	0.1016	152.4	101.6
L3	0.0994	149.1	99.4
	0.1001	150.2	100.1
	0.0979	146.9	97.9
L4	0.0978	146.7	97.8
L5	0.0960	144.0	96.0
	0.0902	135.3	90.2
	0.1006	150.9	100.6
L6	0.0887	133.1	88.7
	0.0924	138.6	92.4
	0.0943	141.5	94.3
L7	0.0970	145.5	97.0
	0.0891	133.7	89.1
	0.0759	113.9	75.9
L8	0.0890	133.5	89.0
	0.0878	131.7	87.8
	0.0942	141.3	94.2
L9	0.0906	135.9	90.6
	0.0926	138.9	92.6
	0.0908	136.2	90.8
L10	0.0963	144.5	96.3
	0.0864	129.6	86.4
	0.0860	129.0	86.0
L11	0.0961	144.2	96.1
L12	0.0968	145.2	96.8
	0.0995	149.3	99.5
	0.0989	148.4	98.9
L13	0.1000	150.0	100.0
	0.0998	149.7	99.8
	0.0855	128.3	85.5
Std. 32	0.0998	149.7	99.8
	0.0993	149.0	99.3

	0.0981	147.2	98.1
C2	0.0993	149.0	99.3
	0.0877	131.6	87.7
	0.0986	147.9	98.6
C1	0.0998	149.7	99.8
	0.1010	151.5	101
	0.0971	145.7	97.1
C5	0.0915	137.3	91.5
WR-01	0.1044	156.6	104.4
	0.1023	153.5	102.3
	0.0929	139.4	92.9
WR-05	0.0948	142.2	94.8
	0.0955	143.3	95.5

*±0.0002 g

Human serum protein binding raw data can be seen in Table 78 and Table 79.

Table 78: Human serum protein binding raw data

	T_R (min)	Peak Area	Concentration calculated from associated calibration curve µg/ml	% Unbound fraction	% Unbound average	Std. dev %	Bound %
Std. 30	4.490	1848	0.3	2.8			
	4.521	2159	0.3	3.1	3.0	4.7	97.0
	4.497	1971	0.3	2.9			
L7	6.374	6996	0.5	5.2	5.2	n/a	94.8
L8	4.430	5153	0.8	8.5			
	4.428	5238	0.9	8.6	8.5	1.3	91.5
	4.427	4941	0.8	8.3			
L9		0	0.0	0.0			
		0	0.0	0.0	0.0	0.0	100.0
		0	0.0	0.0			
L10	5.637	3489	0.8	7.5			
	5.643	5101	0.8	8.1	7.9	2.9	92.1
	5.620	4714	0.8	7.9			

Table 79: Centrifuge data for the compounds where this was measured

	Weight of supernatant* (g)	Corresponding volume (µl)	Throughput filter (%)
L7	0.1008	151	100.8
L8	0.0940	141	94.0
	0.0907	136	90.7
	0.0979	147	97.9

*± 0.0002 g

Porcine full blood protein binding raw data can be seen in Table 80.

Table 80: Porcine full blood protein binding raw data

	Peak Area	Concentration calculated from associated calibration curve (µg/ml)	% Unbound fraction	% Unbound average	Std.dev %	Bound %
Std. 30 plasma	4590	0.6	5.8			
	4424	0.6	5.6	5.6	2.0	94.0
	4408	0.6	5.6			
Std. 30 porcine full blood	1740	0.3	1.3			
	2154	0.3	3.1	2.6	34.0	97.0
	2223	0.3	3.2			

Appendix C: General data concerning both lipophilicity and protein binding

Table 81: Newly synthesized tracers and commercial compounds used in the thesis are shown with their synthesized/commercial name and a test group name for this thesis specifically. First columns are commercial or working names, seconds columns are group names made for this thesis (red color = no protein binding data)

LANSO -series	GROUP NAME	WR-series	GROUP NAME	Diverse	GROUP NAME
		WR-01	W1	Santosh	J1
LANSO-01	L2	WR-02	W2	Gaute	J3
LANSO-02	L3	WR-03	W3	1-21	J4
LANSO-03	L4	WR-04	W4	1-23	J5
LANSO-04	L5	WR-05	W5	1-27	J6
LANSO-05	L6	WR-06	W6	1-75	J7
LANSO-06	L7	WR-07	W7	1-77	J8
LANSO-07	L8	WR-08	W8	1-78	J9
LANSO-08	L9	WR-09	W9	1-79	J10
LANSO-09	L10	WR-10	W10	1-80	J11
LANSO-10	L11	WR-11	W11	1-97	J12
LANSO-11-1	L12	WR-12	W12	1-100	J13
LANSO-11-2	L13	WR-13	W13	1-104	J14
LANSO-12	L14	WR-14	W14	1-106	J15
LANSO-13-1	L15	WR-15	W15	1-117	J16
LANSO-13-2	L16	WR-16	W16	1-136	J17
LANSO-14	L17	WR-17	W17	1-138	J18
LANSO-15-1	L18	WR-18	W18	1-139	J19
LANSO-15-2	L19	WR-19	W19		
		WR-20	W20		

Commercial compounds	GROUP NAME
AH-7921	C1
N- Methyl Lansoprazole	C2
RO-04-5595	C3
Protriptyline	C4
PR04	C5

Pipette calibration can be seen in Table 82.

Table 82: Pipette calibration

M21046D	Avg (µl)	% St.dev reproducibility	Error (µl)	% error
1000 µl	985.5	0.13	14.5	0.01
400 µl	393.6	2.62	6.4	0.02
H30122C				
1000 µl	992.7	0.08	5.3E-3	7.3E-3

Comparison and calibration between two weights and HPLC injector calibration can be seen in Figure 27 below. Mobile phase and testosterone (1 µg/ml) was weighted up with two weights available in the lab, they were measured on the HPLC where the injection volume was set to 10 µl. All measurements were done in triplets. The samples were reweighted after injections to measure the true injection volume.

	before injection	before injection	after injection	after injection	Amount sample injected (g)		Amount sample injected (ml)		Amount sample injected (ul)		
sample	**Mettler weight**	**Ohaus weight**	**Mettler weight**	**Ohaus weight**	**Mettler**	**Ohaus**	**Mettler**	**Ohaus**	**Mettler**	**Ohaus**	
mobile phase	4.0127	4.0149	3.9858	3.9856	0.0269	0.0293	0.0319	0.0348	**10.6**	**11.6**	
testosterone	2.9998	2.9997	2.9721	2.9721	0.0276	0.0276	0.0277	0.0277	**9.2**	**9.2**	
	st.dev Mettler	st.dev Ohaus	st.dev Mettler	st.dev Ohaus							
	0.0000	0.0036	0.0000	0.0001					**expected amount (ul)**		
	0.0001	0.0001	0.0000	0.0004					**10**		
									% dev from expected amount		
	st.dev %	st.dev %	st.dev %	st.dev %					**6.4**	**15.9**	
	0.000	0.090	0.000	0.004					**-7.7**	**-7.7**	
	0.004	0.003	0.002	0.012							
	st.dev		st.dev						**On a 20 ug/ml samples**		
	between the weights		between the weights						**6%**	**1.2**	**ug/ml**
	0.00110		0.00010								
	0.00002		0.00002						**On a 0,01 ug/ml samples**		
									6%	**0.0006**	**ug/ml**

Figure 27: Test of autosampler injection in HPLC and comparison of weights

Abbreviations

ABC transporter	ATP-binding cassette transporter protein family
ATP	Adenosintriphosphate
AUC	Area Under the Curve in a plot of plasma drug concentration as a function of time
BBB	Blood-Brain Barrier
BCEC	Brain Capillary Endothelial Cells
C_{18}	Octadecyl ($C_{18}H_{37}$) functionalized silica stationary phase used in HPLC
CNS	Central Nervous System
CT	Computed Tomography
CYP	Oxidoreductase proteins of the Cytochrome P450 family
D	Distribution coefficient, ratio of concentrations of a compound in a mixture of two immiscible phases at equilibrium
FDT	Free Drug Theory
HPLC	High Performance Liquid Chromatography
IAM	Immobilized Artificial Membranes
IUPAC	International Union of Pure and Applied Chemistry
K_D	Dissociation constant
LC-MS	(High Performance) Liquid Chromatography-coupled with Mass Spectrometry
λ (lambda)	rate constant for radioactive decay [λ] = s^{-1}
Log D	Logarithm of Distribution coefficient
Log k	Logarithm of retention factor, k
Log P	Logarithm of Partition coefficient
MRI	Nuclear Magnetic Resonance Imaging
MRP	Multidrug Resistance-associated Proteins
MW	Molecular Weight, mass of one mole of a substance
nM	Nanomolar
PAMPA	Parallel Artificial Membrane Permeability Assay
PET	Positron Emission Tomography
Pgp	P-glycoprotein
PSA	Polar Surface Area, the polar sum over all polar atoms
R^2	Coefficient of Determination
RP-HPLC	Reversed Phase- HPLC
t_R	Retention time
SPECT	Single-Photon Emission Computed Tomography
SUV	Standard Uptake Units
TLC	Thin Layer Chromatography
UV/VIS	Ultra Violet/Visible